AWARD NUMBER: W81XWH-15-1-0413

TITLE: Targeting quiescence in prostate cancer

PRINCIPAL INVESTIGATOR: Laura Buttitta

CONTRACTING ORGANIZATION: University of Michigan
Ann Arbor, MI 48109

REPORT DATE: December 2019

TYPE OF REPORT: FINAL

PREPARED FOR: U.S. Army Medical Research and Materiel Command
Fort Detrick, Maryland 21702-5012

REPORT DOCUMENTATION PAGE

Form Approved
OMB No. 0704-0188

1. REPORT DATE	2. REPORT TYPE	3. DATES COVERED
DECEMBER 2019	FINAL	15 Sep 2015 - 14 SEP 2019

4. TITLE AND SUBTITLE

Targeting Quiescence in Prostate Cancer

5a. CONTRACT NUMBER
W81XWH-15-1-0413

5b. GRANT NUMBER
PC140656

5c. PROGRAM ELEMENT NUMBER

6. AUTHOR(S)

Laura Buttitta

E-Mail: buttitta@umich.edu

5d. PROJECT NUMBER

5e. TASK NUMBER

5f. WORK UNIT NUMBER

7. PERFORMING ORGANIZATION NAME(S) AND ADDRESS(ES)

University of Michigan
Ann Arbor, MI 48109

8. PERFORMING ORGANIZATION REPORT NUMBER

9. SPONSORING / MONITORING AGENCY NAME(S) AND ADDRESS(ES)

U.S. Army Medical Research and Materiel Command
Fort Detrick, Maryland 21702-5012

10. SPONSOR/MONITOR'S ACRONYM(S)

11. SPONSOR/MONITOR'S REPORT NUMBER(S)

12. DISTRIBUTION / AVAILABILITY STATEMENT

Approved for Public Release; Distribution Unlimited

13. SUPPLEMENTARY NOTES

14. ABSTRACT

A major problem in prostate cancer is finding and eliminating the non-proliferating or "quiescent" cancer cells. This is because early in prostate cancer, a small number of cancer cells metastasize to other tissues such as the bone, where they can lay dormant for years. Most chemotherapies target actively dividing cancer cells causing primary tumor shrinkage, but leave behind quiescent cancer cells which may seed new, more aggressive and chemo-resistant cancers at a later date. Through this research project we have made several important discoveries. 1.We have discovered that PCa cells that metastasize to the bone exhibit dramatically different cell cycle characteristics from those in the liver, suggesting signals from the bone are key to regulating PCa cell cycle and dormancy. 2. We have identified gene expression programs active during dormancy and suppressed during tumor recurrence both in the tumor itself and in the marrow environment. 3. We have generated PCa cell lines that can be sorted based upon a cell cycle reporter for quiescence and identified cell surface molecules that can be used to isolate and quantify dormant cancer cells. 4. We have performed experiments to discern how PCa quiescence modulates the effect of chemotherapies on tumor recurrence.

15. SUBJECT TERMS

tumor dormancy, prostate cancer cell quiescence, cancer recurrence

16. SECURITY CLASSIFICATION OF:			17. LIMITATION OF ABSTRACT	18. NUMBER OF PAGES	19a. NAME OF RESPONSIBLE PERSON
a. REPORT	b. ABSTRACT	c. THIS PAGE			USAMRMC
U	U	U	UU	114	19b. TELEPHONE NUMBER *(include area code)*

Table of Contents

Page

Targeting Quiescence in Prostate Cancer

W81XWH-15-1-0413 PC140656

INTRODUCTION:

Prostate cancer (PCa) is characterized by the early spreading of a small number of tumor cells to other tissues, termed disseminated tumor cells (DTCs). DTCs in the bone are problematic because they may lie dormant for months or even years, yet a percentage of patients will later develop recurrent cancer with significant bone metastases from these cells, which often become resistant to treatment. Understanding how DTCs reside undetected in the marrow for long periods of time and finding ways to eliminate or minimize them, is an important issue in prostate cancer research and treatment.

Hypothesis: We hypothesize that dormant DTCs enter a state of cellular quiescence in the bone marrow, which renders them insensitive to chemotherapies designed to target actively proliferating cancer cells. Recent work has revealed that quiescence may encompass multiple "depths" that impact the speed and ability of dormant cancer cells to re-enter the cell cycle. Our goal is to examine whether dormant DTCs enter into a deep quiescent state known as G0 or arrest in a quiescent but "alert" and ready to re-enter state more similar to G1 in the bone marrow and test whether the disruption of signaling from the marrow that promotes DTC quiescence may reduce tumor burden and improve treatment outcomes by sensitizing quiescent cancer cells to chemotherapies.

Aims: To address this hypothesis we pursued two aims: Aim 1, we developed PCa cell lines expressing novel cell cycle reporters which will allow us to determine the cell cycle state of DTCs during dormancy in a xenograft prostate cancer model. In Aim 2, we address how signals from osteoblasts, osteoclasts or chemotherapy treatments alter DTC quiescence, to determine the impact on tumor dormancy, recurrence and response to current treatments.

Summary of results to date: We successfully generated prostate cancer cell lines carrying fluorescent cell cycle sensors compatible with live imaging and flow cytometry, that together distinguish G0 and G1. We verified that these sensors accurately indicate the cell cycle state of the cells *in vitro* without disrupting their dynamics, and that these cell lines respond to signals from the bone marrow thought to promote dormancy by increasing cell cycle arrest. We used these lines to characterize molecular markers of quiescence in vivo. We found that several components of pathways associated with proliferation (e.g. Her2 and Hippo/YAP) are up-regulated in quiescent cells making them potential molecules to target treatments to quiescent cancer cells. In our xenograft model, we confirmed that these cell lines form tumors and metastasize to the bone marrow. However, in the process of optimizing their recovery from the marrow, we discovered that over time in the mouse, the reporters become silenced. Therefore in our xenograft model for tumor recurrence, we use cell lines using luciferase instead of the

cell cycle reporters to monitor tumor recurrence by bioluminescence. Despite this unexpected challenge, we successfully performed *in vitro* and shorter-term *in vivo* experiments (<1 week) with our cell lines carrying cell cycle reporters. These experiments revealed that DTCs in the bone marrow accumulate in the G1-phase of the cell cycle within 48h of injection, suggesting that entry into a quiescent but "alert" state may be a very early event for DTCs in the marrow. Using *in vitro* co-culture and single cell assays we have also been able to show that signals from osteoblasts such as Gas6 promote quiescence and entry into G0, consistent with our hypothesis that the bone marrow environment promotes quiescence of DTCs over time. By contrast, signaling from the bone marrow via Transferrin or signaling from osteoclasts induces proliferation of PCa in the bone, a result which we have also been able to confirm *in vivo*. In year 1 we provided evidence that treatment with Docetaxel enhanced the effects of Gas6 in promoting PCa quiescence and an increased entry into arrests in G0 and G1. In recent work we show these cells can be targeted by anti-cancer polymers. Toward the goals of manipulating quiescence and cell cycle re-entry of metastasized PCa, we established that the Hippo downstream effector YAP becomes activated to promote tumor recurrence. By inhibiting YAP in our mouse xenograft model we effectively reduced tumor recurrence *in vivo*. Furthermore, using a drug-conjugated HER2 antibody (T-DM1), we show that significant suppression of PCa metastasis can be achieved in a preclinical animal model

KEYWORDS: *Provide a brief list of keywords (limit to 20 words).*

GAS6	Growth arrest specific 6
HSC	Hematopoietic stem cells
HSC Niche	Hematopoietic Stem Cell Niche
PC3	Prostate cancer cell line
PCa	Prostate Cancer
Docetaxel	Chemotherapy agent
G0/quiescence	A reversible quiescent or non-cycling state
Transferrin	Iron transporting protein, high in blood and marrow
FACS	Fluorescence activated cell sorting
G1	Gap1 phase of the cell cycle
S-phase	DNA synthesis phase of the cell cycle
G2	Gap2 phase of the cell cycle
Proliferation	Actively replicating and dividing cells
Osteoblasts	Cells that secrete matrix for bone formation
Osteoclasts	Cells that remodel and resorb bone

ACCOMPLISHMENTS: **Major goals of the project**

STATEMENT OF WORK

START DATE: Sept 15, 2016

Revised SOW (Major tasks 2 and 3) approved Dec. 19 2017

Major Task 1: Generate prostate cancer cell lines stably expressing G0/G1 cell cycle reporters.	Months	status	**Summary of progress**
Subtask 1: Generate Lentivirus and transduce cells	1	completed	-
Subtask 2: Select stable cells lines	2	completed	-
Subtask 3: Verify reporters are correctly expressed	3	completed	-
Milestone(s) Achieved : PC-3 prostate cancer cell lines containing fluorescent cell cycle reporters		completed	PC3 labeled cell lines behave as expected in vitro. This was established in year 1
Major Task 2: Implant labeled cancer cells (or controls) into SCID mice to monitor dormancy			**Major Task 2: Implant labeled cancer cells (or controls) into SCID mice to monitor dormancy**
Subtask 1: Insert labeled cancer cells by i.c. injection or implants	1-4 months	Completed	Subtask 1: Insert labeled cancer cells by i.c. injection or implants
Subtask 2: Remove Collagen Implants if used	1		Subtask 2: Remove Collagen Implants if used
Subtask 3: Isolate tissues and test for metastasis to bone using QPCR of Alu Repeats* and detection of fluorescent labels (Timepoints throughout 1-7 months will be examined)	1-7 months	completed	Subtask 3: Isolate tissues and test for metastasis to bone using QPCR of Alu Repeats* and detection of fluorescent labels (Timepoints throughout 1-7 months will be examined)
Subtask 4: Isolate tissues and perform flow cytometry to identify cell cycle distributions of metastatic populations* (Timepoints throughout 1-7 months will be examined)	1-7 months	completed	Subtask 4: Isolate tissues and perform flow cytometry to identify cell cycle distributions of metastatic populations* (Timepoints throughout 1-7 months will be examined)
Subtask 5: Isolate tissues and perform immunofluorescence to identify cell cycle distributions of cancer cells in the Hematopoietic Stem cell niche* (Timepoints throughout 1-7 months will be examined)	1-7 months	completed	Subtask 5: Isolate tissues and perform immunofluorescence to identify cell cycle distributions of cancer cells in the Hematopoietic Stem cell niche* (Timepoints throughout 1-7 months will be examined)
Subtask 6: Isolate tissues and test for metastasis to bone using QPCR of Alu Repeats and detection of fluorescent labels under chemotherapy treatments* (Timepoints throughout 1-7 months will be examined)	1-7 months	completed	Subtask 6: Isolate tissues and test for metastasis to bone using QPCR of Alu Repeats and detection of fluorescent labels under chemotherapy treatments* (Timepoints throughout 1-7 months will be examined)
Subtask 7: Isolate tissues and perform flow cytometry and immunofluorescence	1-7 months	completed	Subtask 7: Isolate tissues and perform flow cytometry and

to identify cell cycle distributions of metastatic populations under chemotherapy conditions* (Timepoints throughout 1-7 months will be examined)			immunofluorescence to identify cell cycle distributions of metastatic populations under chemotherapy conditions* (Timepoints throughout 1-7 months will be examined)
Milestone(s) Achieved: Measurement of PC3 cell cycle dynamics during dormancy with or without chemotherapy treatment		completed	Milestone(s) Achieved: Measurement of PC3 cell cycle dynamics during dormancy with or without chemotherapy treatment
Major Task 3: Implant labeled cancer cells (or controls) into SCID mice to monitor tumor recurrence			**Major Task 3: Implant labeled cancer cells (or controls) into SCID mice to monitor tumor recurrence**
Subtask 1: Insert stably labeled cancer cells by i.c. injection or implants. Remove implants if used.	1mo	completed	Subtask 1: Insert stably labeled cancer cells by i.c. injection or implants. Remove implants if used.
Subtask 2: Monitor tumor formation in PC3 controls labeled with fluorescent reporters under conditions with vs. without chemotherapy	7-9 months	completed	Subtask 2: Monitor tumor formation in PC3 controls labeled with fluorescent reporters under conditions with vs. without chemotherapy
Subtask 3: Isolate recurrent cancers and perform flow cytometry to identify cell cycle distributions of recurrent tumor populations*	3-4 months	completed	Subtask 3: Isolate recurrent cancers and perform flow cytometry to identify cell cycle distributions of recurrent tumor populations*
Subtask 4: Isolate recurrent tumors and perform immunofluorescence to identify cell cycle distributions of cancer cells *	3-4 months	completed	Subtask 4: Recurrent tumors were prevented
Milestone(s) Achieved: Measurement of PC3 cell cycle dynamics during tumor recurrence- with or without chemotherapy treatment		completed	Milestone(s) Achieved: See Fig. 1

ACCOMPLISHMENTS & GOALS (detailed):

Major activities in year 1:

- Generate PC3 prostate cancer cell lines containing two sets of fluorescent cell cycle reporters
- Verify correct cell cycle reporter expression and cell cycle behavior of cell lines by 3 approaches - flow cytometry, live cell imaging and expression of cell cycle phase molecular markers.
- Examine the cell cycle response of cells *in vitro* to signals thought to promote tumor dormancy in bone
- Examine the cell cycle response of cells *in vitro* to chemotherapeutic agents
- Confirm that cell cycle indicator cell lines form tumors in vivo and metastasize to bone

Major activities in year 2:

- Encountered unexpected challenge that cell cycle reporters in PC3 cells implanted in mice become silenced during timecourse experiments longer than 1 month to model tumor dormancy and recurrence.
- Attempted an CRISPR/Cas9-based strategy to target reporters to endogenous gene loci in PC3 and C4-2B cells

- Determined that cell cycle indicator cell lines that metastasize to bone vs. liver in the short term (less than 1 week) exhibit dramatically different cell cycle characteristics, suggesting signals from the bone are key to regulating PCa cell cycle and dormancy.
- Discovered using single cell tracking assays (described in year 1) that PCa cells *in vitro* undergo asymmetric cell divisions where one daughter enters quiescence while the other re-enters the cell cycle.
- Determined that signals from the marrow environment (Gas6 and GM-CSF) influence the frequency of asymmetric cell divisions and the proliferation vs. quiescence decision in PCa cells providing a possible mechanism for how the bone marrow environment may promote PCa dormancy.
- Performed transcriptome analysis on mouse bone marrow cells with dormant PCa DTCs vs. recurrent PCa to identify secreted host marrow signals that may promote dormancy in PCa cells.

Major activities in year 3:

- Performed in vivo experiments up to 1 week using DiI pre-labeling of cancer cells carrying cell cycle reporters to facilitate recovery.
- Followed up on our *in vitro* results on asymmetric division in PCa cells with an *in vivo* test. We found that similar to our *in vitro* study, treatment with GM-CSF increases the number of PCa cells in the bone and that these cells are poised to cycle in a G1 state.
- Completed a proteomic screen to identify cell surface markers that can be used via FACS to distinguish quiescent (G0) cancer cells from cycling (G1) cells to facilitate cell cycle analysis of recovered cells.
- Identified interactions with osteoclasts that promote PCa proliferation while interactions and signals from osteoblasts inhibit PCa proliferation and promote PCa survival.

Major activities in year 4 during No cost extension:

- Identified Her2 as a molecular marker of quiescent PCa cells. (Yumoto[a] et al., in preparation – see Appendix) **Fig.1**
- Drug-conjugated HER2 antibody (T-DM1) suppressed tumor formation in xenograft model. (Yumoto[a] et al., in preparation – see Appendix) **Fig.1**
- Demonstrated that anticancer polymers can target quiescent PCa cells and effectively kill such cells when combined with Docetaxel (Takahashi et al., *Scientific Reports* 2019, see Appendix) **Fig.1**
- Established that Transferrin (TF) levels induce PCa proliferation and are enhanced in bone marrow in the presence of PCa. This occurs through a positive feedback loop where PCa stimulates TF expression during macrophage to osteoclast differentiation. (Yumoto[b] et al., in preparation, see Appendix). **Fig.1**
- Discovered that quiescent PCa cells express high levels of Hippo/YAP pathway components (**Fig.2**) with YAP/TAZ inhibited by phosphorylation (**Fig 3**). We propose that poises quiescent cells to reactivate YAP/TAZ activity during tumor recurrence. We therefore tested whether inhibition of YAP by shRNA could prevent tumor recurrent in a xenograft model of PCa metastasis. In support of our hypothesis, inhibiting YAP as a regulator of quiescence prevented tumor recurrence in vivo (**Fig.4**).

Significant results and key outcomes

Over the 3 years of funding and no-cost extension period we have encountered unexpected challenges, but also made important discoveries regarding cell cycle status of PCa cells in the bone and the proliferation-quiescence decision in those cells. We have uncovered signals from osteoclasts and osetoblasts that regulate quiescence vs cell cycle entry in PCa. We have also identified the secreted signal Transferrin which may play a role in amplifying the switch between dormancy and proliferation in PCa. We have shown that quiescence in PCa cells increases survival and promotes chemoresistance, and that this state can be targeted using anti-cancer polymers. We have uncovered that PCa cells that initially metastasize to the bone exhibit dramatically different cell cycle characteristics than those that metastasize to the liver. Since the bone is a major site of PCa dormancy and recurrence, we hypothesize that signals from the bone marrow induce cell cycle changes to promote dormancy. Finally, we have discovered that the cell surface molecule Her2 – which is targeted in breast cancer, is a molecular marker for quiescent prostate cancer cells. Using a drug-conjugated HER2 antibody (T-DM1), we demonstrated that targeting cells expressing Her2 can be an effective treatment approach in a preclinical PCa xenograft model.

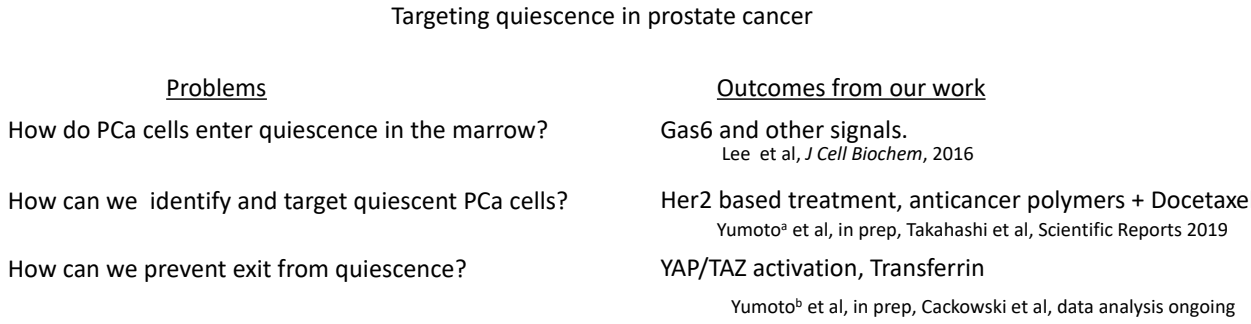

Fig.1. Overview of project questions and challenges with outcomes from the research. We have 2 published studies (most recent one from 2019 in the appendix), 2 manuscripts in preparation to be submitted (in the appendix) and one manuscript under revision for resubmission (in the appendix). We expect to prepare a manuscript on the Hippo/YAP pathway in PCa quiescence in early 2020.

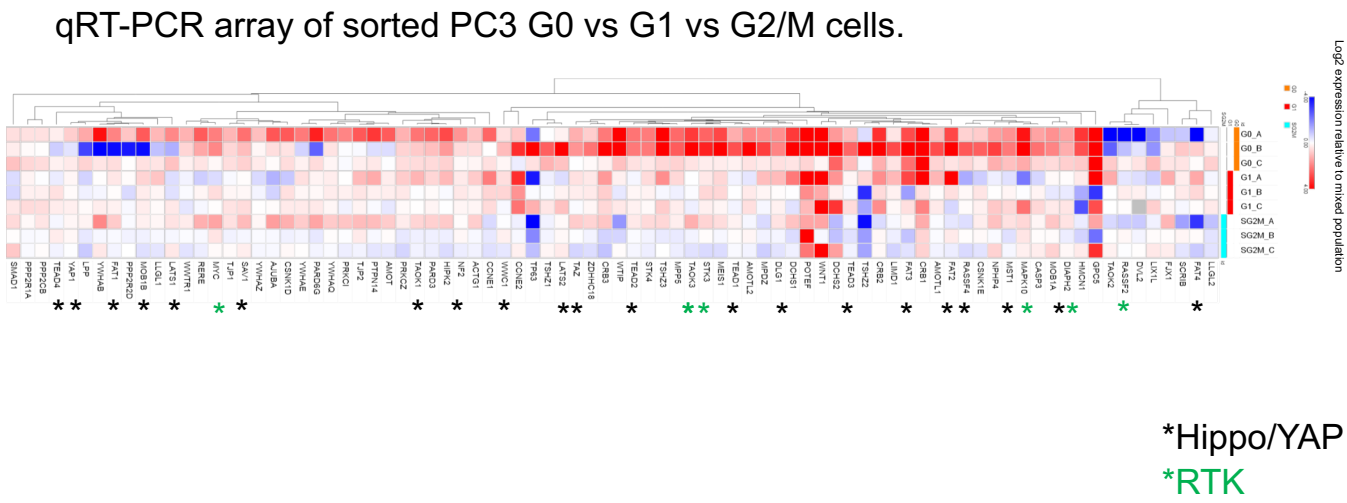

Fig.2. Components of Hippo/YAP and Her2/RTK signaling pathways are highly expressed in quiescent PCa cells.

YAP1 / TAZ Inactivating Phosphorylation Increased in G0

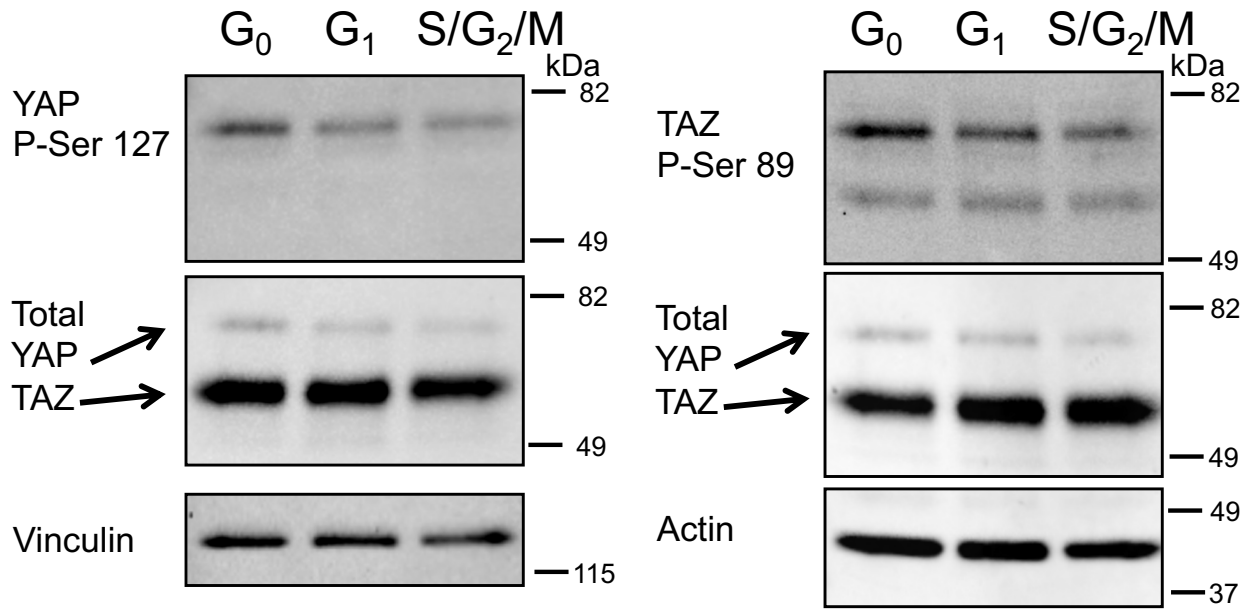

Fig.3. YAP1/TAZ are more abundant in G0, but are in a phosphorylated state which is inactive.

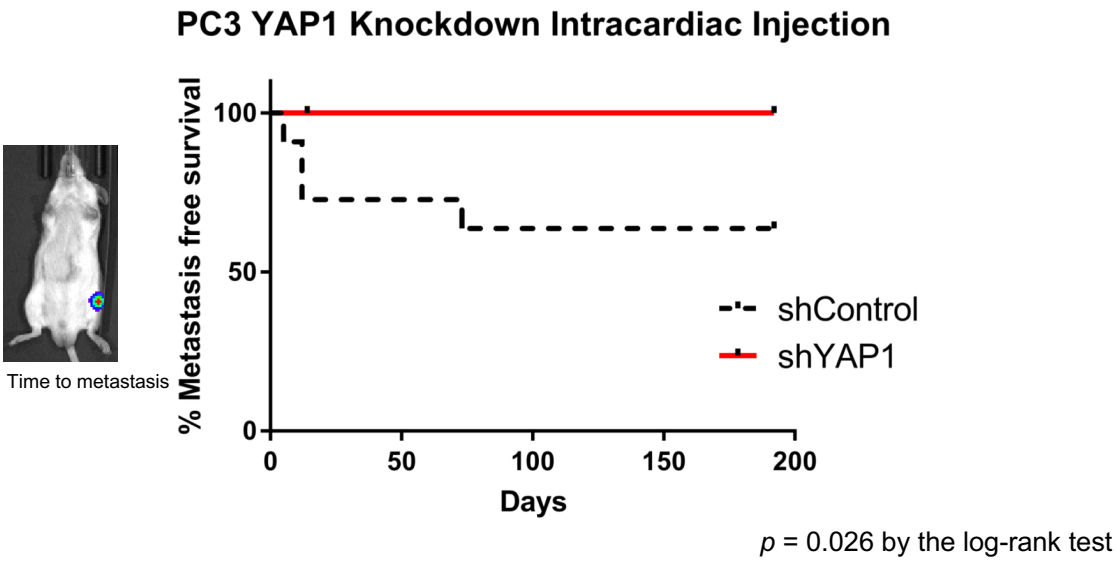

Fig.4. shRNA to YAP1 prevents tumor formation after i.c. injection of PCa cells. (n=11 per cohort).

Other achievements
We have continued to routinely verify that our cell lines are indeed PC3 by sequencing. We feel this is an important precaution, as recent work has emphasized the importance of independently verifying selected cell lines. We also routinely test for mycoplasma contamination and treat when necessary.

Stated goals not yet met: N/A final report

Opportunities for training and professional development.
This project has provided several opportunities for training and professional development as outlined below: *Professional development activities for Dr. Buttitta under PCRP award*: Dr. Buttitta attended the 2018 and 2017 Prostate Cancer Foundation Retreats. This was a great networking opportunity to meet others in the prostate cancer field (which she is relatively new to) and also to learn about the newest work in various realms of prostate cancer research. In addition the work described in year one on the single cell tracking and analysis platform was presented at the AACR 2017 meeting as a poster titled "A computational and statistical approach for interpreting real-time in-vitro gene reporter data"

Dr. Taichman continues to serve as an incredibly valuable co-mentor and facilitator for Dr. Buttitta's emerging work in the prostate cancer field. Dr. Buttitta was also promoted to Associate Professor with tenure at the University of Michigan during year 2 of this award.

- *Collaboration between the Buttitta and Taichman Labs*: This project has provided support and a platform for continued collaboration between the Buttitta and Taichman Labs. Dr. Buttitta's lab is relatively new to the prostate cancer field, while Dr. Taichman's group has extensive experience with models for prostate cancer metastasis and recurrence. The Taichman Lab has developed protocols and techniques that have been approved by the University of Michigan University Committee on the Use and Care of Animals (UCUCA), and students and postdocs working on this project, work in close collaboration with Dr. Taichman's lab members to learn these protocols. In turn, Dr. Buttitta's lab provides the expertise and protocols for the cell cycle studies and the live cell tracking methodology. As described in further detail below, we have had three young scientists, at varying levels of experience, co-mentored by both labs through this project and an additional graduate student and junior faculty has been added this year.

1. *Co-mentorship of undergraduate student Lulia Kana*: Lulia joined the Taichman lab in 2012 where she worked on a project looking at the effects of Gas6 signaling on PC3 cells in vitro. As the collaboration led to development of new tools such as the PC3-FUCCI cell line, Lulia transitioned to being co-mentored by both labs in 2014, resulting in her work being approximately 50% in each lab. Lulia was an excellent and productive student and is now a co-author on two shared publications with the Buttitta and Taichman Labs [1, 10]. Lulia has since graduated with her BS degree and is now in medical school.
2. *Co-mentorship of graduate PhD student Dan Sun*: Dan Sun joined the Buttitta Lab as a PhD student in 2011. After completion of her first project on cell cycle regulation in *Drosophila* in early 2014, she asked to transition to working on mammalian cancer cells, since her future research interests lie in the problem of tumor dormancy. Dan has worked closely with members of the Taichman Lab to learn techniques and helped to generate the cell lines for this project as well as learning FACS protocols, cell sorting etc. This award provided tuition and stipend support for Dan in 2015. Dan was an essential member of the team that developed the cell-tracking pipeline we use for the live image analysis of the cell cycle reporters. In July of 2016 Dan successfully defended her PhD thesis and she is now a postdoc studying cancer in Dr. Julio Aguirre-Ghiso's lab at Mt. Sinai.
3. *Co-mentorship of graduate student Ajai Pullianmackal*: Ajai joined the Buttitta lab in 2015. He has worked on our alternate strategies to deal with the challenges of the cell cycle reporters in PC3 cells. Ajai performed the single-cell experiments shown in the year 2 report and has learned flow cytometry and cell sorting with the assistance of the Taichman Lab. Ajai has contributed to experiments in this report for sorting G0 vs G1 PCa cells and extensively contributed data to our year 3 report. Ajai is a co-author on our manuscript under revision for Scientific Reports (Sun et al, in revision, see appendix).
4. *Co-mentorship of Postdoctoral Fellow Kenji Yumoto*: Dr. Kenji Yumoto, a senior postdoctoral fellow in the Taichman Lab, has contributed to the training of the students on this shared project and helped to

acquire the majority of the data presented here. This award has provided salary support for Dr. Yumoto since the summer of 2016. Dr. Yumoto has provided essential work on the FACS protocols for selecting cell lines, confirming the proper reporter behavior via FACS and use of the cell lines in the mouse model, as well as the studies of Gas6, Transferrin and contributed to studies of osteoclast effects on PCa cell cycle. Dr. Yumoto obtained about half of the data shown in this progress report and is a co-author on 4 manuscripts resulting from this project; in addition to two shared previous publications between the Buttitta and Taichman Labs [1, 2].

5. *Co-mentorship of Junior Faculty Dr. Frank Cackowski, MD PhD*: Dr. Cackowski is a Clinical Lecturer at University of Michigan working with patients and also performing research with Dr. Taichman's group. Dr. Cackowski is working to identify new molecular markers of DTCs has become an expert in working with the mouse xenograft model in the Taichman Lab to model dormancy and recurrence. Dr. Cackowski performed work shown in progress report for year 2 and is spearheading the project to study Hippo/YAP signaling in PCa dormancy. We expect to prepare a manuscript on this where Dr. Cackowski will be first author in 2020. In addition we have a previous co-publication between the Buttitta and Taichman labs with Dr. Cackowski as a first author related to detecting dormant PCa cells in patients [3].

- **How were the results disseminated to communities of interest?**

Dr. Buttitta attended the IMPaCT 2016 conference in Baltimore, MD where she presented a poster on this project to the prostate cancer research community. In addition Dr. Buttitta and collaborators presented a portion of this work as a poster at the 2017 AACR meeting. Dr. Yumoto presented this work at the University of Michigan Research day in a poster. Dr. Buttitta presented a portion of this work at the ASCB meeting cell cycle minisymposium in December 2017 and recently presented a portion of this work at the Prostate Cancer Foundation U.Michigan 2018 site visit. Dr. Buttitta also presented a portion of this work at the UM Rogel Cancer Center Cancer Biology/Genetics Lunch Meeting. Mr. Pulianmackal presented a portion of his work on this project in a poster at the American Society for Cell Biology (ASCB) Meeting in Dec. 2018.

In the past year, Dr. Cackowski presented a portion of the work on this project in five venues; 1. FC Cackowski LB, and Russell Taichman. Detecting, Isolating and Understanding Prostate Cancer Disseminated Tumor Cells. Invited Lecture; 2019; Indianapolis, IN; 2019. 2. Frank Cackowski, Laura Buttitta, and Russell Taichman. Detecting, Isolating and Understanding Prostate Cancer Disseminated Tumor Cells. Invited Lecture; 2019; Cleveland, OH; 2019. 3. Frank Cackowski, Laura Buttitta and Russell Taichman. Prostate Cancer Dormancy and Disseminated Tumor Cells. Invited Lecture; 2019; Portland, OR; 2019. 4. Frank Cackowski, Laura Buttitta, and Russell Taichman. Prostate Cancer Dormancy and Disseminated Tumor Cells. Invited Lecture; 2019; Wayne State University Detroit, MI; 2019 and 5. Frank Cackowski, Laura Buttitta and Russell Taichman. The Hippo Pathway in Prostate Cancer Recurrence and A New Immune Competent, Androgen Responsive Prostate Cancer Bone Metastasis Model. 2019; U.Michigan, Ann Arbor, MI; 2019.

References:

[1] Jung Y, Decker AM, Wang J, Lee E, Kana LA, Yumoto K, Cackowski FC, Rhee J, Carmeliet P, Buttitta L, Morgan TM, Taichman RS. "Endogenous GAS6 and Mer receptor signaling regulate prostate cancer stem cells in bone marrow." **Oncotarget**. 2016 May 3;7(18):25698-711. doi: 10.18632/oncotarget.8365.

[2] Lee E, Decker AM, Cackowski FC, Kana LA, Yumoto K, Jung Y, Wang J, Buttitta L, Morgan TM, Taichman RS. "Growth Arrest-Specific 6 (GAS6) Promotes Prostate Cancer Survival by G1 Arrest/S Phase Delay and Inhibition of Apoptosis During Chemotherapy in Bone Marrow." **J Cell Biochem**. 2016 Dec;117(12):2815-2824. doi: 10.1002/jcb.25582. Epub 2016 Sep 26.

[3] Cackowski FC, Wang Y, Decker JT, Sifuentes C, Weindorf S, Jung Y, Wang Y, Decker AM, Yumoto K, Szerlip N, Buttitta L, Pienta KJ, Morgan TM, Taichman RS. "Detection and isolation of disseminated tumor cells in bone marrow of patients with clinically localized prostate cancer." **Prostate**. 2019 Oct;79(14):1715-1727. doi: 10.1002/pros.23896. Epub 2019 Aug 26.

- **What do you plan to do during the next reporting period to accomplish the goals?**

N/A Final progress report

Technical challenges leading to changes in approach:

The SOW was revised and approved after year 2 (in Dec. 2017).

2. **IMPACT:**

- **Impact on the development of the principal discipline(s) of the project**

1. We are generated PC3 cell lines carrying cell cycle indicators that can be used to monitor cell cycle dynamics of cancer cells *in vitro* and *in vivo*. We expect this to be a useful tool for the scientific community and these cell lines have already been used in 4 published papers and two more currently in preparation.

2. We have also obtained results supporting the hypothesis that prostate cancer cells exposed to specific signals in the bone marrow alter their cell cycle dynamics. This is significant, as we have also shown that prostate cancer cells in G0 exhibit increased resistance to Docetaxel induced cell death. Our results suggest that prostate cancer metastasis to the bone and treatment with traditional chemotherapeutic agents such as Docetaxel likely leads to a relative increase in the fraction of cancer cells in a quiescent or G0 population which may seed recurrent tumors later.

3. We have demonstrated that the bone marrow environment has dramatic effects on the cell cycle state of PCa cells and we have identified candidate signaling pathways that may mediate these effects.

4. In a preclinical model we have demonstrated two effective ways to target quiescence in PCa; 1. with anticancer polymers and 2. By using Her2-antibody based therapies. We expect these results to have a high impact on the prostate cancer community.

- **What was the impact on other disciplines?**

The automated cell tracking method we have developed to monitor cell cycle reporters in PC3 cells can be applied to other cancer and non-cancer cell types. We expect this will be useful pipeline for other academic scientists using these cell cycle indicators in other cell types. We have a paper in revision for publication in *Scientific Reports* on this methodology. We expect our results on candidate signals from the bone marrow that promote cancer dormancy and recurrence to have impacts on the research of other cancers that also metastasize to the bone such as breast cancer. We expect Her2 may also be high on dormant or quiescent breast cancer cells and if our findings also translate to breast cancer this could have strong impacts on the breast cancer field.

- **What was the impact on technology transfer?**

Nothing to Report.

- **What was the impact on society beyond science and technology?**

Nothing to Report

3. **CHANGES/PROBLEMS:**

- **Actual or anticipated problems or delays and actions or plans to resolve them**

The challenges with using our cell cycle reporter cell lines in the xenograft model (described in detail in year 2 report) pushed back our expected timeline for major tasks 2 and 3. We therefore completed our experiments for major task 3 during the no cost extension period.

Changes that had a significant impact on expenditures

The delays in performing the *in vivo* metastasis assays with recovery from the bone marrow shifted a portion of our anticipated animal costs for period 1 to periods 2 and 3 and into the no cost extension period.

Significant changes in use or care of human subjects, vertebrate animals, biohazards, and/or select agents

- **Significant changes in use or care of human subjects**

None

- **Significant changes in use or care of vertebrate animals.**

None.

- **Significant changes in use of biohazards and/or select agents**

None

4. **PRODUCTS:**

- **Publications, conference papers, and presentations**.

Takahashi H, Yumoto K, Yasuhara K, Nadres ET, Kikuchi Y, Buttitta L, Taichman RS, Kuroda K. "Anticancer polymers designed for killing dormant prostate cancer cells." Sci Rep. 2019 Jan 31;9(1):1096. doi: 10.1038/s41598-018-36608-5.

- **Website(s) or other Internet site(s)**

Nothing to report

- **Technologies or techniques**

Nothing to report

- **Inventions, patent applications, and/or licenses**

Nothing to report

- **Other Products**

The automated cell tracking method we have developed to monitor cell cycle reporters in PC3 cells can be applied to other cancer and non-cancer cell types. We expect this will be useful pipeline for other academic scientists using these cell cycle indicators in other cell types. We have a paper in preparation on this methodology, which we expect to be published in the next year. Once this work is published we will make all customized software scripts available to academic not-for-profit researchers as described in our data sharing plan.

5. **PARTICIPANTS & OTHER COLLABORATING ORGANIZATIONS**

Name:	*Laura Buttitta*
Project Role:	*PI*
ORCID ID	0000-0002-5064-0650
Nearest person month worked:	2.0
Contribution to Project:	*Dr. Buttitta is the directing PI for this project and is involved in all aspects of project management, student and postdoc mentorship and writing for publications and reports under this award.*
Funding Support:	*Dr. Buttitta is supported by her nine-month appointment in the College of LS&A at University of Michigan as well as a Scholar Award from the American Cancer Society and a collaborative PCF grant with Dr. Taichman. Dr. Buttitta obtained an NIH R01 award during the no cost extension phase of this project.*

Name:	*Russell Taichman*
Project Role:	*Senior/Key Personnel*
ORCID ID	*0000-0002-7890-0020*
Nearest person month worked:	*0.2*
Contribution to Project:	*Dr. Taichman is a senior co-mentor for Dr. Buttitta and a collaborator for this project. He assists with co-mentorship of all working on this project and provides input and advice on project management and publications.*
Funding Support:	*3P01CA093900-06 (PI: Keller) (PI Project 3: Taichman)* *The Biology of Prostate Cancer Skeletal Metastases* *Project 3: Regulation of the PCa Metastatic Phenotype by the HSC Niche* *05/1/15-04/30/20 NIH/NCI* *Targeting quiescence in prostate cancer* *PI: L. Buttitta, Collaborator: Taichman* *CDMRP, W81XWH-15-1-0413* *8/28/2015-8/30/2018* *Sympathetic Nervous System Control of Disseminated Tumor Cell (DTCs) Dormancy* *PI: Taichman* *CDMRP/ DOD, PC140665 9/1/15-8/31/18* *Mechanisms of PCa Relapse in Marrow (new project)* *Prostate Cancer Foundation (Russell Taichman, PI)* *08/22/2016 – 08/22/2018* *Effort: 1.2 Cal.*
Name:	*Kenji Yumoto*
Project Role:	*Postdoctoral Fellow*
ORCID ID	*None*
Nearest person month worked:	*3*
Contribution to Project:	*Dr. Yumoto is the senior scientist on this project and peforms the majority of the experiments and helps to provide training for students working on this project. Dr. Yumoto also contributes to project management and writing of publications. Dr. Yumoto is an expert in the mouse xenograft model and using shRNA approaches.*
Funding Support:	*Dr. Yumoto is currently supported by this award*
Name:	*Dan Sun*
Project Role:	*Graduate Student Research Assistant*
ORCID ID	*None*
Nearest person month worked:	*4*

Contribution to Project:	*Dr. Sun completed her PhD in the Buttitta Lab in 2016 and worked on this project together with Dr. Yumoto.*
Funding Support:	*Dr. Sun was supported by this award as well as a Scholar Award (PI: Buttitta) from the American Cancer Society*
Name:	*Lulia Kana*
Project Role:	*Undergraduate research assistant*
ORCID ID	*None*
Nearest person month worked:	*2*
Contribution to Project:	*Ms Kana was an undergraduate co-mentored by the Taichman and Buttitta labs from 2013-2016. She worked for research credit and assisted Dr. Sun and Dr. Yumoto with experiments. She graduated in 2016.*
Funding Support:	*Ms. Kana's position was an unpaid position for research credit.*
Name:	*Frank Cackowski MD PhD*
Project Role:	*Clinical Lecturer and Research Associate*
ORCID ID	*None*
Nearest person month worked:	*0.2*
Contribution to Project:	*Dr. Cackowski is a new collaborator on this project and has worked with Dr. Yumoto on the in vivo bone metastasis assays*
Funding Support:	*Dr. Cackowski is supported by a collaborative PCF Challenge Grant on which he is a New Investigator*
Name:	*Ajai Pulianmackal*
Project Role:	*Graduate student Research Assistant*
ORCID ID	*None*
Nearest person month worked:	*1*
Contribution to Project:	*Mr. Pulianmackal has worked with Dr. Yumoto on optimizing the flow cytometry and single cell live imaging assays.*
Funding Support:	*Mr. Pulianmackal is supported by a Scholar Award (PI: Buttitta) from the American Cancer Society*

- **Has there been a change in the active other support of the PD/PI(s) or senior/key personnel since the last reporting period?**

New Funding for Dr. Buttitta (PI) since Sept. 2017:
Dr. Buttitta obtained an NIH R01 on an unrelated project studying cellular quiescence in *Drosophila* wings.

New Funding for Dr. Taichman (Senior/Key Personnel) since Sept. 2018:
None

6. **SPECIAL REPORTING REQUIREMENTS**

- **COLLABORATIVE AWARDS:** Not applicable
- **QUAD CHARTS:** Not applicable

7. **APPENDICES:**

Four manuscript files (pdf)

1. Sun et al in Revision 2019 (Manuscript under revision for resubmission to Scientific Reports)
2. Takahashi et al 2019 (Recent publication on anticancer polymers targeting quiescent PCa cells)
3. Yumoto et al A 2019 (Manuscript in preparation for submission on Her2 expression and targeting in PCa)
4. Yumoto et al B 2019 (Manuscript in preparation for submission on Transferrin expression and effects on quiescence in PCa)

ATCQ: A method for analysis of the proliferation-quiescence transition

Dan Sun [1*], Zhengda Li [2*], Ajai Pulianmackal[1], Kenji Yumoto[3], Russell Taichman[3] Qiong Yang [2+], Alexander T. Pearson [4+] and Laura Buttitta [1+]

1. Dept. of Molecular, Cellular and Developmental Biology, University of Michigan, Ann Arbor MI, 48109
2. Dept. of Biophysics, University of Michigan, Ann Arbor MI, 48109
3. Dept. of Periodontics and Oral Medicine, University of Michigan School of Dentistry, Ann Arbor, MI 48109
4. Division of Hematology/Oncology, Department of Internal Medicine, University of Michigan School of Medicine, Ann Arbor MI, 48109

Additional affiliations

*equal contribution
[+]authors for correspondence: qiongy@umich.edu, pearsona@med.umich.edu, buttitta@umich.edu

Abstract

The proliferation-quiescence decision is a dynamic process that remains incompletely understood. Live-cell imaging with fluorescent cell cycle sensors now allows us to visualize the dynamics of this cell cycle transition, and has revealed the proliferation-quiescence decision to be highly heterogeneous in culture. Here we describe an, automated cell-cycle state identification platform to monitor and quantify cell behaviors after mitosis at the proliferation-quiescence decision. Our approach involves treating cell populations as a cohort of individuals, where cell cycle phase changes serve as unbiased censored time-to-event information. This allows the application of survival statistical methods to analyze the proliferation-quiescence decision, analogous to a clinical trial for cells. To demonstrate the accuracy and sensitivity of this tool called Automated Temporal tracking of Cellular Quiescence (ATCQ), we monitored the proliferation-quiescence decision under various conditions to examine several features of this cell cycle decision point. First, we show that cells can enter into transient or prolonged quiescence after mitosis prior to the next cell cycle in the presence of abundant nutrients. Second, we show that under serum starvation, cells not only enter into a G0 quiescent state, but a fraction of cells also arrest in G1. Finally, we inhibit the PP2A complex, which normally promotes entry into quiescence and show that cells exclusively shorten the median G0 phase by approximately 14%, consistent with a role for PP2A in maintaining G0. Altogether our results show that states of cellular quiescence can be heterogeneous emphasizing a need to monitor the proliferation-quiescence decision in many cells over time. ATCQ is a sensitive and accurate tool for monitoring the dynamics of the proliferation-quiescence decision in cultured cells.

Introduction

Cycling cells tend to enter quiescence, a reversible, non-cycling state in response to contact inhibition, reduced levels of mitogens, or various stress conditions. Quiescent cells retain the ability to re-enter the cycle upon the addition of serum or under favorable conditions. However, recent studies in mammalian cells found that many cells enter a reversible G0-like state in cell culture even in the presence of mitogens and abundant nutrients[1] (additional refs, Meyer Yang Nature paper,Arora spencer paper, Barr nature comm 2017 paper). This suggests the proliferation-quiescence decision is constantly

regulated - even under optimal growth conditions. The relative percentage of cells that enter a temporary G0-like state after mitosis varies with cell type and culture conditions, suggesting many signaling inputs influence the proliferation-quiescence decision. This is also consistent with findings in several cancer cell lines, where some cells enter a temporary quiescent state while others do not[2]. This leads to heterogeneity in cell culture, with a subpopulation of cells entering and leaving temporary quiescent states of varying duration[3]. This proliferative heterogeneity is thought to be related to cancer therapeutic resistance[2].

The difficulties in monitoring the proliferation-quiescence decision and distinguishing G0 from G1 has limited our ability to learn how signals such as changes in oxygen supply, growth factors and interactions with the extracellular matrix impact quiescence entry on a single cell basis in a population. Most assays for cell cycling status use immunostaining of cell cycle phase markers or nucleotide analogue incorporation, both of which assess static conditions in fixed samples[4]. More recently, cell cycle reporters such as the FUCCI system (Fluorescent Ubiquitination-based Cell Cycle Indicator), have been used to track cell cycle dynamics live in individual cells[5] (additional refs – cook paper and refs therein). The FUCCI system and its derivatives are able to differentially label cells in G1, S and G_2/M phases, allowing us to visualize the G_1-M transition, however G0 cannot be distinguished from G1 in this approach.

Single-cell assays are essential for revealing heterogeneous behaviors that are mostly masked by single time point or population averaging (bulk) assays. However, time-lapse microscopy of hundreds or thousands of cells produces large amounts of data, which ranges from tedious to impossible for manual analysis. Cells also move over time, creating additional challenges for accurately tracking individual cells over longer timecourses. To facilitate the study of cell cycle dynamics, a single-plasmid system with semi-automated cell tracking named CycleTrak was developed. CycleTrak provides a fluorescent readout for G0/G1 and tracking of G2-M based on nuclear morphology using a constitutive histone-eGFP[6]. Although CycleTrak is able to detect the G_1-S phase transition, one major limitation is that the single G0/G1 cell marker is insufficient to distinguish quiescent G0 cells from cells in G1. Furthermore, the G0/G1 phase is marked by the fluorescence intensity from a single vector above a user designated threshold, a parameter which may vary from cell to cell in pooled populations or transient transfections, leading to inconsistent G0/G1 readouts in situations or cell types where clonal lines cannot be used.

Chittajallu *et al.* extended this approach by integrating two FUCCI reporters able to detect the G1-M transition and developed a workflow for automated *in vivo* 3-dimentional cell cycle profiling[7]. This system identifies cell-cycle state of each cell based on the image features extracted from a histone-CFP fusion protein and two cell cycle reporters. The constitutively expressed histone-CFP facilitates tracking cells throughout different cell cycle phases and provides an advantage for lineage tracing. The major drawback of this approach though is that the reporters are unable to distinguish cells in G0 from cells in G1. In addition the cell-cycle status identification relies on a supervised Random Forest classification, a machine learning method, which needs manual supervision prior to each cell line or experiment. Thus an approach that can distinguish G0 from G1 and automatically correct for variations in cell cycle reporter expression levels on a cell-by-cell basis would be advantageous for monitoring the mitosis - G1 cell cycle transition that encompasses the proliferation-quiescence decision.

In order to better understand the spatiotemporal patterns of the proliferation-quiescence decision in cells without artificial synchronization, we have taken advantage of cell cycle reporters that distinguish G0 from G1 in live imaging. A novel cell cycle indicator, mVenus-p27K$^-$, was generated to work in combination with the G0/G1 FUCCI reporter mCherry-hCdt1(30/120) (double check this in Oki paper and see if it contains PIP), to specifically label quiescent cells[8]. This probe is a fusion protein consisting of a fluorescent protein mVenus and a Cdk binding defective mutant of p27 (p27K-). p27 accumulates during quiescence, and is degraded by two ubiquitin ligases: the Kip1 ubiquitination-promoting complex (KPC) at the G0-G1 transition, and the SCF^{Skp2} complex at S/G2/M phases[9]. When used in combination with the G0/G1 FUCCI reporter, cells can be tracked from a few hours after mitosis until early S phase with distinct colors. This allows us to examine the dynamics of the proliferation-quiescence transition after mitosis on a single-cell level without artificial synchronization.

To quantitatively measure the cell cycle transitions after mitosis until S-phase entry, we developed a new, automated cell-cycle state identification platform to define, assign, and quantify cell cycle behaviors: Automated Temporal tracking of Cellular Quiescence (ATCQ). Here we show that ATCQ captures several recently discovered features of the proliferation-quiescence decision after mitosis and is sensitive enough to capture perturbations of as little as 14% of the time spent in G0 for cells within an asynchronous population.

Results

Validation of G0/G1 cell cycle indicators

To characterize the proliferation-quiescence transition at single-cell resolution in mouse 3T3 cells, we used the cell cycle indicator mVenus-p27K$^-$ combined with the G0/G1 reporter from the FUCCI cell cycle system, mCherry-hCdt1(30/120) to distinguish G0 cells from G1 cells (Fig. 1A). We first manually examined movies of asynchronously proliferating 3T3 cells stably expressing these reporters under full serum conditions to monitor reporter dynamics (Movie 1,2). With this combination of cell cycle reporters, mVenus-p27K$^-$ expression begins approximately 2-6h after cytokinesis is complete, followed by mCherry-hCdt1expression approximately 2-6h later. Many cells then exhibit a rapid reduction in mVenus-p27K$^-$ within approximately 3h, signaling G1 entry followed by mCherry-hCdt1 degradation at G1 exit (Fig. X). However for a fraction of cells we observed mVenus-p27K$^-$ and mCherry-hCdt1 to both continue to accumulate for up to 21h and beyond, signaling G0 entry[8] (Fig. X). This ordered progression of reporter expression from mVenus-p27K$^-$ positive to mVenus-p27K$^-$ and mCherry-hCdt1 double positive to mCherry-hCdt1 was invariant in the movies, although we did observe cell to cell variation in reporter expression intensity (Fig. X). Somehting about observing temp quiescence in full serum at a percentage that matches the spencer paper.

We also observed asynchronous decisions in pairs of daughters born from mitosis, where one cell would enter into G1 and degrade the mVenus-p27K$^-$ while the other daughter, born of the same mitosis would remain in G0 for an additional X-X hours (Fig. X). This type of asymmetric proliferation-quiescence decision after mitosis has been described (ref) although the source of the asymmetry remains unclear (purvis nature preview ref). Altogether our live imaging of asynchronous cells suggests this reporter combination can capture temporary states of quiescence as well as quiescence heterogeneity.

Through single-cell tracking of over 400 cells under normal conditions and serum starvation thus far, we have verified that: 1. G0-Venus always precedes G1-Cherry after mitosis 2. Cells that are double positive for more than 4h do not enter G1 for at least 12h and 3. G1-Cherry single positive cells enter S-phase within ~5hr. By using these reporters for cell sorting we have also verified that double-positive G0-Venus/G1-Cherry cells have low phospho-RB, low Cdk2 T-loop phosphorylation and high levels of the Cdk2 inhibitor p27, indicative of G0 (see Additional Experimental Detail). Using our cell tracking system, we have observed that under normal serum, un-crowded culture conditions 65% of 3T3 cells enter a double positive state consistent with quiescence, while under serum starvation for 24h this jumps to 80% and by 72h over 90% have become double positive. Our findings under normal growth conditions are roughly consistent with the 77% of $Cdk2^{low}$ 3T3 cells measured by Spencer et al., using a Cdk2 activity reporter. We therefore propose that our system provides a proliferation vs. quiescence readout resulting from the Cdk2 activity bifurcation.

(emphasize that it enriches by FACS) A distinct advtange of this reporter system over other sensors that are localization-based is the ability to enrich and sort for specific cell populations by FACS. To confirm that the mVenus-p27K$^-$ / mCherry-hCdt1 double positive population represents G0 phase with molecular markers, we performed either a short-term (24h,1%FBS) or a long-term (72h,1%FBS) serum starvation treatment, and monitored the accumulation of double positive cells by Fluorescence Activated Cell Sorting (FACS) (Fig. 1C,D). After 72h serum starvation, almost 90% cells are double positive (Fig. 1E), consistent with the previous study describing this reporter combination[8]. However we also noted that double positive cells accounted for almost 30% of the total cell population even when cells were cultured under normal, full nutrient conditions (Fig. 1B,E). A recent single-cell tracking study revealed a novel "G0-like" quiescent phase after mitosis in a fraction of cells under full nutrient conditions[1]. In our manual processing of movies we observed that under normal growth conditions, this reporter combination was possibly also capturing this temporary "G0-like" quiescence in a fraction of asynchronously proliferating cells.

To examine whether the mVenus-p27K$^-$ / mCherry-hCdt1 double positive population under full serum conditions represents a temporary G0 state, we examined G0 and G1 molecular markers in these cells. To do this, we sorted cells into mVenus-p27K$^-$/mCherry-hCdt1(30/120) double positive, mCherry-hCdt1 single positive and, mVenus-p27K$^-$/mCherry-hCdt1 double

negative populations and performed western blots for molecular markers of G0 vs. G1 phase. As a positive control for G0, cells cultured under serum deprivation were sorted in a similar manner. p130, one of the retinoblastoma family members, is abundant in quiescent cells and largely involved in the repression of gene expression in G0[10,11]. As cells enter G1, p130 is phosphorylated, and targeted for degradation[12]. We observed an enriched level of un/hypo-phosphorylated p130 in double positive G0 cells under serum starvation and full nutrient conditions compared to cycling cells or single positive cells in G1 (Fig. 1F). The Cdk inhibitor p27 also increases in G0 cells[13]. We observed an increase in endogenous p27 in the double positive G0 cells under serum starvation as well as double positive cells in full nutrient conditions compared to cycling cells or single positive cells in G1 (Fig. 1G). Finally, we examined a molecular marker of G1 entry, pCdk2^{T160}, the phosphorylation of the T-loop of the G1-S regulator Cdk2[14]. We observed an increase in Cdk2 T-loop phosphorylation in the mCherry-hCdt1 single positive G1 population compared to the mVenus-p27K$^-$/mCherry-hCdt1 double positive G0 populations under serum starvation and full serum conditions (Fig.1G). This suggests that the mVenus-p27K$^-$/mCherry-hCdt1 double positive cells under full serum conditions enter a temporary G0. This was further supported by cell sorting and peforming qRT-qPCR for transcripts previously shown to be upregulated in G0 cells (Sup. 1E)[8,15].

An automated cell tracking and analysis pipeline for live-cell imaging of the proliferation-quiescence decision

To monitor and quantitatively measure the dynamic transitions of cell cycle states—from cytokinesis to S phase entry, we developed the Automated Temporal Tracking of Quiescence (ATCQ) analysis platform that includes a computational framework for automated cell segmentation (identification of individual cells in an image), tracking, cell cycle state identification, and quantification from movies (Fig.2A). The cell segmentation and tracking allows us to record the fluorescent reporter intensity changes within individual cells in real-time imaging, without the aid of a constitutive nuclear marker. The single-cell fluorescence changes over time, in turn, are used to obtain cell cycle state identification (G0, G1, or early S phase) and quantification, which allows us to examine the kinetics of the proliferation-quiescence transition.

The single-cell trace of fluorescent reporters, mVenus-p27K$^-$ and mCherry-hCdt1, graphed by ATCQ is consistent with what we manually observed in movies (Fig.2B).

We used the temporal changes in the fluorescence intensity readings of both reporters to create a classification that automatically assigned cell cycle phases for single cells (Fig. 2). To quantitatively assess the relative change of two fluorescent reporters, we converted the relative change of the intensity readings from two adjacent time frames, t and t+1, into radian values (Fig. 2C). That is, the vector from time t to time t+1 on a plot of mCherry vs. mVenus fluorescence intensities is calculated into radian values over the range from –180° to 180°. A radial histogram of all recorded fluorescent vectors therefore appropriately reflects three primary clusters of cellular behaviors, corresponding to G0 entry, G0 exit or G1 entry, and G1 exit or early S entry (Fig. 2E). For example, a radian of -90° indicates cells exit G1 and enter into early S phase as mCherry signal decreases, while a radian of –180° indicates cells exit G0 and enter G1 as mVenus signal decreases while mCherry remains high.

This allows us to quantitatively visualize three distinct cell cycle behaviors at the proliferation-quiescence transition from the analysis of over 1,000 single-cell traces. The radial histogram exhibits the frequency and variability of three cell cycle behaviors in a population of asynchronously growing cells under normal, unperturbed conditions. The length of the bars depicts the frequency of individual cells with two fluorescent reporters exhibiting a specific behavior assigned to each radian. The clustering of cells into three distinct states is marked by the local minima of the frequency in radial histogram. Therefore, a given cell at any internal time is associated with state 1: G0, state 2: G1, or state 3: S phase. To facilitate the visualization of this, cells in G0 state are labeled in blue, while cells that exit G0 and progress into G1 phase are labeled in orange. When cells enter into S phase, they are labeled in grey (Fig. 2D-F).

To assess the accuracy of our approach, we generated a plot to show all the cell-level radian assignment values for temporally adjacent movie frames. In this plot, all the radian values defining cell state can be compared among all cells in any movie frame *t* and the next frame *t+1* (Fig. 2F). Each dot represents a single cell with the radian vectors drawn from adjacent time frames. Therefore, cells remaining in the same state within a time interval lie on the diagonal of the plot, while cells that transit between two states scatter above or below the diagonal. We considered cells to be correctly assigned if they either remained in their current state in the next

frame, or cycle forward in the next frame. Our approach had a very high correct assignment rate (Sup.2C), with 97-98% of frame intervals assigned with the correct cell-cycle transition order. This validates the feasibility of using ATCQ to investigate cell cycle dynamics. Furthermore, because ATCQ uses the relative changes in intensity of the two cell cycle reporters over time to assign a cell cycle state, correct assignments are not affected by cell to cell variation in fluorescence intensity.

Monitoring how serum deprivation and PP2A inhibition impact the proliferation-quiescence decision.

Single-cell, real-time imaging produces large amounts of data, which is advantageous when assessing heterogeneous cell dynamics in a population. In order to quantify the proliferation-quiescence decision with the large amount of imaging data, we used Kaplan-Meier (K-M) curves to estimate the time cells spent in a certain state (Fig. 3). The Kaplan-Meier estimator is a common statistical analysis tool to estimate clinical study survival functions that allows for individuals to be censored when they leave the study population[16]. For our application, we took an advantage of it to estimate the probability of individual cells remaining in each state as a function of time. In the K-M curve, each step-down means cells exit that certain state. To compare time-in-states between treatment conditions, the time each cell spends in each state is first recorded, as well as whether a transition to the next state was observed. If the completion of the state was not observed, that cell was censored. Censorship would occur for example, if a cell underwent apoptosis or if it moved out of the observation frame.

To test whether ATCQ is able to capture impacts of environmental stimuli on the proliferation-quiescence decision, we performed a serum starvation to promote G0 entry. As expected, cells under serum deprivation exhibit a significant difference in G0 (blue) but not early S phase (grey) (Fig. 3A-C). The increase in prolonged G0 upon serum starvation, is evident from the slower decline of the curve compared to the full serum conditions. However, cells also tended to have a longer G1 phase under serum starvation compared to full serum conditions. This result was initially unexpected, but may be consistent with a recent study showing that cells in G1phase can delay DNA replication in response to serum starvation[17]. ATCQ thus reveals

dynamics of the proliferation-quiescence decision consistent with single-cell studies of others, and will facilitate further studies of this transition under various environmental perturbations.

Previously, we revealed a role for PP2A complex in restricting Cdk2 activity after mitosis to modulate the proliferation-quiescence decision in tissue development[18]. We found that compromising PP2A activity caused 10% cells to fail to enter a developmentally regulated G0 state at the proper time. To examine whether PP2A affects G0 in cell culture, we performed a short-term (1h) treatment with the pan-PP2A inhibitor Okadaic Acid (OA) prior to imaging. As expected, analysis of the survival distributions showed that OA treatment results in a modest but statistically significant decrease in the median time in G0 (160 minutes vs. 140 minutes, $p < 0.001$). By contrast, no significant difference was observed for the time spent in the other two states (G1 and early S phase) (Fig.3D-F). Importantly the modest decrease observed in the G0 state is consistent with that expected if approximately 10% of cells are affected as previously shown[18,19]. This suggests that PP2A plays a role in promoting entry and maintenance of the G0 state in a fraction of cells and that ATCQ system can be sensitive enough to quantify the effects of perturbations that affect the proliferation-quiescence decision in a small fraction of cells.

Cells move less when they enter into prolonged quiescence

Monitoring the proliferation-quiescence decision via live-cell imaging provided us with an opportunity to characterize cellular behaviors at M-G1/G0 cell cycle transition. One quantifiable characteristic we obtained from ATCQ analysis is cellular movement. By comparing the euclidian distance between the center of individual nuclei at adjacent time frames, we could obtain information about cellular movement for cells assigned into different cell cycle states. Using linear regression analysis with repeated measurements (to account for multiple measurements on each cell), we found there was a significant effect of the time spent in G0 and the distance each cell moved. The longer cells stay in G0, the less they move, even under full serum conditions ($p < 0.0001$) (Fig. 4A). Interestingly, cells in G1 display a dynamic mobility pattern: at early timepoints into G1 cells tend to increase movement while later in G1, cell movement decreases. A peak in cell movement is observed around 3 hours after G1 entry (Fig. 4B). This suggests a window of G1 may be compatible with migration, as suggested by a recent study of migrating cells *in vivo*[20]. We next compared the movement of G0 and G1 cells under

serum starvation. Under limiting nutrients, both G0 and G1 cells moved less, consistent with longer cell cycle arrests leading to decreased movement (Fig. 4C,D). However G1 cells displayed greater heterogeneity than G0 cells, with a subpopulation of G1 cells exhibiting movement similar to that of G1 cells under full serum conditions and a fraction exhibiting reduced movement with prolonged G1 arrest, more similar to G0 cells. We then directly compared the movement of G0 cells under full serum and serum starved conditions and found that cells under prolonged G0 arrests (>20h) exhibited similar declines in cell movement, suggesting that the prolonged G0 observed in a fraction of cells under full nutrient conditions shared features with the G0 observed under serum starvation (Fig. 4E).

Discussion

Here, we present a sensitive, high-throughput method to quantitatively investigate the dynamics of the proliferation-quiescence decision at single-cell resolution in asynchronous cell culture populations. We show that this system can capture and quantify the transition after mitosis through G0 and G1, states that have been difficult to distinguish from each other. One major advantage in our approach is that the cell cycle readout is determined by the kinetics of nuclear-localized fluorescence signal changes, rather than by single-time-point signal localization or appearance. This makes this system robust and effective even when there is cell to cell variability in reporter expression levels. However one limitation of this approach is that we are unable to track multiple successive rounds of divisions due to the loss of fluorescent cell cycle markers for the S/G2/M phases. This issue could be remedied by incorporating a third constitutively nuclear fluorescent construct such as a histone-CFP. This would allow for tracking of cell lineages to determine whether cells that enter a temporary quiescence after mitosis also give rise to daughters more likely to enter temporary G0.

With ATCQ, we show that cells tend to spend longer time in both G0 and G1 states in response to serum deprivation. This suggests that either G0 or G1 cells could enter into a non-cycling state, and is consistent with recent work showing there to be two reversible windows for the proliferation-quiescence decision[17]. Furthermore we show that compromising PP2A function after mitosis, shortens the G0 phase in temporarily quiescent cells under full nutrient conditions. This adds a new regulator, in addition to p21, to this recently described phenomenon that

contributes to proliferative heterogeneity[1,3]. Further studies using ATCQ are likely to reveal additional players that also impact quiescence and contribute to the heterogeneous cell cycle behavior observed in many cell lines.

Several cancers contain heterogeneous populations with varying levels of proliferation[2,21,22]. Some studies suggest that quiescent tumor cells contribute to drug-resistance, by providing a population of non-cycling cells that survive cytotoxic chemotherapy[23,24]. Understanding the molecular basis of proliferative heterogeneity therefore may assist in developing better therapeutic approaches for cancer. Additionally, recent studies in cancer cells show that heterogeneous cells exhibit differential patterns in migration dynamics and invasive activity[21,25,26]. G0/G1 cancer cells in 3D Gelform histoculture displays invading activity exclusively and cancer cells cease movement upon entry into S/G2/M states. However in this study G0 vs G1 cells could not be distinguished[25]. Here, we show that 3T3 cells in G0 exhibit reduced movement the longer they are quiescent, while G1 cells move robustly upon entry into G1. This suggests that G1 cells may be the major contributors to the robust cell mobility observed in culture. In the future, ATCQ can be used to help us better understand the dynamics of cellular proliferation-quiescence decision under different physiological conditions or in various cancer models.

Materials and Methods

Cells and cell culture

The mouse embryonic fibroblast 3T3 cell line containing the G0 and G1 cell cycle reporters were kindly provided by Dr. Toshihiko Oki (University of Tokyo). These cells were grown in Dulbecco's modified Eagle's medium (DMEM; Gibco) supplemented with 10% fetal bovine serum (FBS) and 1% penicillin-streptomycin. Serum levels were reduced as indicated in the figures and text for serum starvation experiments.

Flow Cytometry analysis and FACS

For flow cytometry analysis of DNA content, cells were fixed with 4% paraformaldehyde, and then stained with the FxCycle Violet DNA Stain (Thermo Fisher, F10347). Resuspended cells were analyzed on an Attune flow cytometer using the violet laser for DNA measurements.

For cell sorting, cells were cultured in DMEM supplemented with either 10% FBS or 1%FBS for 24-72 hr, then subpopulations were sorted according to the intensity of their fluorescent reporters, mVenus-p27^{K-}(+)/mCherry-hCdt1(30/120)(+) NIH3T3 cells (G0) or mVenus-p27^{K-}(-)/mCherry-hCdt1(30/120)(+)NIH3T3 cells (G1) or mVenus-p27^{K-}(-)/mCherry-hCdt1(30/120)(-) NIH3T3 cells (S/G2/M), using a BD FACS Aria II system. Cells were sorted into SDS-PAGE loading buffer or TRIZOL for immediate protein extraction or RNA isolation. A minimum of ~10^5 cells were collected for each experiment.

Live-cell imaging

Cells were cultured at low density (to avoid contact inhibition) on 12-well plates in phenol red-free DMEM/10%FBS or 1%DMEM. Cells were imaged using an EVOS FL cell imaging system with a 20X objective lens or an IncuCyte Zoom at 37ºC , 5% CO_2. The imaging intervals were 20-30 minutes. For PP2A inhibition, cells were exposed to Okadaic Acid (OA) at 50nM or DMSO (control) for 30 minutes. Media containing OA or DMSO was then removed, and fresh complete medium was added. Cells were imaged one hour later.

Image processing & analysis

Individual cell identification (segmentation) and tracking were performed using a custom MATLAB program that automates these processes as described below. The program interface provides interactive adjustment of the parameters used at each step in the segmentation process, allowing the user to tailor the segmentation process to accommodate the characteristics of each image under analysis. Then, cell tracking is done with the Simple Tracker tool available on the MATLAB File Exchange. This tool uses the Hungarian algorithm to link cells from frame to frame into connected tracks using user-entered parameters for maximum movement distance allowed between frames and maximum gap in frames allowed between occurrences of the same

cell track. Cells were tracked for the entire time they were visible in the field of view. A subset of tracks were verified by hand, to be sure that one track represented the same cell for the duration of the track. The output of this software is an Excel file containing the identified cells, the frame number(s) in which they appear, the size, approximate radius, and cell center location in each frame, and the average and maximum intensity values in the cell on both the red and green channels in each frame, as well as the segmentation settings used to obtain these results.

Statistical analysis

Fluorescence Intensity smoothing:

Analysis was restricted to cells tracked over at least 3 video frames. The mCherry and mVenus fluorescence signals were smoothed using a nearest neighbor proportion localized polynomial approach. The localized polynomial nearest neighbor value parameter was chosen using an Akaike Information Criteria [27] based optimization with leave one out cross-validation. Calculations were performed using the Locfit package (2) in the software program R 3.0.1(R Core Team, 2014).

Transformation to survival time data:

For each cell, the cell cycle state over each pair of time points was assigned as described as before. For each cell, the aggregated time spent in each state was calculated. The event class for the last time point in each state was assigned as either “correct cycle” or “censored”. Cells that were not assigned to progress forward in the cell cycle were censored from the analysis.

Statistical calculations:

Associations between experimental time and overall fluorescence intensity were calculated via the Pearson’s correlation coefficient and associated test[28]. Survival curves were generated via the Kaplan-Meier method and compared using the log-rank test. Survival time statistics were calculated using the survival package in R 3.0.1 (https://github.com/therneau/survival). Repeated measures linear regression was performed using generalized least squares regression using the nlme package with individual cells as the within-factor level[29,30].

Western Blotting

Antibodies used: anti-mouse Rb2/p130 (BD Biosciences, 610261,1:1000), anti-mouse phospho-Cdk2^{T160} (Cell Signaling, 1:500), anti-mouse Cdk2(Santa Cruz, M2, 1:1000), anti-rabbit p27 (Cell Signaling, #2552, 1:1000) or anti-mouse GAPDH (Cell Signaling, 14C10, 1:2000) were used as loading controls with the appropriate HRP-conjugated secondary antibody. Enhanced Chemi-luminescence detection (Amersham) was performed and band signal intensity was quantified using NIH Image J.

RT-qPCR

For RT-qPCR, RNA was isolated from sorted cells per the TRIzol manual, resuspended in water, and then treated with TURBO™ DNase to remove contaminating DNA. Using 500ng of RNA per sample, cDNA was synthesized using oligo(dT)$_{20}$ and the Superscript III First-Strand Synthesis System (Invitrogen 18080051). qPCR using 0.5µL of cDNA per reaction was then performed using the 7500 Fast Real-Time PCR and StepOnePlus Real-Time PCR Systems (Applied Biosystems)

Primer sequences

Primer name	Sequence
Forward-GAPDH	ATGTGTCCGTCGTGGATCTGA
Reverse-GAPDH	TTGAAGTCGCAGGAGACAACCT
Forward-PCNA	TTTGAGGCACGCCTGATCC
Reverse-PCNA	GGAGACGTGAGACGAGTCCAT
Forward-Mki67	CCTTGGCTTAGGTTCACTGTCC
Reverse-Mki67	TGCAGAATCCAGATGATGGAGC
Forward-Geminin	GGGAGCCCAAGAGAATGTGAA
Reverse-Geminin	CAAGCCTTTTGGCAACTCATTT

Forward-SOD3	CCTTCTTGTTCTACGGCTTGC
Reverse-SOD3	GCGTGTCGCCTATCTTCTCAA
Forward-PDCD4	CCACTGACCCTGACAATTTAAGC
Reverse-PDCD4	TTTTCCGCAGTCGTCTTTTGG

Acknowledgements:

This work in the Buttitta Lab was supported by funding from the American Cancer Society (RSG-15-161-01-DDC) and the Dept. of Defense (W81XWH-15- 1-0413). Work in the Yang Lab is supported by the National Science Foundation (Early CAREER Grant #1553031) and the National Institutes of Health (MIRA #GM119688). Work in the Pearson lab is supported by the National Institutes of Health (K08-DE026500). We thank Dr. T. Oki for providing the Venus/Cherry labeled 3T3 cell line and Chris A. Edwards, manager of Microscopy & Image-analysis Laboratory (MIL) from University of Michigan for help with live-cell imaging. We thank Dr. Kenji Yumoto for help with cell sorting, Abbey Roelofs (U. Michigan LSA-IT) for help with improving the cell tracking and analysis program and the O'Shea lab for the use of their Incucyte. We thank "The Tribe" (ATCQ) for musical inspiration.

Figure 13. (A) Diagram of the fluorescence changes we observe with the G0-Venus/G1-Cherry reporters. Note the initial Venus-only state just after mitosis and the very brief double-positive window as cells enter into the next G1. (B) We sorted cells into the indicated phases based upon Venus/Cherry fluorescence. Western blot confirms the expected patterns for p27, phospho-RB and Cdk2 T-Loop phosphorylation. Note that with 3T3 cells, we always have two cross-reacting bands with the phospho-RB antibody just below the correct band. The correct pRB band is indicated by the red arrow. Cdk2 T-Loop phosphorylation is highest just before S-phase entry. (C-D) Still images from 3 movies including tracking from M-phase are provided showing 3 different patterns to quiescence entry after mitosis. Daughters from the same mitosis are indicated by black and white arrows. In C, the two daughters make “asymmetric decisions, one enters G1 while the other enters quiescence. In D, both daughters enter G1. In E both daughters enter quiescence.

Figure 14. (A) Example outputs of our cell-tracking system. Each cell is represented by a dot, which changes in color from blue to red over time, graphed according its to Venus/Cherry fluorescence. Three “behaviors” are observed over time, G0 Entry, G1 Entry and G1 Exit/S-phase entry. The percentages of the population exhibiting behaviors are shown. We find that even under normal full serum conditions, 65% of 3T3 cells enter G0. (B) Time spent in each phase transition under normal or serum starved conditions.

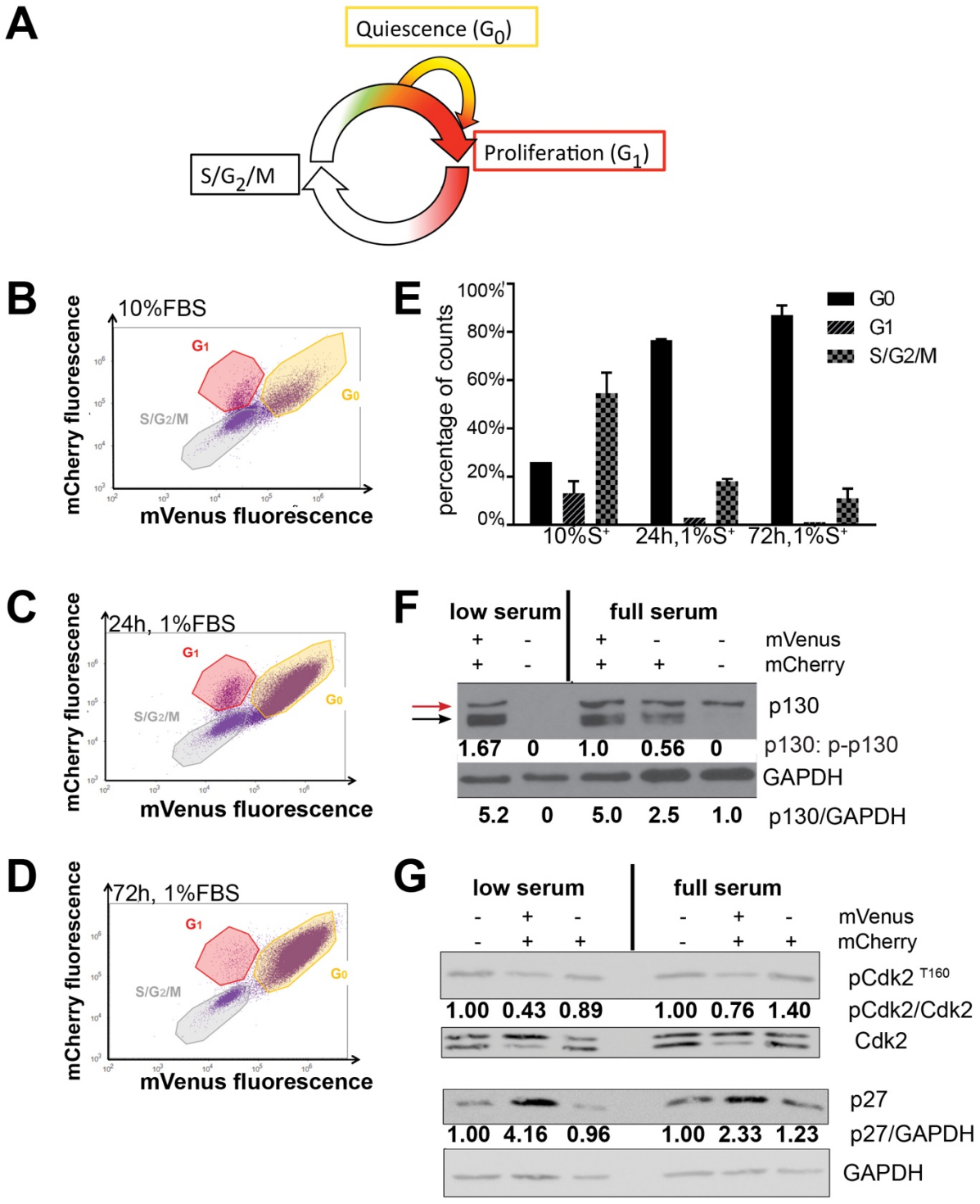

Figure. 1 G0 and G1 cell cycle indicators

(A) Diagram of the signal changes of the G0/G1 mVenus-p27K$^-$ (green) & mCherry-hCdt1(30/120) (red) cell cycle reporters. Cells in G0 are double positive (yellow) and cells in G1

are single positive (red). (B-D) The dot plots from flow cytometer analysis are generated from 3T3 cells expressing mVenus-p27K$^-$ and mCherry-hCdt1(30/120) probes, cultured with full 10% serum media (B), or low 1% serum media for 24hr (C) or 72hr (D). A sub-population of double positive cells increases as cells are treated with serum starvation. (E) Bar graph of flow cytometry analysis shows the composition of distinctively labeled cell sub-populations under different growth conditions. Western blot analysis is performed (F,G) using protein extracts from fluorescence-activated cell sorting of 3T3 under full or low serum conditions. (F) The western blot showed that a 2-fold increase in the ratio of un/hypo-phosphorylated to hyper-phosphorylated form p130 in double positive cells, compared to mCherry single positive cells under full serum condition. The un/hypo-phosphorylated form and hyper-phosphorylated form are indicated by the black and red arrows, respectively. (G) Cdk2 complex is a positive regulator in G1 phase, and the blots show the active form of Cdk2, phosphoCdk2^{T160} is enriched in mCherry-hCdt1(30/120) single positive cells compared to double positive cells. In contrast, the cyclin-dependent kinase inhibitor (CKI) protein, p27 is highly expressed in double positive cells.

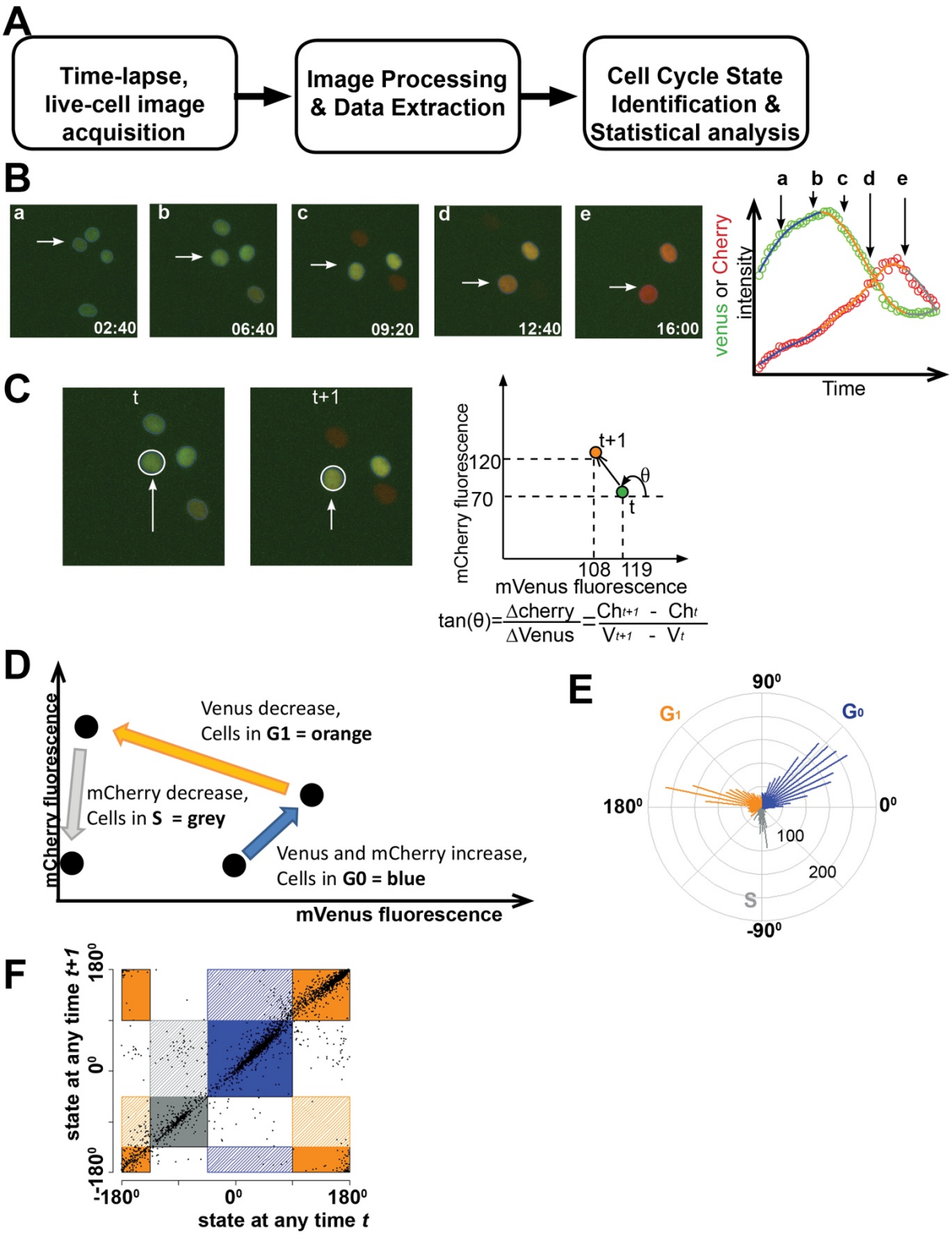

Figure. 2 ATCQ analysis displays three distinct states at the proliferation-quiescence decision under normal unperturbed conditions

(A) A workflow of the ATCQ system (B) (a-e) partitioning images from the single-cell tracking process. White arrow points out the same cell traced at different time points. Representative single-cell trajectory of two fluorescent probes in time-lapse, live-cell imaging. Each circle depicts one fluorescent intensity reading at a given time in either mVenus or mCherry channel. (C) Representative images show the same cells traced at two adjacent time frames. The calculation is generated to convert fluorescent intensity readouts to radial readings over time. (D) Three distinct cell cycle behaviors in order were observed from G0/G1 cell cycle reporter fluorescent intensity changes in asynchronously growing cells. When cells in state G_0, both mVenus reporter and mCherry accumulate together, colored in blue. Then cells transit into G_1 when mVenus fluorescent signal decreases while mCherry still keeps high, colored in orange. The third state is S phase entry, when mCherry signal decreases, colored in grey. (E) The radial histogram shows the conversion of the two fluorescent intensity readouts from each time frame to the radian readings over two adjacent time frames. The length of the spikes depicts the frequency of individual cells exhibiting a certain cell cycle behavior at a particular radian. The transition from one state to another is marked by the local minima of the frequency in radial histogram. (F) The dot plot shows all the cell-level, post-smoother radian assignment values for temporally adjacent movie frames. In this plot, all the radian values defining cell state can be compared among all cells in any movie frame t and the next frame $t+1$.

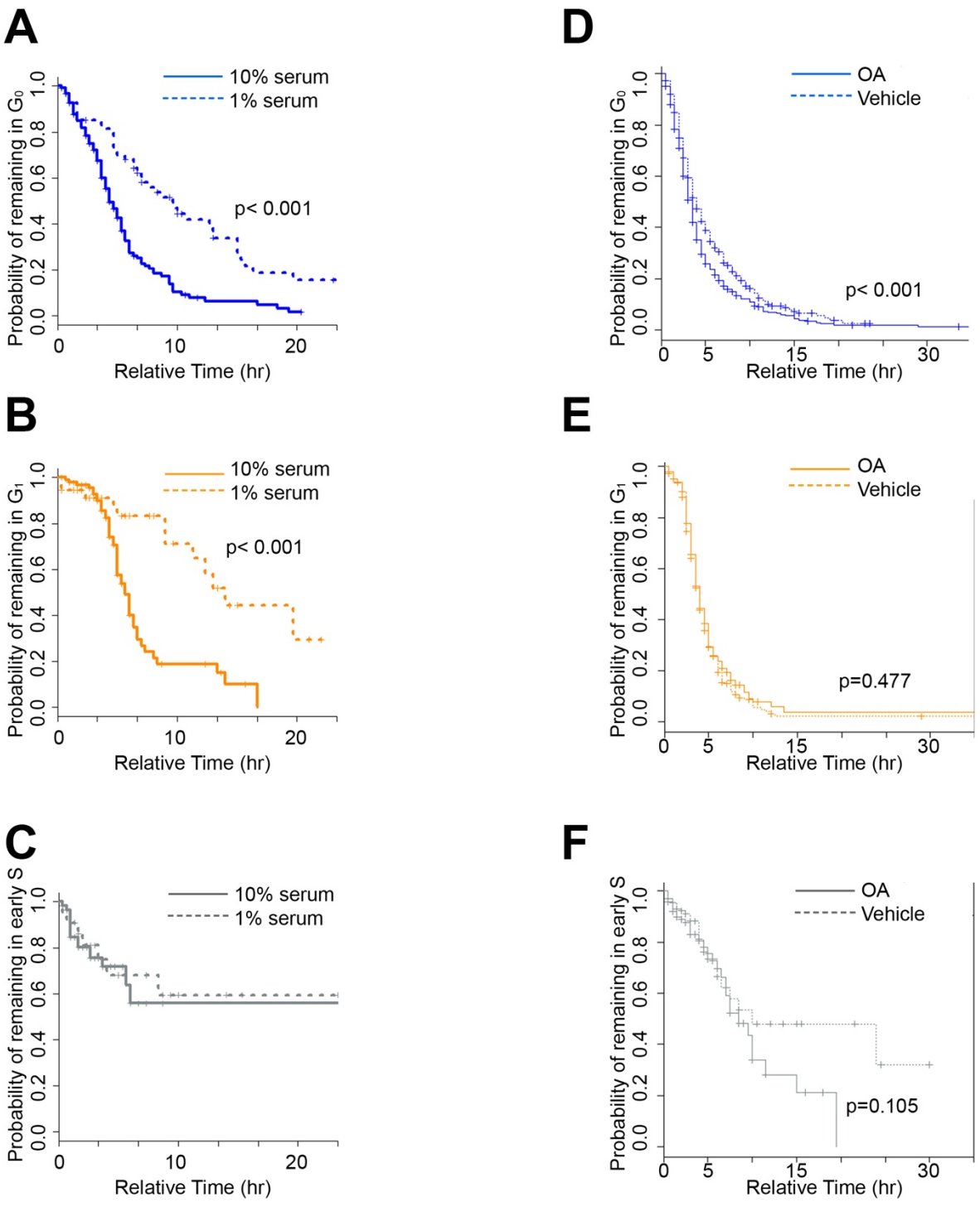

Figure. 3 Serum deprivation and PP2A impact the proliferation-quiescence transition. (A-C) The Kaplan-Meier curves of each state estimates the time cells remaining in each state under either full serum (10%) or low serum (1%) conditions. The analysis shows that cells tend to spend longer time in both G_0 and G_1 states in response to serum starvation (p value<0.001).

(D-F) 50nM Okadaic Acid (OA) is used to inhibit PP2A functions for 30min prior to live, time-lapse imaging. The Kaplan-Meier curves reflect that cells treated with OA tend to spend less time in G_0 than cells in vehicle treatment. There is statistically significant decrease in the probability of cells entering a prolonged G_0. The Kaplan-Meier curves also showed cells with OA treatment exhibit no significant difference in time spent in G_1 state (E) or early S phase entry (F).

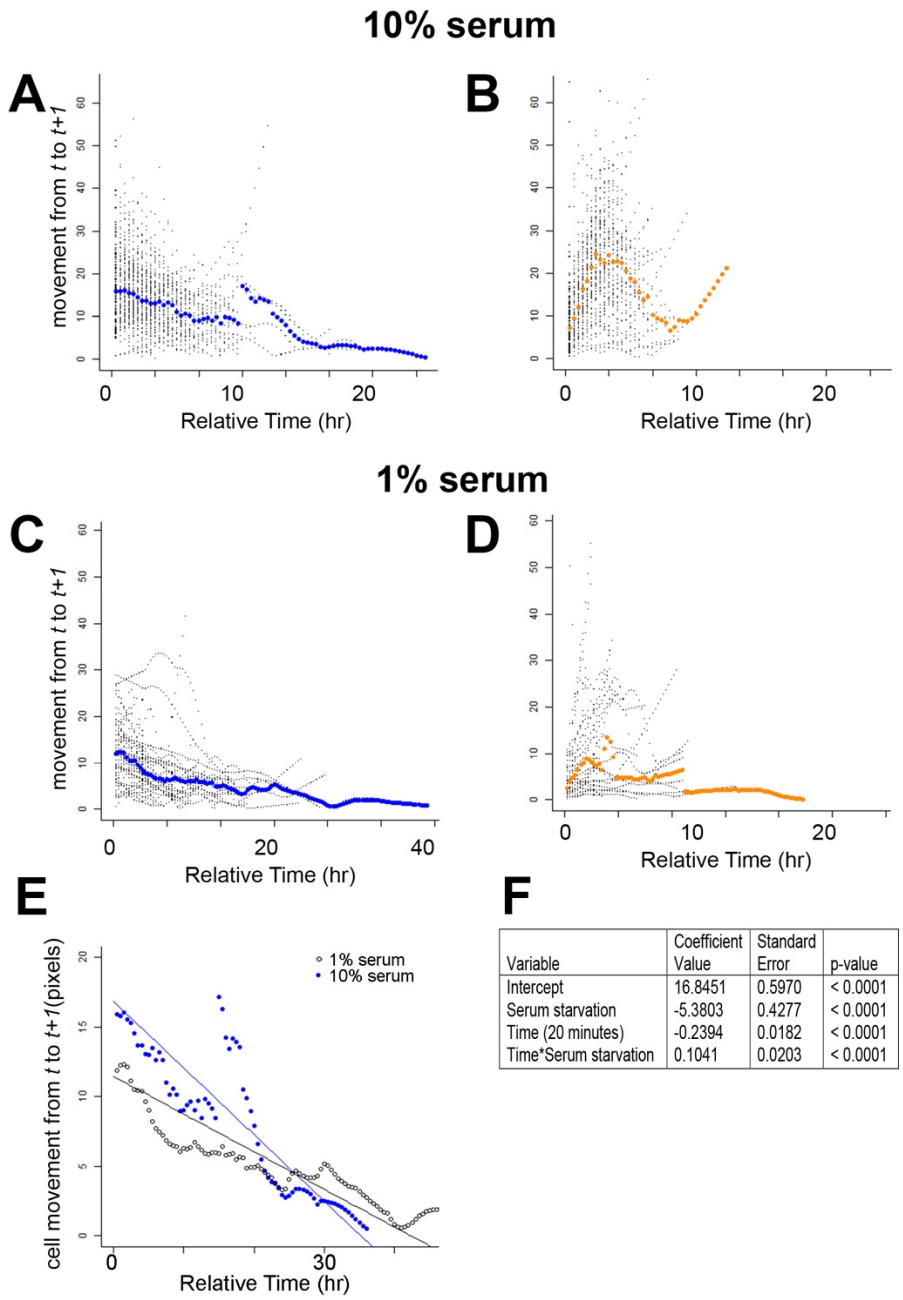

Variable	Coefficient Value	Standard Error	p-value
Intercept	16.8451	0.5970	< 0.0001
Serum starvation	-5.3803	0.4277	< 0.0001
Time (20 minutes)	-0.2394	0.0182	< 0.0001
Time*Serum starvation	0.1041	0.0203	< 0.0001

Figure 4. Cell movement decreases in prolonged G0.

Cells were grown in either 10% serum or 1%serum medium. The graphs show the distance (in pixels) cells traveled from adjacent time frames as cells stay in G0 (A,C) or the G1(B,D) state. A significant decrease in distance traveled is observed the longer cells remain in G0 ($p<0.001$). (E) The median values for the distance cells traveled as a function of time spent in G0. Blue dots indicate average values for cells cultured in full serum medium, and black empty circles indicate

average values for cells cultured under low serum conditions. Lines represent the predicted movement-by-time relationship generated from the repeated measures linear regression model, for full serum and serum starved cells, respectively. (F) Multivariate repeated measures linear regression reveals that both the amount of time spent in G0 and the presence of serum affect cell movement.

Supplemental Data

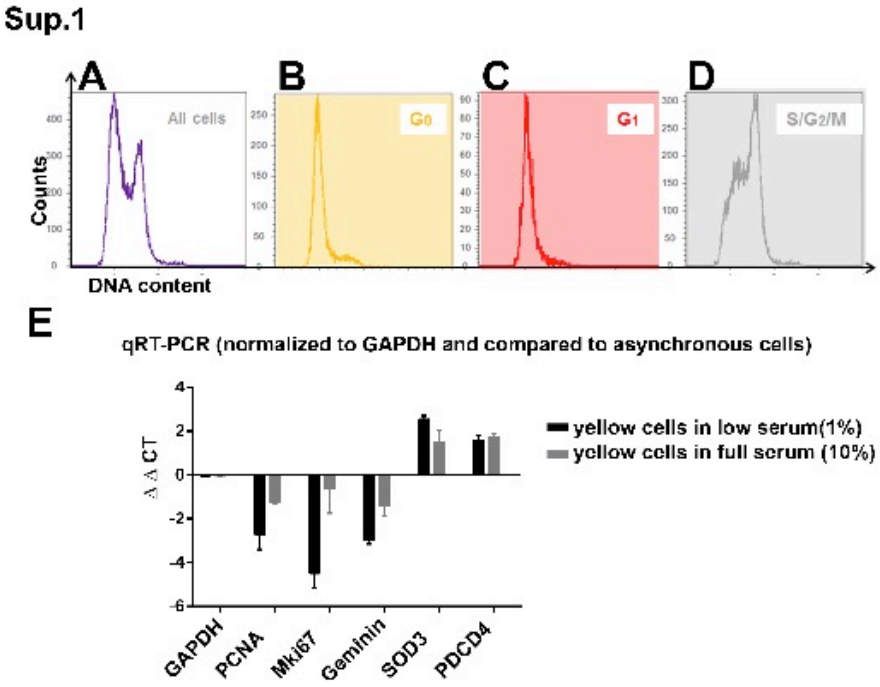

Supplement 1. Cell sorting by flow cytometry followed by RT-qPCR were used to validate additional G0 and G1 markers.

(A-D) Cell cycle profiles from sub-populations gated in Fig. 1D. Double positive cells with mVenus-p27K$^-$(+)/mCherry-hCdt1(30/120)(+) or single positive cells with mVenus-p27K$^-$(-)/mCherry-hCdt1(30/120)(+) labels contain 2C DNA content. On the contrary, majority of S/G2 cells with low mVenus-p27K$^-$ or mCherry-hCdt1(30/120) expression contain greater than 2C DNA content. (E) RT-qPCR shows that active cell cycle regulators are downregulated in mVenus-p27K$^-$(+)/mCherry-hCdt1(30/120)(+) yellow cells, whereas genes associated with G0 are enriched[8,15], compared to the gene expression level from mCherry-hCdt1(30/120) single positive cells. Δ CT = log2 of the fold difference from mCherry-hCdt1(30/120) single positive cell samples.

A

	Hazard ratio = 1.2		Hazard ratio = 1.5		Hazard ratio = 2	
α	β = 0.8	β = 0.9	β = 0.8	β = 0.9	β = 0.8	β = 0.9
0.05	526	707	110	148	40	53
0.01	786	1001	163	207	59	75
0.001	1148	1406	238	291	86	105

Assuming 90% of cells observed to correctly exit cycle of interest

B

	Hazard ratio = 1.2		Hazard ratio = 1.5		Hazard ratio = 2	
α	β = 0.8	β = 0.9	β = 0.8	β = 0.9	β = 0.8	β = 0.9
0.05	594	795	125	165	45	60
0.01	864	1126	183	223	66	84
0.001	1292	1581	257	327	97	118

Assuming 80% of cells observed to correctly exit cycle of interest

C

Growth Conditions	Error Rate	Treatment	Error Rate
Full Serum (10%FBS)	1.8%	Vehicle	1.5%
Low Serum (1%FBS)	1.1%	OA	2.5%

Supplement 2. (A-B) Power calculations and (C) error rates. The correct assignment rate is 1- the error rate, and here we find the majority cells (97-98%) are assigned the correct G0-G1-S/G2/M order.

Movie 1. 3T3 cells cultured in full serum media in a 30hr movie

Movie 2. 3T3 cells cultured in low serum media in a 30hr movie

References

1 Spencer, S. L. *et al.* The proliferation-quiescence decision is controlled by a bifurcation in CDK2 activity at mitotic exit. *Cell* **155**, 369-383, doi:S0092-8674(13)01143-4 [pii] 10.1016/j.cell.2013.08.062 (2013).

2 Dey-Guha, I. *et al.* Asymmetric cancer cell division regulated by AKT. *Proc Natl Acad Sci U S A* **108**, 12845-12850, doi:1109632108 [pii] 10.1073/pnas.1109632108 (2011).

3 Overton, K. W., Spencer, S. L., Noderer, W. L., Meyer, T. & Wang, C. L. Basal p21 controls population heterogeneity in cycling and quiescent cell cycle states. *Proc Natl Acad Sci U S A*, doi:1409797111 [pii] 10.1073/pnas.1409797111 (2014).

4 Matson, J. P. & Cook, J. G. Cell cycle proliferation decisions: the impact of single cell analyses. *FEBS J* **284**, 362-375, doi:10.1111/febs.13898 (2017).

5 Sakaue-Sawano, A. *et al.* Visualizing spatiotemporal dynamics of multicellular cell-cycle progression. *Cell* **132**, 487-498, doi:S0092-8674(08)00054-8 [pii] 10.1016/j.cell.2007.12.033 (2008).

6 Ridenour, D. A., McKinney, M. C., Bailey, C. M. & Kulesa, P. M. CycleTrak: a novel system for the semi-automated analysis of cell cycle dynamics. *Dev Biol* **365**, 189-195, doi:S0012-1606(12)00103-0 [pii] 10.1016/j.ydbio.2012.02.026 (2012).

7 Chittajallu, D. R. *et al.* In vivo cell-cycle profiling in xenograft tumors by quantitative intravital microscopy. *Nat Methods* **12**, 577-585, doi:10.1038/nmeth.3363 (2015).

8 Oki, T. *et al.* A novel cell-cycle-indicator, mVenus-p27K-, identifies quiescent cells and visualizes G0-G1 transition. *Sci Rep* **4**, 4012, doi:srep04012 [pii] 10.1038/srep04012 (2014).

9 Kamura, T. *et al.* Cytoplasmic ubiquitin ligase KPC regulates proteolysis of p27(Kip1) at G1 phase. *Nat Cell Biol* **6**, 1229-1235, doi:ncb1194 [pii] 10.1038/ncb1194 (2004).

10 Litovchick, L. *et al.* Evolutionarily conserved multisubunit RBL2/p130 and E2F4 protein complex represses human cell cycle-dependent genes in quiescence. *Mol Cell* **26**, 539-551, doi:10.1016/j.molcel.2007.04.015 (2007).

11 Smith, E. J., Leone, G., DeGregori, J., Jakoi, L. & Nevins, J. R. The accumulation of an E2F-p130 transcriptional repressor distinguishes a G0 cell state from a G1 cell state. *Molecular and cellular biology* **16**, 6965-6976 (1996).

12 Tedesco, D., Lukas, J. & Reed, S. I. The pRb-related protein p130 is regulated by phosphorylation-dependent proteolysis via the protein-ubiquitin ligase SCF(Skp2). *Genes Dev* **16**, 2946-2957, doi:10.1101/gad.1011202 (2002).

13 Sherr, C. J. & Roberts, J. M. CDK inhibitors: positive and negative regulators of G1-phase progression. *Genes Dev* **13**, 1501-1512 (1999).

14 Jeffrey, P. D. *et al.* Mechanism of CDK activation revealed by the structure of a cyclinA-CDK2 complex. *Nature* **376**, 313-320, doi:10.1038/376313a0 (1995).

15 Coller, H. A., Sang, L. & Roberts, J. M. A new description of cellular quiescence. *PLoS Biol* **4**, e83, doi:04-PLBI-RA-0946R4 [pii] 10.1371/journal.pbio.0040083 (2006).

16 Kaplan, E. L. & Meier, P. Nonparametric-Estimation from Incomplete Observations. *J Am Stat Assoc* **53**, 457-481, doi:Doi 10.2307/2281868 (1958).

17 Cappell, S. D., Chung, M., Jaimovich, A., Spencer, S. L. & Meyer, T. Irreversible APC(Cdh1) Inactivation Underlies the Point of No Return for Cell-Cycle Entry. *Cell* **166**, 167-180, doi:10.1016/j.cell.2016.05.077 (2016).

18 Sun, D. & Buttitta, L. Protein phosphatase 2A promotes the transition to G0 during terminal differentiation in Drosophila. *Development* **142**, 3033-3045, doi:10.1242/dev.120824 (2015).

19 Naetar, N. *et al.* PP2A-Mediated Regulation of Ras Signaling in G2 Is Essential for Stable Quiescence and Normal G1 Length. *Mol Cell* **54**, 932-945, doi:S1097-2765(14)00357-8 [pii] 10.1016/j.molcel.2014.04.023 (2014).

20 Matus, D. Q. *et al.* Invasive Cell Fate Requires G1 Cell-Cycle Arrest and Histone Deacetylase-Mediated Changes in Gene Expression. *Dev Cell* **35**, 162-174, doi:10.1016/j.devcel.2015.10.002 (2015).

21 Haass, N. K. *et al.* Real-time cell cycle imaging during melanoma growth, invasion, and drug response. *Pigment Cell Melanoma Res* **27**, 764-776, doi:10.1111/pcmr.12274 (2014).

22 Pyaskovskaya, O. N., Kolesnik, D. L., Kolobov, A. V., Vovyanko, S. I. & Solyanik, G. I. Analysis of growth kinetics and proliferative heterogeneity of Lewis lung carcinoma cells growing as unfed culture. *Exp Oncol* **30**, 269-275 (2008).

23 Yano, S. *et al.* Spatial-temporal FUCCI imaging of each cell in a tumor demonstrates locational dependence of cell cycle dynamics and chemoresponsiveness. *Cell Cycle* **13**, 2110-2119, doi:29156 [pii] 10.4161/cc.29156 (2014).

24 Doherty, M. R., Smigiel, J. M., Junk, D. J. & Jackson, M. W. Cancer Stem Cell Plasticity Drives Therapeutic Resistance. *Cancers (Basel)* **8**, doi:10.3390/cancers8010008 (2016).

25 Yano, S. *et al.* Invading cancer cells are predominantly in G0/G1 resulting in chemoresistance demonstrated by real-time FUCCI imaging. *Cell Cycle* **13**, 953-960, doi:27818 [pii] 10.4161/cc.27818 (2014).

26 Yano, S. *et al.* Cell-cycle-dependent drug-resistant quiescent cancer cells induce tumor angiogenesis after chemotherapy as visualized by real-time FUCCI imaging. *Cell Cycle* **16**, 406-414, doi:10.1080/15384101.2016.1220461 (2017).

27 Akaike, H. A new look at the statistical model identification. *IEEE Transactions on Automatic Control* **19**, 716-723, doi:10.1109/tac.1974.1100705 (1974).

28 Tukey, J. W. Comparing Individual Means in the Analysis of Variance. *Biometrics* **5**, 99-114, doi:Doi 10.2307/3001913 (1949).

29 Cox, D. R. Regression Models and Life-Tables. *Journal of the Royal Statistical Society. Series B (Methodological)* **34**, 187-220 (1972).

30 Pinheiro, J., Bates, D., DebRoy, S., Sarkar, D. & Team}, R. C. in https://CRAN.R-project.org/package=nlme Vol. R package version 3.1-131 (2017).

SCIENTIFIC REPORTS

Corrected: Author Correction

OPEN

Anticancer polymers designed for killing dormant prostate cancer cells

Received: 9 January 2018
Accepted: 23 November 2018
Published online: 31 January 2019

Haruko Takahashi[1,2], Kenji Yumoto[3], Kazuma Yasuhara[4], Enrico T. Nadres[1], Yutaka Kikuchi[2], Laura Buttitta[5], Russell S. Taichman[3] & Kenichi Kuroda[1]

The discovery of anticancer therapeutics effective in eliminating dormant cells is a significant challenge in cancer biology. Here, we describe new synthetic polymer-based anticancer agents that mimic the mode of action of anticancer peptides. These anticancer polymers developed here are designed to capture the cationic, amphiphilic traits of anticancer peptides. The anticancer polymers are designed to target anionic lipids exposed on the cancer cell surfaces and act by disrupting the cancer cell membranes. Because the polymer mechanism is not dependent on cell proliferation, we hypothesized that the polymers were active against dormant cancer cells. The polymers exhibited cytotoxicity to proliferating prostate cancer. Importantly, the polymer killed dormant prostate cancer cells that were resistant to docetaxel. This study demonstrates a new approach to discover novel anticancer therapeutics.

The design and development of molecules effective in eliminating dormant cancer cells remain a significant challenge in drug discovery. Dormant cancer cells are not proliferating but are largely resistant to conventional chemotherapies which target only rapidly proliferating cells, leading to recurrence and metastasis[1,2]. The design of drugs which are able to target dormant cancer cells must meet at least two conditions: (i) the target mechanism/pathway and molecular target in cancer cells are not dependent on cell proliferation, and (ii) the molecular target must be distinctive from normal cells for selectivity. To that end, we hypothesize that cell membranes would serve as an anticancer target in dormant cancer cells to meet these requirements. Specifically, physically compromising the barrier function of cell membrane would be lethal, but not necessarily be dependent on the stages of cell cycle. For the second requirement, cancer cells overexpress phosphatidylserine (PS) on their cell membrane surfaces relative to normal cells, which could provide a cancer selective binding target[3,4]. Therefore, designer molecules capable of binding to PS lipids and disrupting cell membranes may effectively kill dormant cancer cells.

In this study, we report the design of new class of anticancer polymers that are effective in killing dormant prostate cancer (PCa) cells. The design is inspired by membrane-active host-defense peptides with anticancer activity[5–7]. This class of peptides, which we denote as anticancer peptides (ACPs), are relatively small (2,000–5,000 Da) and adopt cationic amphiphilic α-helical structures. Cationic ACPs selectively bind to PS lipid-rich anionic cancer cell membranes preferentially to normal cells by electrostatic interactions. The bound ACPs insert the hydrophobic domain of their helix into the membranes, which causes membrane disruption, leakage of cellular components, and ultimately cancer cell death. The anticancer polymers used here are low molecular weight methacrylate copolymers with random-sequences of binary monomer compositions consisting of cationic and hydrophobic side chains, serving as a model platform to test our approach. We hypothesize that the ACP-mimetic polymers are selective to PCa cells and kill dormant PCa cells resistant to conventional anticancer drugs. Synthetic polymer platforms are more resistant to proteolytic degradation in physiological environments and are more chemically tunable for activity modulation than peptides. The anticancer activity of natural and

[1]Department of Biologic and Materials Sciences, School of Dentistry, University of Michigan, Ann Arbor, MI, 48109, USA. [2]Department of Biological Science, Graduate School of Science, Hiroshima University, 1-3-1 Kagamiyama, Higashi-hiroshima, Hiroshima, 739–8526, Japan. [3]Department of Periodontics & Oral Medicine, School of Dentistry, University of Michigan, Ann Arbor, MI, 48109, USA. [4]Division of Materials Science, Graduate School of Science and Technology, Nara Institute of Science and Technology, Ikoma, Nara, 630–0192, Japan. [5]Molecular, Cellular and Developmental Biology, University of Michigan, Ann Arbor, MI, 48109, USA. Haruko Takahashi and Kenji Yumoto contributed equally. Correspondence and requests for materials should be addressed to R.S.T. (email: rtaich@umich.edu) or K.K. (email: kkuroda@umich.edu)

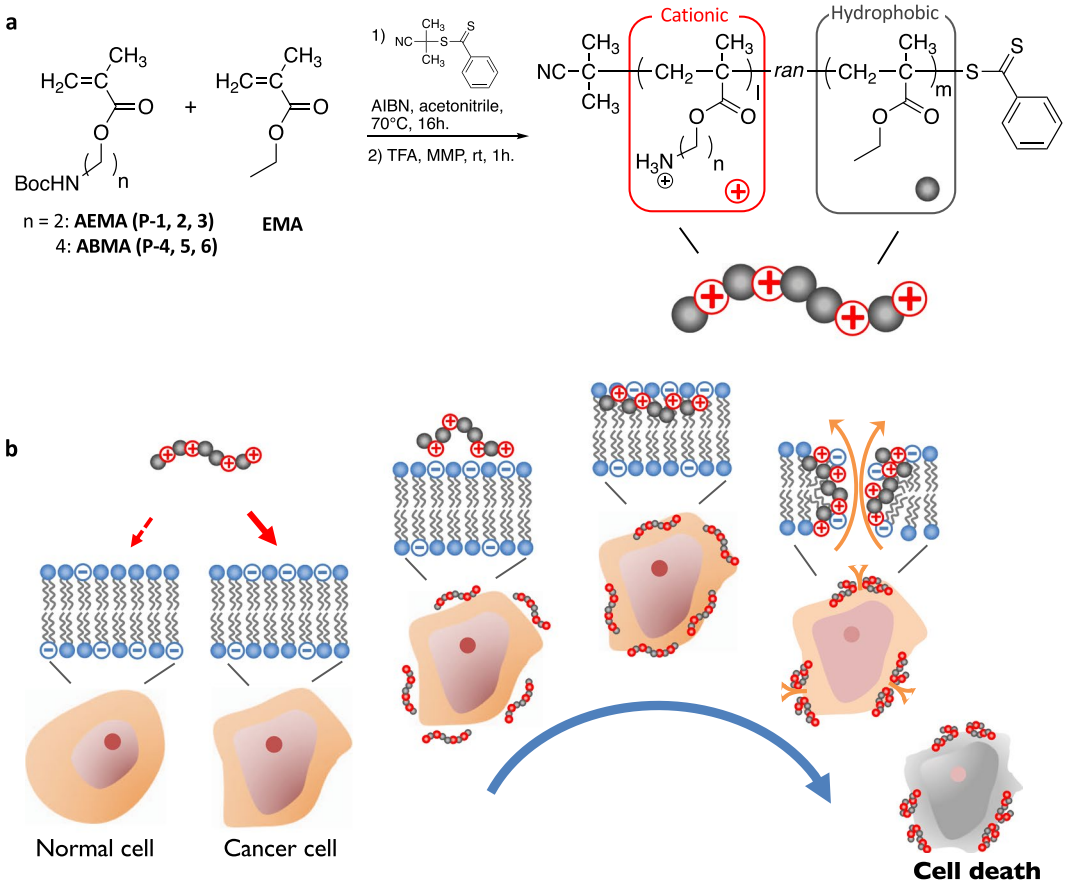

Figure 1. Synthesis and proposed mechanisms of anticancer copolymers. (**a**) Synthesis of methacrylate random copolymers with cationic and hydrophobic side chains. The polymers with low molecular weights (~2,000 g/mol.) and narrow molecular weight distribution were prepared by RAFT controlled radical polymerization. The composition of hydrophobic monomer EMA was varied. (**b**) The proposed anticancer mechanism of polymers.

synthetic cationic polymers has been previously examined and were shown to induce apoptosis in cancer cells[8,9]. However, the molecular mechanism is not clear, and thus it is difficult to control the activity by design or develop structure-activity relationships. In addition, many synthetic polymers used in anticancer therapeutics are simply drug delivery carriers in the forms of drug conjugates or drug-encapsulated particles where the anticancer activity originates primarily from the drugs, not the polymers[10–12]. Recently, Yang and Hedrick demonstrated cationic polymer assemblies with anticancer activity by lysing cancer cell membranes[13]. The membrane-targeting mechanism would be a new strategy to treat drug-resistant cancer cells.

Results and Discussion

Polymer design and synthesis. Learning from ACPs, our first hypothesis is that the cationic and hydrophobic properties of ACPs are the essential functionalities, but also the minimum requirements that govern their membrane-targeting anticancer activity and cancer cell-selectivity. To test the design hypothesis, we prepared methacrylate random copolymers consisting of cationic and hydrophobic side chains (Figs 1a and S1). To identify the optimal compositions, a series of cationic amphiphilic random copolymers were synthesized (Tables 1 and S1). The primary ammonium group was chosen to mimic the cationic lysine side chains of ACPs, which should bind to the anionic PS lipids by electrostatic interaction, imparting selectivity to cancer cells over human cells (Fig. 1b). The ethyl side chains of ethyl methacrylate (EMA) monomers serve as the hydrophobic groups for insertion into the cell membranes, causing membrane disruption. The molecular weights of polymers are 2,000 to 3,000 g/mol., in a similar range to the molecular size of ACPs[5], and the molecular weight distributions of the polymers are relatively narrow (dispersity $Đ = 1.1–1.3$) (Table 1). The polymers are highly soluble in both water and cell culture media.

Cytotoxicity against proliferating prostate cancer cells vs. normal cells. To test our design approach, the copolymers were first examined for their *in vitro* cytotoxicity to proliferating cancer cells. We selected three established metastatic PCa cell lines C4-2B, DU145, and PC-3 which are associated with bone tropism and brain metastasis (C4-2B and DU145) and bone metastasis (PC-3)[14]. The copolymers caused concentration-dependent cytotoxicity in these PCa cells and exhibited 100% killing in the culture at high polymer concentrations (Figs 2a and S2). The EC_{50} value, the concentration of copolymers that gives half-maximal

Polymer	Composition	DP[a]	M_n[b] (NMR) (g/mol.)	M_n[c] (GPC) (g/mol.)	M_w[c] (GPC) (g/mol.)	M_w/M_n[c]
P-1	AEMA100 - EMA0	15	2,200	2400	2700	1.15
P-2	AEMA72 - EMA28	13	1,800	1800	2000	1.13
P-3	AEMA60 - EMA40	13	1,800	1700	1900	1.10
P-4	ABMA100 - EMA0	14	2,400	2200	2900	1.32
P-5	ABMA69 - EMA31	16	2,500	2800	3100	1.12
P-6	ABMA52 - EMA48	17	2,500	2100	2400	1.12

Table 1. Characterization of anticancer peptide-mimetic copolymers. [a]The degree of polymerization was calculated by comparing the integrated areas of signals from the side chains to that from the phenyl group (RAFT agent) at the polymer end. [b]The number average molecular weight (M_n) was calculated from the degree of polymerization (DP), and molecular weights of monomers and chain transfer agent. The molecular weight of trifluoroacetate was excluded in M_n in order to compare the size of copolymers to that of ACPs. [c]M_n and M_w were determined using GPC for boc-protected polymers.

reduction in cell viability, decreased significantly for the first 4-hour incubation with **P-5** (Figs 2b and S3 for dose-cell viability curves), but leveled off for longer incubation times. This indicates that the copolymers act relatively quickly, in contrast to docetaxel that generally needs several days to be effective *in vitro*. The EC_{50} values after 24 hour treatment varied from 10 to 500 μg/mL, depending on the cell lines and monomer compositions (Table 2). In general, the polymers were more active (lower EC_{50} values) against C4-2B and DU145 than PC-3 cells. The EC_{50} values decreased as the mole percentage of EMA monomer increased (Fig. 2c), indicating that the hydrophobicity of polymers potentiates the anticancer activity due to the role of hydrophobic groups causing membrane disruption. The copolymers with longer cationic side chains (ABMA monomers) showed higher activity (smaller EC_{50} values) compared to those with shorter cationic side chains (AEMA monomers). We have previously demonstrated that the elongation of cationic side chains of methacrylate random copolymers increases the depth of polymer insertion in anionic bacterial cell membranes (snorkeling effect), leading to higher antibacterial activity[15]. Similarly, the longer cationic side chains might enhance the polymer insertion into cancer cell membranes and disrupt the membranes more effectively. As a reference, the EC_{50} values of lytic peptide melittin were 2–6 μg/mL under the same assay conditions. While melittin exhibited higher activity than the polymers, it is highly toxic to normal cells, thus limiting its use as an anticancer agent[16,17].

The cytotoxicity of copolymers to non-cancerous normal cells was also evaluated to determine selectivity. Lysis of human red blood cells (hemolysis) was used as a measure of membrane-mediated acute cytotoxicity of copolymers. In general, the hemolytic activity of copolymers depended on their hydrophobicity. The percent hemolysis increased as the mole percentage of EMA increased, indicating that the copolymers with higher hydrophobicity are more hemolytic (Table 2 and Fig. S4 for dose-hemolysis curves). The cytotoxicity of copolymers to proliferating normal cells after 24 hour exposure to the copolymers was first examined using human dermal microvascular endothelial cells (HDMECs) (Fig. 2a and Table 2). The viability of HDMECs after incubation with **P-5** for 24 hours was higher than that of similarly treated DU145 cells. Similar to DU145, the EC_{50} values for HDMECs also decreased as the mole percentage of EMA increased (Fig. 2c). These results suggest that the high hydrophobicity of polymers led to undesired cytotoxicity against normal human cells, that is likely due to non-specific hydrophobic binding to normal cell membranes.

We further examined the cytotoxicity of copolymers against primary human cells including normal human dermal fibroblasts (NHDF) and human prostate epithelial cells (HPrECs). The EC_{50} values after 24 hour incubation with the selected copolymers were smaller than those against HDMEC and PCa cells (Table 2 and Fig. S2), indicating that the copolymers showed higher cytotoxicity against these primary human cells as compared to HDEMC and PCa cells. These results suggest that the cytotoxicity of copolymers to primary normal cells is largely dependent on the cell types.

Membrane-disruptive mechanism. To probe the mechanism of action by the copolymers, we further examined the effect of **P-5** on the cell membranes. We selected **P-5** as a model copolymer because it showed a potent activity against PCa cells and relative selectivity to PCa cells over HDMECs among the polymers tested in this study. We first observed the DU145 cells and HDMECs under a microscope after incubation with **P-5** for 24 hours (Fig. 3a). Because of cell death, DU145 cells were detached, and the remaining cells were collapsed. The surfaces of these cells were severely damaged. On the other hand, the cell surfaces of HDMECs treated with **P-5** for 24 hours appear to be little damaged compared to those of DU145. To quantify the damages to the cell membranes, an extracellular leakage of the cytoplasmic enzyme lactate dehydrogenase (LDH) from DU145 cells treated with **P-5** for 24 hours was examined. **P-5** caused significant LDH leakage at high polymer concentrations, suggesting that the cell membranes were permeabilized (Figs 3b and S5). The percentage of released LDH was correlated to cell viability of cells treated by **P-5** (Fig. 3c) and other copolymers (Fig. S6). On the other hand, the conventional anticancer drug docetaxel, which interferes with cell division of rapidly proliferating cells and causes apoptotic cell death[18], caused little or no LDH release although it reduced cell viability (Figs 3c and S5–S7). In addition, the EC_{50} values of all the polymers for the cell viability and LDH leakage were well correlated (Fig. 3d). These results suggest that the polymer-induced cancer cell death was primarily caused by cell membrane disruption.

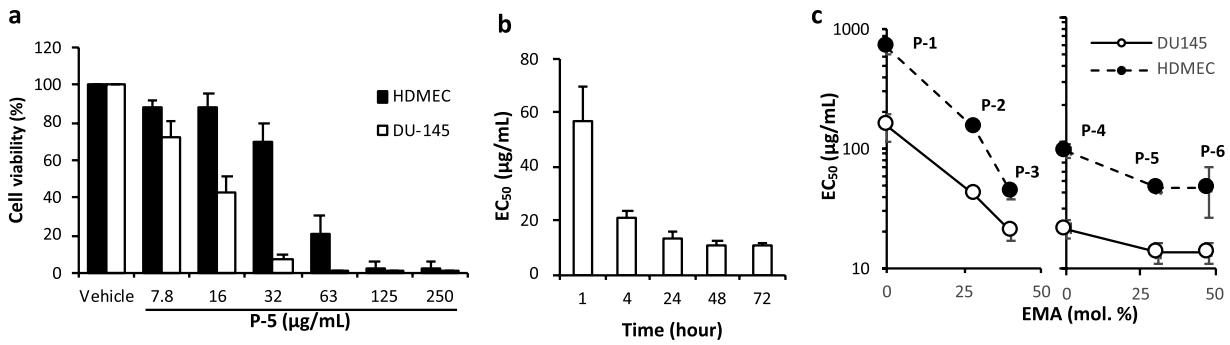

Figure 2. Cytotoxicity of copolymers to prostate cancer cells and HDMEC. (**a**) Cytotoxicity of **P-5** to DU145 and human dermal microvascular endothelial cells (HDMEC) after 24 hour incubation at 37 °C. The percentage of cell viability after 24 hour treatment was calculated relative to the viability of cells treated by a vehicle (0.01% acetic acid, the final concertation of 0.001% in the assay cell culture.) for the copolymer as 100%. (**b**) Time dependence of EC_{50} of **P-5** for DU145. The EC_{50} values were determined from dose-response curves of each incubation time. (**c**) Relationship between the hydrophobic EMA monomer composition and anticancer activity. The EC_{50} values of all polymers for DU145 cells after 24 hour treatment with the copolymers were plotted against the mol. percentage of EMA in a polymer chain. The data points and error bars for panels represent average value ± standard deviation (S.D.) of three independent assays, performed in triplicate for each (n = 3).

	EC_{50} [24 h] (μg/mL)						HC_{50} (μg/mL)
	Human prostate cancer cells			Human primary cells			Human red blood cells
Entry	C4-2B	DU145	PC-3	HDMEC	NHDF	HPrEC	
P-1	207 ± 33	157 ± 42	457 ± 21	700 ± 82	n.d.	n.d.	(2.8 ± 1.0%)[†]
P-2	46.7 ± 9.6	42.0 ± 1.6	113 ± 32	153 ± 5	45.3 ± 4.1	28.0 ± 5.0	(11.7 ± 9.3%)[†]
P-3	39.6 ± 6.2	20.0 ± 3.3	70.7 ± 7.4	43.3 ± 4.7	n.d.	n.d.	137 ± 95
P-4	18.7 ± 3.8	21.0 ± 3.7	54.7 ± 10.5	86.0 ± 9.9	13.3 ± 5.3	16.5 ± 0.5	(0.9 ± 0.2%)[†]
P-5	18.7 ± 1.9	13.3 ± 2.5	30.7 ± 3.4	43.0 ± 2.4	9.3 ± 2.5	11.0 ± 1.0	(26.9 ± 9.6%)[†]
P-6	20.0 ± 1.6	13.7 ± 2.6	27.3 ± 1.9	44.3 ± 19.4	n.d.	n.d.	71.3 ± 23.0
Melittin	6.3 ± 0.2	1.8 ± 0.2	2.8 ± 0.4	3.5 ± 0.3	n.d.	n.d.	2.7 ± 0.8

Table 2. Cytotoxicity of copolymers to prostate cancer cells and non-cancerous cells. The cell viability was measured by a colorimetric cell viability assay CCK-8 or XTT and the EC_{50} values were determined from the dose-cell viability curves (Fig. S2) after incubation with the copolymers for 24 hours. The data points and error bars represent average value ± standard deviation (S.D.) of three independent assays, performed in triplicate (n = 3). [†]The percent hemolysis at 1,000 μg/mL is presented in parentheses.

We also determined damages to the cell membranes of HDMEC by **P-5** after 24 hour treatment. **P-5** also caused LDH leakage (Fig. 3b), which indicate that **P-5** also cause membrane disruption in the HDMEC cell membranes. The level of LDH leakages was smaller than that of DU145, which appears to reflect the selectivity of **P-5** to DU145 over HDMECs in their cell viabilities (Fig. 2a). Similar to DU145 cells, the percentage of released LDH was also correlated to the cell viability of HDMECs treated by **P-5** for 24 hour exposure to **P-5** (Fig. 3c). This result suggests that the cytotoxicity of **P-5** to HDMECs was also primarily caused by cell membrane disruption. However, the LDH leakage was suppressed (leakage ~20%) after 72 hour incubation at high **P-5** concentrations (Fig. S8) while these cells showed no viability (Fig. S9). We speculate that the cells might form junctions and seal the damaged membranes, but we cannot rule out other mechanisms to cause toxicity in cells, which involve cellular targets. At this point, the toxicity mechanism of copolymers is not clear, which is beyond the scope of this report.

The role of PS lipids in the cytotoxicity mechanism of copolymers. The results described above indicated that the cytotoxicity of copolymers depends on cells, and the copolymers appear not to be selective to cancer cells over normal cells. We wondered if these normal cells might also express significant PS lipids on the cell surfaces, and then the cytotoxicity of copolymers might be correlated to the level of PS lipid exposure on the surfaces of these cells. To test this hypothesis, we examined the PS lipid exposure of these cells using Annexin V. Annexin V is a biomarker which binds specifically to PS lipids on cell surfaces, and the Annexin V binding to cells was further analyzed by flow cytometry (Fig. S10). To quantify the level of Annexin V binding to cells, we gated regions which give higher than the high end of 5% in the cell population without Annexin V (control) for each cell type, and the percentage of cells stained by Annexin V in these gates was determined. The PCa cells all displayed high Annexin V binding levels (~98%), as compared to the primary normal cells NHDF (71%) and HDMEC (75%), while HPrEC (89%) showed a relatively high level of Annexin V binding. The EC_{50} values of

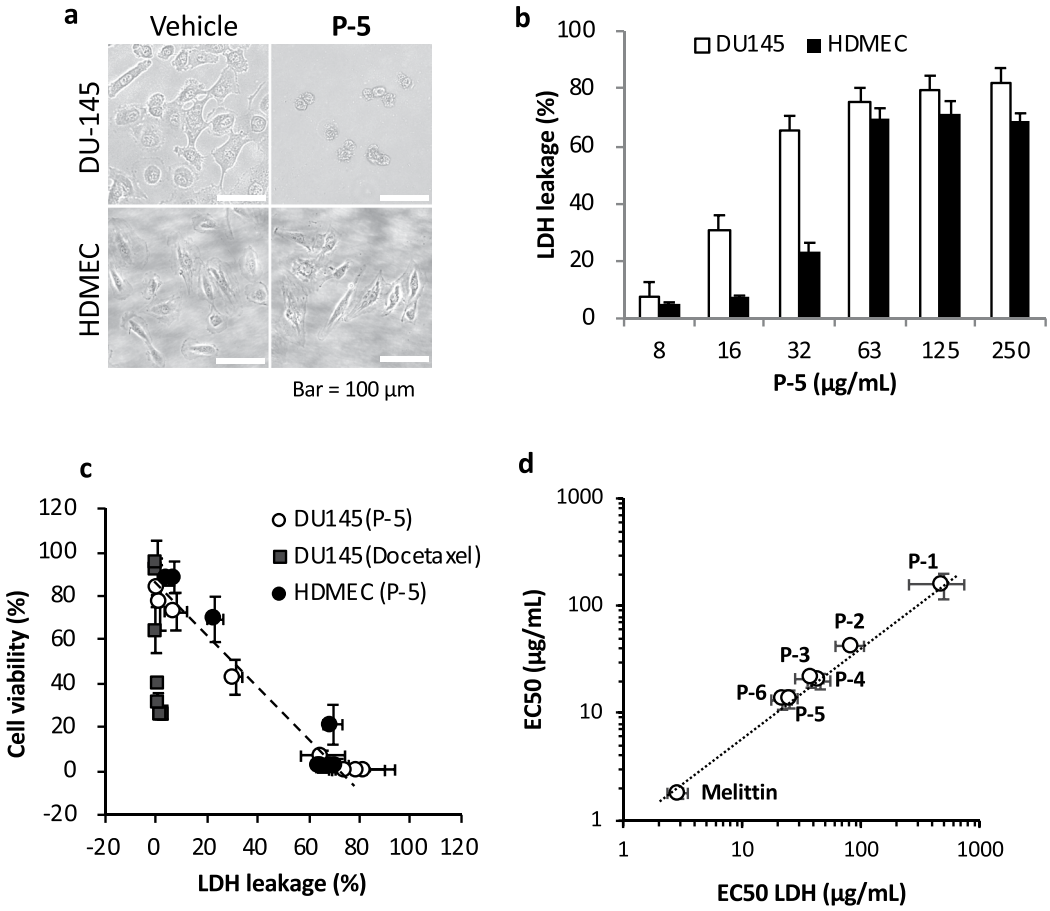

Figure 3. Membrane-targeting action of copolymers. (**a**) Effect of **P-5** on cell surfaces of DU145 and HDMEC cells. The cells in a 6-well plate were incubated with **P-5** for 24 hours at concentration of 32 µg/mL, and the cell morphologies were observed. 0.01% acetic acid was used as vehicle (the final concertation of 0.001%). (**b**) Polymer-induced LDH leakage from DU145 cells and HDMEC. The cells in a 96-well plate were incubated with **P-5** for 24 hours. Each assay was performed in triplicate, and the data points and error bars represent average value ± standard deviation (S.D.) of three independent assays (n = 3). (**c**) Correlation between the percentages of cell viability and LDH leakage for DU145 cells treated with **P-5**. (**d**) Correlation between the EC_{50} values for the cell viability reduction and for the LDH leakage by **P-5** after incubation with **P-5** for 24 hours.

cell viability was plotted as a function of level of Annexin V binding (Fig. 4a), and there appears to be no direct correlations, indicating that the cytotoxicity of copolymers may not directly reflect the level of PS lipid exposure on the cell surfaces.

Based upon our results we next wondered what roles do PS lipids have in regulating the anticancer activity of copolymers? The results of LDH leakage (Fig. 3) suggested that the copolymers acted by disrupting cancer cell membranes. Here we examined the ability of **P-5** to target and disrupt a lipid bilayer with PS lipids. We prepared giant unilamellar vesicles (GUVs) with (DOPC/DOPS) or without PS lipids (DOPC). Lipid vesicles have been previously used to probe the mechanism of anticancer peptides[19–21]. It has been reported that the total amount of PS lipids in cells were largely different in cancer cell types, ranging from 2% to 10%[22]. In order to examine the effect of PS lipids on the copolymer activity evidently, we used GUVs with 10% PS lipids, which would be potentially the maximum amount of PS lipids exposed on the cancer cell surfaces. **P-5** completely lysed all GUVs with PS lipids at high **P-5** concentrations, although the GUVs without PS lipids remained intact (Figs 4b and S11), indicating that the PS lipids enhanced the membrane disruption by **P-5**. The selective activity of **P-5** against the membranes with PS lipids can be explained by the electrostatic binding of cationic side chains of **P-5** to anionic PS lipids. Therefore, the PS lipids could be the first binding target. However, increasing the amount of PS lipids from 10% to 35% did not enhance the lysis of GUVs (Fig. 4b). In addition, it has been also reported that phosphatidylethanolamine (PE) lipids are also externalized to the cancer cell surfaces[23]. The anticancer peptide Polybia-MP1 lysed GUVs containing PE more than those without PE, while PE lipids are zwitterionic, but not anionic, indicating that the PE lipids play an important role in the membrane-disruptive mechanism of the peptide. This suggests that lipids other than PS lipids and/or their combinations with PS lipids may be important for membrane disruption by the copolymers. Taken together, the PS lipids may be involved as an initial binding site in the membrane disruptive mechanism of copolymers, but they are not only the factor to determine the activity of copolymers against cell membranes. This may corroborate with our conclusion on no clear correlation between

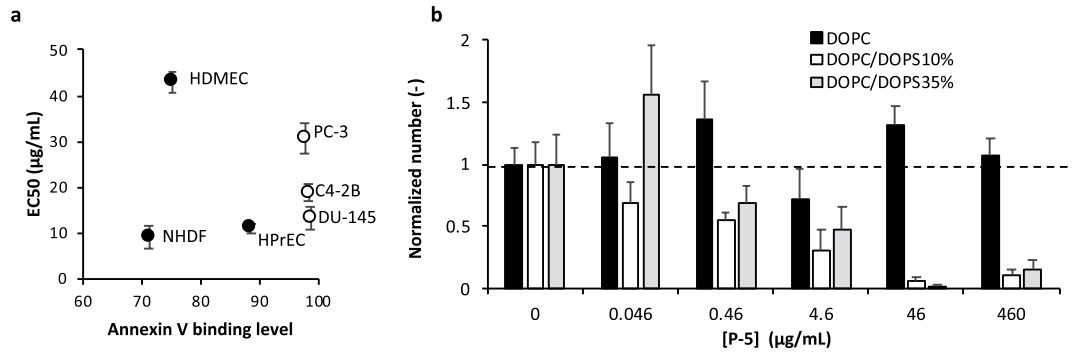

Figure 4. Role of PS lipids in the anticancer mechanism of P-5. (**a**) The relationship between the EC_{50} values and Annexin binding level. (**b**) Lysis of GUVs consisting of DOPC/DOPS (65:35 or 90:10) or only DOPC by **P-5**. The number of GUVs with diameters larger than 5 nm, relative to those of control (0 μg/mL), was determined as a measure of **P-5** induced lysis. The data points and error bars represent average value ± standard deviation (S.D.) of 4 or 5 images.

the cytotoxicity (EC_{50}) of copolymers and the level of Annexin binding (Fig. 4a). In addition, detailed mechanistic studies would be also need to directly prove that the copolymers indeed target PS lipids on the actual cell surfaces. One potential approach would be use of lacadherin which binds to PS lipids and blocks the effect of polymers by preventing the interactions with PS lipids[24], which will be a subject of our future study.

Anticancer activity against dormant cancer cells. We next examined the efficacy of **P-5** to kill dormant cancer cells. We used an *in vitro* cellular model prepared under low serum conditions to induce dormant cell behavior. In general, when cells were cultured in a reduced serum medium, the cell cycle becomes slow or arrested, inducing cell dormancy[25]. However, the cell viability of PC-3 cells still increased after being cultured in a 0.5% FBS medium for 48 hours, indicating that some sub-populations of cells were proliferating (Fig. S12). To examine the cell cycle and to isolate dormant cells, we integrated cell cycle reporters (p27 and Cdt1) into PC-3 cells, which report the stage of cell cycle by fluorescence[26]. The reporters-integrated PC-3 cells were cultured in a 0.5% FBS medium for 48 hours. The dormant cells (p27(+)/Cdt1(+)) made up 64% of the total cell population, while the actively proliferating cells (p27(-)/Cdt1(-)) were 19% (Fig. 5a). The dormant cells were sorted by flow cytometry and cultured in a 0.5% FBS medium. The dormancy of the isolated cells was confirmed by low expression of the endogenous proliferation marker Ki-67 protein[27] (Fig. S13) and no substantial increase in the cell proliferation over 48 hours in the same culture medium (Fig. S14). Importantly, the dormant and proliferating cells showed the same level of Annexin V-APC binding (Fig. 5b), suggesting that anionic PS lipids exposed on the cell surfaces are viable targets for both proliferating and dormant PC-3 cells.

The isolated dormant PC-3 cells were treated with docetaxel or **P-5** for 48 hours. The cell viability-based assay was not suitable to determine their cytotoxicity due to the low viability readings from dormant cells. Therefore, their effect on treated cells was determined by flow cytometric analysis using DAPI and Annexin V-APC, which report membrane-damaged cells and apoptotic cells, respectively[28]. DAPI diffuses into the cytosol and nucleus of cells with damaged cell membranes and bind to DNA. Annexin V binds to the elevated level of PS lipids on apoptotic cell surfaces. It should be noted that the fluorescence signals from Annexin V bound to apoptotic cells were typically one or two orders of magnitude higher than those from Annexin V bound to viable cancer cells. In the case that cells are doubly positive, the cell membrane integrity is significantly compromised (necrotic), in which PS lipid exposure is no longer regulated and/or Annexin V freely binds to PS lipids in the inner leaflet of the cell membranes.

The flow cytometry analysis indicates that docetaxel caused little or no changes in the dormant PC-3 cells as compared to the untreated control (Fig. 5c). The percent cell death of docetaxel-treated dormant cells was 20%, which was not significantly different from 17% dead cells of control (Fig. 5d). The extremely high concentration of docetaxel (1,000 ng/ml) increased dead cells only slightly to 28%. These results suggest that docetaxel was inherently inactive against the dormant PC-3 cells. On the other hand, the cells treated with **P-5** were stained by both DAPI and Annexin V, suggesting significant membrane damage or necrotic cell death. At the **P-5** concentrations of 15 μg/mL and 30 μg/ml, in which the cell viabilities of HDMECs were larger than 70% (Fig. 2a), ~100% of the dormant PC-3 cells were dead (Fig. 5d). These results support our hypothesis that the ACP-mimetic copolymer is capable of killing dormant cancer cells.

To further probe the anticancer mechanism of the copolymer, we treated the cells with **P-5** for 1 hour because we anticipated that early stage apoptosis or intermediate membrane damage can be detected in flow cytometry analysis. The flow cytometry results showed that only double positive and double negative cell sub-populations were observed (Fig. S15), indicating that **P-5** caused deleterious damages in the cell membranes without any intermediate steps of membrane permeabilization or apoptosis. The cell surfaces of dormant PC-3 cells treated with **P-5** for 1 hour were visualized by electron microscopy and showed large pores or a sponge-like morphology (Fig. 5e–j), along with many pieces of small debris around the cells. However, the cells treated with docetaxel and vehicle remained intact. The cells also appear to partially adhere to the substrate. These results indicate that **P-5** caused significant membrane damage in a relatively short timeframe.

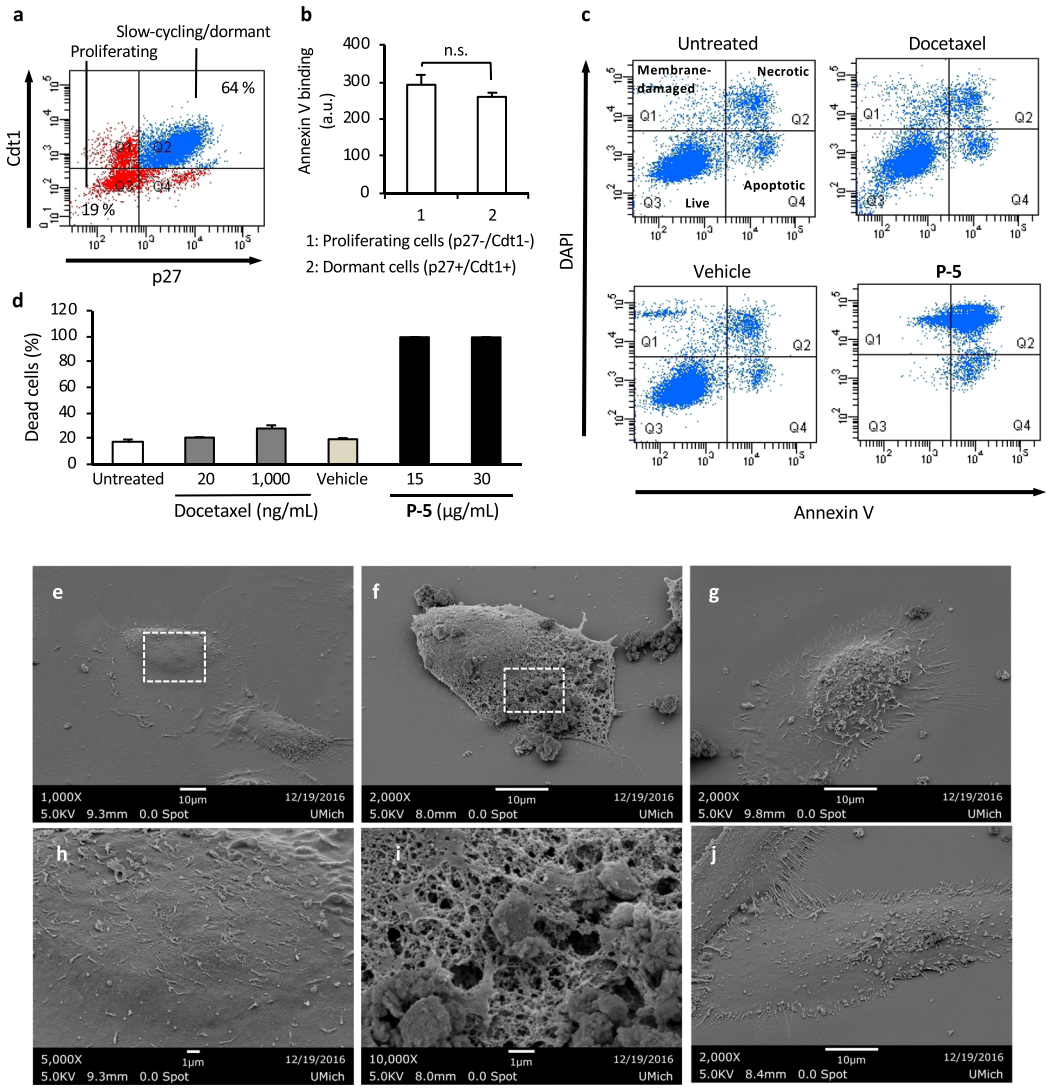

Figure 5. Anticancer activity of **P-5** against isolated dormant PC-3 cells. (**a**) Cell populations. The cells were cultured in a 0.5% FBS medium for 48 hours, and the sub-populations of cells in different cell cycles were identified by fluorescence signals associated with the reporters p27 and Cdt1 in flow cytometry. (**b**) Levels of PS exposure on proliferating and dormant PC-3 cells. (**c**) Flow cytometric analysis of treated isolated dormant PC-3 cells. The dormant PC-3 cells were incubated with **P-5** at 30 μg/mL, docetaxel at 20 ng/mL, or vehicle (0.001% acetic acid) for 48 hours in a 0.5% FBS culture medium. (**d**) Cytotoxicity of **P-5** to dormant PC-3 cells. The percent cell death is calculated as 100%- live cell subpopulation (DAPI(−)/Annexin V(−)). Each group was measured with three replicates (n = 3), and the error bars indicate the standard deviation. (**e**–**j**) Effect of copolymer **P-5** on dormant PC-3 cells observed by SEM. The isolated dormant PC-3 cells were untreated (**e**,**h**) or treated with **P-5** at 30 μg/mL (**f**,**i**), docetaxel at 20 ng/ml (**g**), or vehicle (0.01% acetic acid, the final concertation of 0.001%) (**j**) for 1 hour in a 0.5% FBS culture medium. The panels of (**d**,**e**) are magnified images of areas indicated by broken lines in the panels of (**h**,**i**), respectively.

Copolymer activity against dormant cells in a solid tumor model. Within solid tumors, some cell sub-populations located far from blood vessels are metabolically inactive or dormant due to depletion of oxygen and nutrients[29,30]. These dormant cells do not respond to anticancer drugs which target proliferating cancer cells. It is also known that poor penetration of drug molecules into solid tumor tissues also reduces their efficacy[31,32]. As the copolymer effectively killed dormant cancer cells in monolayer cultures, we further tested the copolymer for the activity against those in an *in vitro* tumor spheroid model, which provides more clinically relevant tumor-like microenvironment[33].

Spherical aggregates or spheroids were prepared by culturing DU145 and PC-3 cells in ultra-low attachment cell culture plates for 24 hours (Fig. 6). The cells showed low expression of Ki-67 protein, indicating slow proliferation or cell dormancy (Fig. S16)[27]. Docetaxel treatment showed little or no effect on the percentage of DU145 cell death, while docetaxel was more active against proliferating cells cultured on a standard cell culture plate (Fig. 6). The drug resistance is likely due to cell dormancy as well as limited diffusion of drug molecules into the spheroids. However, the treatment by **P-5** killed >90% cells in DU145 and PC-3 spheroids. The cell images

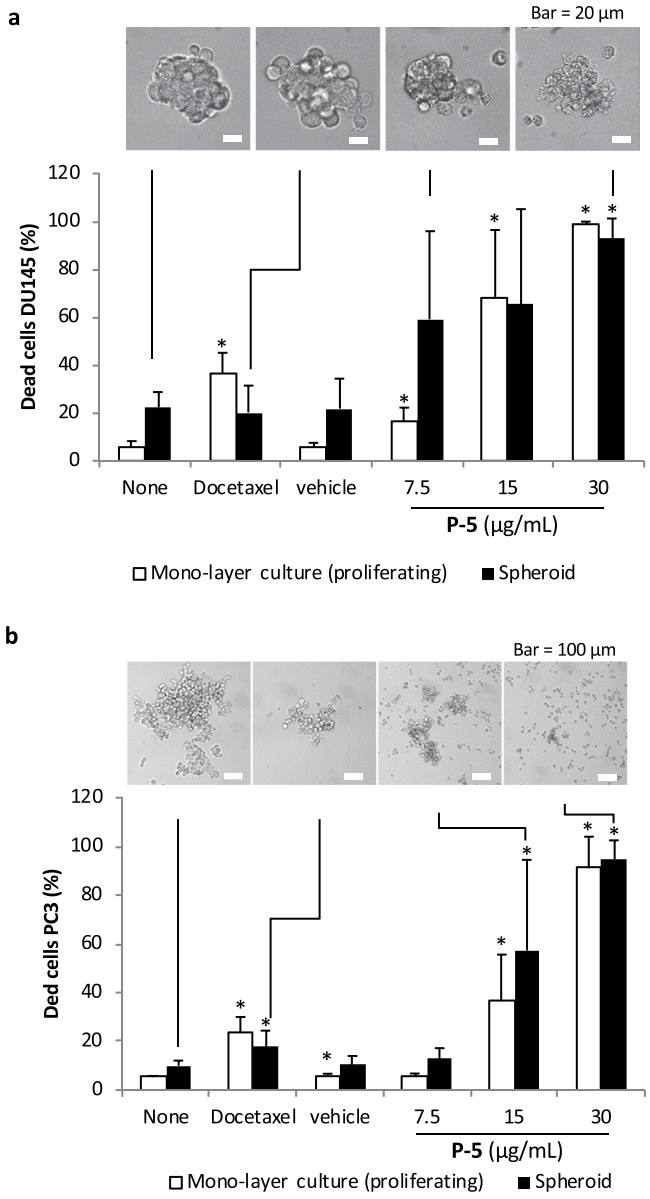

Figure 6. Anticancer activity of **P-5** against PCa cells in mono-layer and spheroid cultures. The cell death (**a**) DU145 and (**b**) PC-3 was determined by staining the cells with Annexin V and DAPI, and the percentage of dead cells was quantified by flow cytometry after dissociating the cell aggregate. Vehicle 0.01% acetic acid (the final concertation of 0.001% in the assay culture). The concertation of docetaxel is 20 ng/mL. The data are expressed as mean ± standard deviation (PC-3; n = 9, DU145; n = 4). Two-tailed, unpaired Student's t-test was used for data analysis. The statistical significance was determined against the control (None) values. *$p < 0.05$.

indicated that the surfaces of cells treated with **P-5** were lysed, and the DU145 spheroids were no longer densely packed, while the cell aggregates treated with docetaxel were rather intact (Fig. 6a). Surprisingly, **P-5** dispersed the PC-3 spheroids and reduced their sizes, indicating that the membrane disruption may also compromise the cell-cell adhesion (Fig. 6b).

Conclusion

In this study, we demonstrated the molecular design of membrane-active copolymers as a synthetic mimic of ACPs. The copolymers showed anticancer activity against proliferating PCa cells. The copolymers exert their anticancer effects by disrupting the cell membranes. The anticancer activity and selectivity of copolymers could be tuned by altering their cationic and hydrophobic monomer compositions. The anticancer activity of copolymers does not directly reflect the amount of PS lipids exposed on the cell surfaces, and other lipids may be also involved in their mechanism. Importantly, the copolymer killed isolated dormant PCa cells inherently resistant to docetaxel. The copolymer was also effective in killing dormant cells in the *in vitro* tumor spheroid model, resulting in shrinkage or dispersion of *in vitro* tumor spheroid models.

The synthetic polymer platform provides simple, but diverse chemical structures for tuning their physiological properties, providing an approach to improve their efficacy and cancer selectivity. While further specific testing is required, we believe that these traits of polymeric materials will allow rational design and screening of many functional polymers such as degradable polymers[34], polymer architectures and morphologies such as polymer micelles[35], and chemical modifications including cancer-homing ligand groups or pro-drug moieities[36–39], which would lead to identification of clinically potent, selective compounds. In addition, the bio-distribution or systemic toxicity of these polymers are unknown. Synthetic polymers may also induce an immune response, which should be also thoroughly evaluated for clinical translation. Further investigations on therapeutic efficacy and the development of delivery system would be necessary for future clinical implementation. We also envision that anticancer polymers could be used in conjunction with conventional chemotherapies or when conventional chemotherapies fail to treat dormant cancer cells, rather than simply replacing the traditional drugs. Taken together, we believe that the design principle for anticancer polymers demonstrated in this study opens up a new research field to discover new anticancer materials and therapeutics to treat dormant cancer cells.

Methods

Polymer synthesis (P-5). The copolymers were synthesized by RAFT polymerization according to the previous report[40]. For **P-5**, 4-((*tert*-butoxycarbonyl)amino)butyl methacrylate (Boc-ABMA) (7.0 mmol, 1.5 mL of 2 M solution in acetonitrile), ethyl methacrylate (EMA) (3.0 mmol, 1.5 mL of 2 M solution in acetonitrile), 2-cyanoprop-2-yl-dithiobenzoate (1.0 mmol, 221 mg, 10 mole% relative to total amount of monomers), and AIBN (0.1 mmol, 16 mg, 1 mole% relative to total amount of monomers) were mixed in a flask. The oxygen of reaction mixture was removed by nitrogen gas bubbling for 5 minutes, and the reaction solution was stirred at 70 °C for 16 hours. The reaction was stopped by cooling the vial in a dry ice-acetone bath. The solvent was removed by evaporating under reduced pressure. The residue was dissolved in in dichloromethane, and the polymer was isolated by precipitation in excess hexanes twice. The mole percentage of EMA (MP_{ethyl}) was determined by comparing integrated peaks of butylene groups of Boc-ABMA and ethylene groups of EMA in the ^{1}H NMR spectrum. The DP was calculated by comparing integrated peaks of phenyl group of chain transfer agent at the polymer ω-end and side chains. The number average molecular weight (M_n) was calculated using the DP, MP_{ethyl}, and the molecular weights of monomers and RAFT agent. Gel permeation chromatography (a calibration curve based on 10 standard samples of poly(methyl methacrylate)): M_n = 2,800 g/mol., M_w = 3,100 g/mol., dispersity ($Đ$) = 1.12. ^{1}H NMR ($CDCl_3$, 400 MHz) δ: 7.90–7.26 (m, 4H, phenyl end group), 5.25–4.70 (brs, 1H, -N*H*Boc), 4.20–3.83 (m, 2H, side chain of ABMA and EMA -OCH_2-), 3.25–2.92 (brs, 2H, -NCH_2-), 2.15–1.77 (m, 2H, polymer backbone -CH_2-), 1.70–1.45 (m, 4H, side chain of ABMA -NCH$_2$CH_2CH_2CH$_2$O-), 1.42 (brs, 9H, Boc group), 1.32–1.17 (m, 3H, methyl group of EMA side chain -CH_3), 1.16–0.80 (m, 3H, methyl group of polymer backbone -CH_3). DP (^{1}H NMR) = 15.0, MP_{ethyl} (^{1}H NMR) = 30 mole %, M_n (^{1}H NMR) = 3,400 g/mol.

Boc-protected **P-5** copolymer (1.00 g) was mixed with methyl 3-mercaptopropionate (MMP) (500 μL), followed by the addition of trifluoracetic acid (TFA) (5 mL). After stirring for 30 min, the TFA was removed by blowing with nitrogen gas. The residue was dissolved in methanol, and the deprotected **P-5** was isolated by precipitating in excess diethyl ether. Subsequently, the precipitate was dissolved in distilled water and lyophilized to yield a light pink fluffy product (0. 94 g, Yield = 90%). ^{1}H NMR (methanol-d_4, 400 MHz) δ: 7.90–7.40 (m, 4H, phenyl end group), 4.20–3.90 (m, 2H, side chain of ABMA and EMA -OCH_2-), 3.10–2.90 (m, 2H, -NCH_2-), 2.20–1.80 (m, 2H, polymer backbone -CH_2-), 1.80–1.65 (m, 4H, side chain of ABMA -NCH$_2$CH_2CH_2CH$_2$O-), 1.50–1.10 (m, 3H, methyl group of EMA side chain -CH_3), 1.20–0.80 (m, 3H, methyl group of polymer backbone -CH_3). DP (^{1}H NMR) = 15.9, MP_{ethyl} (^{1}H NMR) = 31 mole %, M_n (^{1}H NMR) = 2,500 g/mol.

Cell culture. The human prostate cancer cell lines, PC-3 (Cat #: CRL-1435), DU145 (Cat #: HTB-81) and HPrPC (Cat #: PCS-440-010) were obtained from the American Type Culture Collection. All prostate cancer cell lines were routinely grown in RPMI 1640 (Life Technologies, Carlsbad, CA, USA) supplemented with 10% (v/v) fetal bovine serum (Invitrogen), 1% (v/v) penicillin-streptomycin (Invitrogen) and maintained at 37 °C, 5% CO_2, and 100% humidity. Human dermal microvascular endothelial cells (HDMECs) were obtained from the PromoCell (Heidelberg, Germany) and maintained in endothelial cell growth medium MV2 (PromoCell, Heidelberg, Germany) at 37 °C, 5% CO_2, and 100% humidity. NHDF was obtained from PromoCell.

Anticancer assays using dormant PC-3 cells. PC-3 cells expressing cell-cycle indicators were incubated with **P-5**, docetaxel, and vehicle (0.01% acetic acid, final concertation of 0.001%) in a culture medium RPMI 1640 containing 0.5% FBS for 48 hours at 37 °C, 5% CO_2, and 100% humidity. Apoptotic cells or necrotic cells were detected by flow cytometry using APC Annexin V Apoptosis Detection Kit (cat. 640932, BioLegend, San Diego, CA).

Tumor spheroid model. PC-3 or DU145 cells (5×10^4 cells) were seeded in ultra-low attachment 6-well cell culture plates (Corning #3471) or normal 6-well cell culture plates (Thermo Scientific #140675) in RPMI 1640 containing 10% (v/v) fetal bovine serum, and 48 hours later, Docetaxel or **P-5** was added to the wells (Docetaxel; 20 ng/ml, **P-5**; 7.5, 15, 30 μg/ml). Cell apoptosis/necrosis assay was performed 72 hours after the drug administration.

Data Availability

The datasets generated during and/or analyzed during the current study are available from the corresponding author on reasonable request.

References

1. Kim, J. J. & Tannock, I. F. Repopulation of cancer cells during therapy: An important cause of treatment failure. *Nat. Rev. Cancer* **5**, 516–525 (2005).
2. Aguirre-Ghiso, J. A. Models, mechanisms and clinical evidence for cancer dormancy. *Nat. Rev. Cancer* **7**, 834–846 (2007).
3. Riedl, S. *et al*. In search of a novel target - Phosphatidylserine exposed by non-apoptotic tumor cells and metastases of malignancies with poor treatment efficacy. *Biochim. Biophys. Acta* **1808**, 2638–2645 (2011).
4. Utsugi, T., Schroit, A. J., Connor, J., Bucana, C. D. & Fidler, I. J. Elevated expression of phosphatidylserine in the outer-membrane leaflet of human tumor-cells and recognition by activated human blood monocytes. *Cancer Res.* **51**, 3062–3066 (1991).
5. Papo, N. & Shai, Y. Host defense peptides as new weapons in cancer treatment. *Cell. Mol. Life Sci.* **62**, 784–790 (2005).
6. Riedl, S., Zweytick, D. & Lohner, K. Membrane-active host defense peptides - Challenges and perspectives for the development of novel anticancer drugs. *Chem. Phys. Lipids* **164**, 766–781 (2011).
7. Yeung, A. T. Y., Gellatly, S. L. & Hancock, R. E. W. Multifunctional cationic host defence peptides and their clinical applications. *Cell. Mol. Life Sci.* **68**, 2161–2176 (2011).
8. Gakhar, G. *et al*. Anti-tumor Effect of Novel Cationic Biomaterials in Prostate Cancer. *Anticancer Res.* **34**, 3981–3989 (2014).
9. Jiang, M. *et al*. Chitosan Derivatives Inhibit Cell Proliferation and Induce Apoptosis in Breast Cancer Cells. *Anticancer Res.* **31**, 1321–1328 (2011).
10. Duncan, R. Polymer therapeutics: Top 10 selling pharmaceuticals - What next? *J. Controlled Release* **190**, 371–380 (2014).
11. Yang, J. Y. & Kopecek, J. Macromolecular therapeutics. *J. Controlled Release* **190**, 288–303 (2014).
12. Zhao, Y., Alakhova, D. Y. & Kabanov, A. V. Can nanomedicines kill cancer stem cells? *Adv. Drug Del. Rev.* **65**, 1763–1783 (2013).
13. Park, N. H. *et al*. Addressing Drug Resistance in Cancer with Macromolecular Chemotherapeutic Agents. *J. Am. Chem. Soc.* **140**, 4244–4252 (2018).
14. Wu, X. Y., Gong, S. C., Roy-Burman, P., Lee, P. & Culig, Z. Current mouse and cell models in prostate cancer research. *Endocr. Relat. Cancer* **20**, R155–R170 (2013).
15. Palermo, E. F., Vemparala, S. & Kuroda, K. Cationic Spacer Arm Design Strategy for Control of Antimicrobial Activity and Conformation of Amphiphilic Methacrylate Random Copolymers. *Biomacromolecules* **13**, 1632–1641 (2012).
16. Gajski, G. & Garaj-Vrhovac, V. Melittin: A lytic peptide with anticancer properties. *Environ. Toxicol. Pharmacol.* **36**, 697–705 (2013).
17. Hoskin, D. W. & Ramamoorthy, A. Studies on anticancer activities of antimicrobial peptides. *Biochim. Biophys. Acta* **1778**, 357–375 (2008).
18. Pienta, K. J. Preclinical mechanisms of action of docetaxel and docetaxel combinations in prostate cancer. *Semin. Oncol.* **28**, 3–7 (2001).
19. Sinthuvanich, C. *et al*. Anticancer β-Hairpin Peptides: Membrane-Induced Folding Triggers Activity. *J. Am. Chem. Soc.* **134**, 6210–6217 (2012).
20. Leite, N. B. *et al*. PE and PS Lipids Synergistically Enhance Membrane Poration by a Peptide with Anticancer Properties. *Biophys. J.* **109**, 936–947 (2015).
21. Wang, C. *et al*. Cell surface binding, uptaking and anticancer activity of L-K6, a lysine/leucine-rich peptide, on human breast cancer MCF-7 cells. *Sci. Rep.* **7**, 8293 (2017).
22. Wang, D.-Y., Done, S. J., Mc Cready, D. R. & Leong, W. L. Validation of the prognostic gene portfolio, ClinicoMolecular Triad Classification, using an independent prospective breast cancer cohort and external patient populations. *Breast Cancer Res.* **16**, R71 (2014).
23. Stafford, J. H. & Thorpe, P. E. Increased Exposure of Phosphatidylethanolamine on the Surface of Tumor Vascular Endothelium. *Neoplasia* **13**, IN1–IN2 (2011).
24. Blanco, V. M. *et al*. Phosphatidylserine-selective targeting and anticancer effects of SapC-DOPS nanovesicles on brain tumors. *Oncotarget* **5**, 7105–7118 (2014).
25. Yao, G. Modelling mammalian cellular quiescence. *Interface Focus* **4** (2014).
26. Oki, T. *et al*. A novel cell-cycle-indicator, mVenus-p27K-, identifies quiescent cells and visualizes G0-G1 transition. *Sci. Rep.* **4**, 4012 (2014).
27. Gerdes, J., Schwab, U., Lemke, H. & Stein, H. Production of a mouse monoclonal-antibody reactive with a human nuclear antigen associated with cell-proliferation. *Int. J. Cancer* **31**, 13–20 (1983).
28. Cummings, B. S. & Schnellmann, R. G. In *Curr. Protoc. Pharmacol.* (John Wiley & Sons, Inc., 2001).
29. Cox, M. C., Reese, L. M., Bickford, L. R. & Verbridge, S. S. Toward the Broad Adoption of 3D Tumor Models in the Cancer Drug Pipeline. *ACS Biomater. Sci. Eng.* **1**, 877–894 (2015).
30. Katt, M. E., Placone, A. L., Wong, A. D., Xu, Z. S. & Searson, P. C. *In Vitro* Tumor Models: Advantages, Disadvantages, Variables, and Selecting the Right Platform. *Front. Bioeng. Biotechnol.* **4**, 12 (2016).
31. Minchinton, A. I. & Tannock, I. F. Drug penetration in solid tumours. *Nat. Rev. Cancer* **6**, 583–592 (2006).
32. Tannock, I. F., Lee, C. M., Tunggal, J. K., Cowan, D. S. M. & Egorin, M. J. Limited penetration of anticancer drugs through tumor tissue: A potential cause of resistance of solid tumors to chemotherapy. *Clin. Cancer. Res.* **8**, 878–884 (2002).
33. van den Brand, D., Massuger, L. F., Brock, R. & Verdurmen, W. P. R. Mimicking Tumors: Toward More Predictive *In Vitro* Models for Peptide-and Protein-ConjugatedDrugs. *Bioconj. Chem.* **28**, 846–856 (2017).
34. Gutekunst, W. R. & Hawker, C. J. A General Approach to Sequence-Controlled Polymers Using Macrocyclic Ring Opening Metathesis Polymerization. *J. Am. Chem. Soc.* **137**, 8038–8041 (2015).
35. Elsabahy, M., Heo, G. S., Lim, S. M., Sun, G. R. & Wooley, K. L. Polymeric Nanostructures for Imaging and Therapy. *Chem. Rev.* **115**, 10967–11011 (2015).
36. Dharap, S. S. *et al*. Tumor-specific targeting of an anticancer drug delivery system by LHRH peptide. *Proc. Natl. Acad. Sci. USA* **102**, 12962–12967 (2005).
37. Ellerby, H. M. *et al*. Anti-cancer activity of targeted pro-apoptotic peptides. *Nat. Med.* **5**, 1032–1038 (1999).
38. DeFeo-Jones, D. *et al*. A peptide-doxorubicin 'prodrug' activated by prostate-specific antigen selectively kills prostate tumor cells positive for prostate-specific antigen *in vivo*. *Nat. Med.* **6**, 1248–1252 (2000).
39. Lee, J., Huang, W., Broering, J. M., Barron, A. E. & Seo, J. Prostate tumor specific peptide-peptoid hybrid prodrugs. *Bioorg. Med. Chem. Lett.* **25**, 2849–2852 (2015).
40. Enrico, N. T., Takahashi, H. & Kuroda, K. Radical-Medicated End-Group Transformation of Amphiphilic Methacrylate Random Copolymers for Modulation of Antimicrobial and Hemolytic Activities. *J. Polym. Sci. Pol. Chem.* **55**, 304–312 (2017).

Acknowledgements

This research was supported by the National Science Foundation (NSF CAREER Award DMR-0845592 to K.K.), the National Cancer Institute (CA093900, CA163124 to R.T.), the Department of Defense (PCRP Idea award W81XW-15-1-0413, to L.B., and W81XWH-14-1-0403 to R.T.), the Prostate Cancer Foundation (Challenge Award 16CHAL05 to R.T.), Grants-in-Aid for Challenging Research (Exploratory, No. 17K19353 to K. Yasuhara) from the Japan Society for the Promotion of Science (JSPS), and Department of Biologic and Materials Sciences, School of Dentistry, University of Michigan. R.T. receives support as the Major McKinley Ash Collegiate

Professor. This work was also supported by JSPS Postdoctoral Fellowships for Research Abroad (No. 26-774 to H.T.). We also thank Dr. Robertson Davenport at University of Michigan Hospital for providing RBCs. We thank Dr. Yuji Mishina and Dr. Maiko Omi for help on cell imaging and Dr. Dan Sun for assistance with generating cell lines.

Author Contributions

H.T. synthesized and characterized the copolymers, evaluated the cytotoxicity of copolymers to proliferating cancer cells and normal cells, performed LDH leakage assay and cell imaging. K. Yumoto characterized the primary normal cells and dormant cancer cells, evaluated the cytotoxicity of copolymer to normal cells and dormant cancer cells, and prepared cell samples for SEM. K. Yasuhara performed the lipid vesicle assays. E.T.N. synthesized and characterized the copolymers. Y.K. supervised the assays using primary normal cells. L.B. devised and supervised the development of cell lines to monitor dormancy. R.S.T. devised the project and supervised the assays using dormant cancer cells. K.K. devised the project, helped with data analysis, and prepared the manuscript. All authors assisted with editing the manuscript.

Additional Information

Supplementary information accompanies this paper at https://doi.org/10.1038/s41598-018-36608-5.

Competing Interests: The authors declare no competing interests.

Publisher's note: Springer Nature remains neutral with regard to jurisdictional claims in published maps and institutional affiliations.

HER2 is a cell surface marker for dormant prostate cancer cells

Kenji Yumoto[1], Frank C. Cackowski[1,3], Yu Wang[1], Maiko Omi[2], Ann Decker[1], Younghun Jung[1], Dan Sun[4], Henriette A. Remmer[5], Yuji Mishina[2], Laura Buttitta[4] and Russell S. Taichman[1,6]

[1]Department of Periodontics and Oral Medicine, University of Michigan School of Dentistry, Ann Arbor, MI 48109, USA
[2]Department of Biological and Materials Sciences, University of Michigan School of Dentistry, Ann Arbor, MI 48109, USA
[3]Department of Internal Medicine, Division of Hematology and Oncology, University of Michigan School of Medicine, Ann Arbor, MI 48109, USA
[4]Department of Molecular, Cellular and Developmental Biology, University of Michigan, Ann Arbor, MI, 48109, USA
[5]Proteomics & Peptide Synthesis Core, Biomedical Research Core Facilities, University of Michigan Medical School, Ann Arbor, MI 48109, USA
[6]Department of Periodontics, University of Alabama at Birmingham School of Dentistry, Birmingham, AL 35233, USA.

Corresponding Author:
Russell S. Taichman D.M.D., D.M.Sc.
Department of Periodontics
University of Alabama at Birmingham School of Dentistry
SDB #406
1720 2nd Avenue South
Birmingham, AL 35294-0007
Telephone: 205.934.4720
Email: taichman@uab.edu

Abstract

Disseminated prostate cancer (PCa) cells can survive for years as dormant cells, maintaining the capacity to initiate relapse. Unfortunately, disseminated tumor cells (DTCs) are relatively resistant to current chemotherapies, which target proliferating cells. Therefore, there is a significant unmet need to understand the biology of dormant DTCs to devise strategies that target these cells. One approach is to identify cell surface markers that are unique to dormant tumor cells that would enable dissection of the biology of these cells and ultimately provide opportunities to target them with specific therapies. In this study, we examined cell surface proteins on dormant PCa cells using a proteomics approach coupled with flow cytometry analysis. We identified HER2 as being highly expressed on the surface of dormant PCa cells. Using a drug-conjugated HER2 antibody (T-DM1), significant suppression of PCa metastasis can be achieved in a preclinical animal model. We propose that these findings may be instrumental in new strategies for targeting dormant DTCs.

Introduction

Prostate cancer (PCa) is the most common cancer among men worldwide, often leading to bone metastases [1] [2] [3]. Accumulating evidence suggests that disseminated tumor cells (DTCs) can survive in a dormant state through engagement of specialized "niches" in the bone marrow microenvironment [4] [5] [6] [7]. Dormant DTCs are thought to be the cause of relapse and disease progression through reactivation of proliferative pathways. Unfortunately, dormant DTCs are largely resistant to current chemotherapies designed to target proliferating cancer cells. Once DTC proliferation is reactivated, halting disease progression is nearly impossible. Therefore, understanding the biology of DTCs, the processes that regulate dormancy and how to target them with therapy, remain critical challenges for the field.

Once tumors arrive in the bone marrow (BM), DTCs are likely to undergo apoptosis, become dormant or begin to proliferate. What regulates these choices remains largely unknown although recent work has identified key signaling pathways which regulate dormancy [8] [9]. Previously, we showed that DTCs home to the bone marrow, where many become localized near osteoblasts (OBs) where they become dormant [5]. In this osteoblast-rich niche, osteoblast secretion of cytokines, such as growth arrest specific 6 (GAS6) [10] [11], transforming growth factor-beta 2 (TGF-β2) [12], bone morphogenetic protein 7 (BMP7) [13] and protein acidic and rich in cysteine (SPARC) [14], cooperate to establish DTC dormancy. Positive-feedback signaling loops further reinforce dormancy as GAS6 induces the expression of both TGF-β and its receptors on PCa cells to mediate TGF-β2-induced cell growth suppression [11]. Likewise, SPARC stimulates the expression of BMP7 by marrow stromal cells [14]. In turn, TGF-β2 and BMP7 induce cellular dormancy by activating p38 and increasing expression of the cell cycle inhibitor p27 [12] [13]. Wnt5a from OBs also induces dormancy of PCa cells through induction of Siah E3 ubiquitin protein ligase 2 (SIAH2), which represses Wnt/β-catenin signaling [15].

Traditionally, dormant cells are defined by high expression of p27 protein, a cell cycle inhibitor or by low expression of the proliferation marker Ki-67 protein. In addition, low rates of BrdU incorporation have been used to identify cells as dormant or non-proliferative. Unfortunately, these methods require fixation of the cells and permeabilization of the cell membranes. This limits the isolation of dormant cells to fixed samples and prevents further dissection of their biology. To address this drawback, we set out to identify methods to isolate dormant prostate cancer cells that do not compromise their integrity or viability.

We approached the problem of isolating viable dormant DTCs through trying to find a unique maker of dormant PCa cells using a proteomics analysis. We took an advantage of cell cycle indicators, which in conjunction with fluorescence-activated cell sorting (FACS), permitting a rapid segregation of cells in G_0 phase from other phases of the cell cycle. We combined this approach with membrane preparations and proteomic mass spectrometry analysis for identification of cell surface expressed proteins identifiable by FACS.

In this study, we show that cell surface expression of HER2 (ERBB2) is relatively high both on dormant PCa cells *in vitro* and DTCs in early stages *in vivo*. HER2 is a transmembrane, tyrosine kinase receptor whose overexpression is associated with adverse prognosis in breast cancer (BCa) [16]. HER2 is a member of the human epidermal growth factor receptor (HER) family, along with 3 other receptors including epidermal growth factor receptor (EGFR, HER1), HER3 and HER4. The HER family are involved in regulating a diverse repertoire of cellular processes that control cell growth, survival, differentiation, and migration [17] [18]. In breast cancer, HER2 is overexpressed in 15-20% of breast carcinomas and is associated with a more aggressive disease, higher recurrence rate, and increased mortality [19]. Trastuzumab, a humanized monoclonal antibody against HER2, has become the standard of care for the treatment of HER2 positive BCa. Trastuzumab in combination with chemotherapy significantly improves both the survival of patients with metastatic and early stage, HER2-positive BCa [20] [21] [22] [23] [24]. Amplification and overexpression of HER2 has also been observed in patients with PCa [25], and overexpression of HER2 was associated with cancer progression, a poor prognosis and development of androgen independency [26]. More recently, overexpression of HER2 proteins have been associated with PCa progression and bone metastasis [27]. However the relationship between cell surface expression levels of HER2 and cancer growth or cancer cell proliferation has not been well investigated.

Based on these observations, we hypothesized that dormant DTCs could be targeted using HER2 antibodies in order to prevent metastasis. To test this hypothesis, we evaluated Trastuzumab emtansine (T-DM1), which is a humanized monoclonal antibody against HER2 (Trastuzumab) conjugated to the highly potent cytotoxic agent DM1, in an animal model of PCa metastasis. Our approach was to provide T-DM1 treatments only at the earliest stages of the metastatic processes, prior to tumor formation. We found that T-DM1 significantly suppressed PCa

metastasis in our model. Our study may lead to a new strategy to prevent PCa metastasis by targeting dormant DTCs by HER2 antibody drugs.

Results

Proteomics on membrane proteins extracted from dormant vs. proliferating PC3 cells

We recently showed that a combination of fluorescent ubiquitin-based cell cycle reporters designed to label cells in G_0, mVenus-p27K- and mCherry-30-120hCdt1 (Cdt1), could be used in prostate cancer PC3 cells to isolate quiescent cells by flow cytometry [28]. We refer to this stable dual-reporter cell line as PC3 Venus Cherry (PC3VC) [29] [28]. PC3VC cells were cultured in the presence of 5% fetal bovine serum (FBS) for 48 hours, and cells in G0 ($Venus^+$ $Cherry^+$) and G1 cells ($Venus^-$ $Cherry^+$) were sorted by FACS separately (Fig. 1). Subsequently, membrane proteins were extracted and analyzed by proteomic mass spectrometry. Initially, 3,791 proteins were identified (Supplemental data 1). Many of these proteins demonstrated significant differences in expression between samples isolated from cells in G0 and G1 cell cycle phases. Of these, 27 proteins from the proteomic results were selected for further analysis based upon the commercial availability of antibodies that can be used for FACS analyses (Table 1).

Cell surface HER2 expression is increased on dormant PCa cells induced by serum starvation

To identify differentially expressed cell markers that correlate with cell cycle phases, cellular dormancy was induced by serum starvation. As predicted, serum starvation significantly suppressed cell proliferation, with a 60 % suppression in cell numbers compared to the cells cultured in 10 % FBS (Fig. 2A). Critically, serum starvation for 3 days did not induce cell death in PC3 cells (Supplemental Fig. 1A). Serum starvation also increased expression of endogenous p27, a cell cycle inhibitor and a marker of dormant cells, which was not detected in cells cultured in 10% FBS (Fig. 2B).

Using the serum starvation model, cell surface expression of the selected targets identified by proteomics (Table 1) was confirmed using specific antibodies and FACS. With this approach, 13 proteins were reliably detected on the surface of PC3 cells (Fig. 2C, Supplemental Fig. 1B). Interestingly, HER2 levels on the cell surface were dramatically increased by serum starvation (Fig. 2C), while CD146 and CD71 cell surface expression were remarkably reduced by serum starvation (Fig. 2C, Supplemental Fig. 1C) consistent with the proteomics data (Table 1).

Since HER2 is overexpressed in 15-20% of breast carcinomas, and is associated with a more aggressive breast cancer, we focused on HER2 and examined HER2 cell surface levels across different PCa cell lines and normal prostate epithelial cells (Fig 2D). HER2 expression was detected on the membranes of both highly metastatic PC3 and DU145 cells, and significant levels were detected on the LNCaP and C4-2B subline in the presence of 10 % FBS (Fig 2D). PNT2, normal prostate epithelial cells have low expression of HER2 on the cell surface (Fig 2D). We next induced dormancy using serum starvation in these cell lines. Similar to PC3, cell proliferation was suppressed and p27 expression was increased in each cell line by serum starvation (Supplemental Fig. 1D, E). Critically, HER2 cell surface expression was significantly increased for the DU145, LNCaP and C4-2B cell lines (Fig 2E, F). However, normal prostate cells, PNT2 cells failed to increase cell surface levels of HER2 (Fig 2E, F).

To explore whether HER2 is generally expressed on the cell surface by dormant/quiescent cells, we sought to extend our studies beyond PCa. Therefore, we examined cell surface expression of HER2 in BCa cell lines (BT-474, SKBR3) in response to serum starvation. The serum starvation suppressed cell proliferation in these cells (Supplemental Fig. 1F). Similar to the prostate cancer cell lines, HER2 levels on the cell surface was also enhanced by serum starvation on BCa cells (Supplemental Fig. 1G).

HER2 cell surface expression is associated with the expression of p27

Next double staining using specific antibodies against HER2 and p27 on PC3 and C4-2B cells cultured in serum free conditions was performed. Cell surface HER2 and cytoplasmic p27 expression were examined by FACS, and a HER2 low intensity population (10% of total cells) and a HER2 high intensity population (10% of total cells) were gated separately (Fig 3A, top). Next, p27 levels were compared between the two populations (Fig 3A, bottom). As expected, significantly higher expression of p27 was detected in the HER2 high population both in PC3 and C4-2B, showing that HER2 cell surface expression is associated with dormancy (Fig. 3A). To further confirm these results, immunocytochemistry was performed to observe p27 and HER2 expression in PCa cells after serum starvation (Fig. 3B). In agreement with the FACS results (Fig. 3A), strong expression of HER2 was detected on the surface of both p27 positive PC3 and C4-2B cells, whereas in the cells cultured in 10% FBS, p27 was undetectable and expression of HER2 was less (Fig. 3B).

HER2 levels on the cell surface are augmented by a cyclin-dependent kinase inhibitor

Inhibition of cyclin-dependent kinases (CDK) 4/6 activity leads to retinoblastoma (Rb) dephosphorylation and repression of E2F activity, which promotes a G0/G1 arrest, therefore, CDK4/6 is an attractive target for cancer therapies to inhibit cancer growth [30] [31] [32]. Abemaciclib is an FDA-approved drug for the treatment of advanced or metastatic breast cancers, which selectively inhibits CDK4/6 [33] [34]. Treatment of PCa cells with abemaciclib (1 μM) significantly reduced cell numbers compared to vehicle (0.01% ethanol)-treated cells (Fig. 4A). For both C4-2B and LNCaP, 20-30 percent of cells had died during the treatment period, but PC3 and DU145 were seemingly resistant (Fig. 4B). Therefore, after live cell gating, cell surface expression of HER2 was evaluated. Overall, HER2 was significantly increased in PCa cells except for DU145 when cells were treated by abemaciclib (Fig. 4C). Similarly, for BCa cells, HER2 cell surface expression was elevated by abemaciclib, whereas abemaciclib inhibited proliferation without the induction of cell death (Supplemental Fig. 2A, B, C). Taken together, these results suggest that high expression of HER2 on the cell surface is one of the signatures of dormant or cell cycle arrested cells although not in all instances.

Enhanced expression of HER2 on the surface of PCa cells co-cultured with osteoblasts

Osteoblasts are critical components of the bone marrow niche and are known to play a significant role in regulating DTC proliferation in the marrow [5] [35]. Previously we demonstrated that a murine pre-osteoblastic cell line, MC3T3-E1, dramatically decreases the proliferation of PCa cells when they are co-cultured together [11]. Here we analyzed HER2 cell surface expression of PCa cells (PC3, DU145 and C4-2B) when they were co-cultured with MC3T3-E1 (Fig. 5). To segregate the two species, the murine MC3T3-E1 cells were stained by an antibody against the mouse major histocompatibility complex (MHC) (Fig. 5A) and cell surface HER2 levels were assayed on the MHC-negative human PCa cells. HER2 expression on PC3 cells was increased by co-culture with MC3T3-E1 cells and relative expression levels, as measured by mean fluorescence intensity (MFI), clearly showed enhanced expression of HER2 on PCa cells by the co-culture (Fig. 5B).

HER2 is highly expressed on the surface of DTCs *in vivo*

In order to examine cell surface expression of HER2 on DTCs, PC3 cells were injected into male CB.17. SCID mice by intracardiac (i.c.) injection. After 48 hours, the pelvis, femora, tibiae and

liver were collected. Cells were obtained from the bones and liver and stained using human leukocyte antigen (HLA) antibodies and mouse MHC antibodies. DTCs were identified as HLA positive, and mouse-MHC negative cells (Fig. 6A), and the cell surface expression of HER2 on DTCs was measured by FACS. Compared to PC3 cells before injection, HER2 cell surface expression became significantly increased on DTCs derived from mouse BM or liver (Fig. 6B).

Targeting HER2 reduces the viability of PC3 cells *in vitro*

Trastuzumab (T-DM1) is a HER2 antibody conjugated to the highly potent cytotoxic agent DM1. We tested the impact of T-DM1 on dormant PCa cells. Cell viability was evaluated after 4 days of culture in the presence of T-DM1. Cell viability was measured using Cell Counting Kit-8, which detects live cells by measuring mitochondrial activity. T-DM1 significantly reduced the viability of PC3 cells and the efficiency of 10 μg/ml of T-DM1 on PCa survival is comparable to Docetaxel (1μg/ml) when cells are cultured in 10% FBS (Fig. 7A, top). Next, to examine the effect of T-DM1 on the viabilities of dormant PC3 cells, the cells were cultured in 0.5% FBS. Cell viability was suppressed by T-DM1 (10 μg/ml), and was even more effective than docetaxel (1μg/ml) (Fig. 7A, bottom). T-DM1 is thought to kill cells in part through the induction of antibody-dependent cellular cytotoxicity (ADCC) [36] [37]. We therefore tested whether T-DM1 induces ADCC on PC3 cells using splenocytes collected from severe combined immunodeficient (SCID) mice. PC3 cells were labeled with the fluorescent dye, DiD, and cultured in 1% FBS for 24 hours, and then incubated with T-DM1 and splenocytes. After 18 hours, PC3 cells could be identified as DiD-positive cells, and dead cells were detected as DAPI positive (Fig. 7B). Our results showed that T-DM1 kills ~ 20 % of the target cells by ADCC (Fig. 5C).

Targeting HER2 reduces metastasis in an animal model

Based on our results demonstrating that HER2 is highly expressed on DTCs before the DTCs expand *in vivo* (Fig. 6) and that T-DM1 has a potent cytotoxic effect on dormant PCa cells (Fig. 7), we hypothesized that it may be possible to target and eliminate dormant DTCs as an adjuvant therapy in early stages of dissemination to prevent metastasis using HER2 targeted therapies. To explore this possibility we evaluated the impact of T-DM1on an animal model of metastasis (Fig. 8). In this model, luciferase-labeled PC3 cells were injected in the left ventricle of SCID mice, and the mice were treated with T-DM1 alone or IgG control up to day 12 after tumor inoculation (Fig. 8A). Mice treated with control IgG began to demonstrate the first evidence of metastasis by

4 weeks, and only 40 % of the mice survived without metastasis after 160 days (Fig. 8B). By contrast, T-DM1 treatments significantly inhibited the development of metastasis with 80% of mice surviving without metastasis throughout the experiments up to 160 days after the tumor injection (Fig. 8B). Representative images of bioluminescence from the control group and T-DM1-treated groups are shown (Fig. 8C). These results suggest that T-DM1 reduces or eliminates DTCs during dormancy, before DTCs are activated to proliferate and form detectable metastases.

Discussion

Using a proteomics approach coupled with cell cycle indicators and FACS, we sought to identify a cell surface marker which could distinguish dormant PCa cells from those cells in proliferative phases of the cell cycle. We found that elevated HER2 expression was a feature of dormant PCa and BCa cells. Critically, HER2 targeted therapies significantly reduced metastasis in an animal model of PCa. It is important to note that we designed the animal model to mimic adjuvant therapy delivered to men at high risk of prostate cancer recurrence. Therefore, the animals were only treated with T-DM1 in the early stages of metastasis before tumors were detectable by imaging. These observations suggest that T-DM1 may serve as a useful adjuvant therapy for men at high risk for disease progression and relapse.

Over-expression of HER2 has been shown to play an important role in the development and progression of several subtypes of aggressive BCa [16] [19] [38] and other tumors [39] [40] [41] [42]. It is important to note that although HER2 expression is associated with dormancy of the tumor cells we evaluated, HER2 expression alone may not be sufficient to distinguish all dormant from proliferating cells by FACS and will likely require additional antibodies such as CD146 or CD71 which appear to mark proliferating cells.

Although the extracellular ligands which bind to HER2 have not yet been identified, HER2 signaling promotes cell proliferation and cell survival [43]. Pathways which have been implicated in the downstream HER2 signaling after receptor phosphorylation include the mitogen-activated protein kinase, phosphatidylinositol 3-kinase (PI3K)/AKT/mTOR, phospholipase C, protein kinase C, and signal transducer and activator of transcription pathways [43]. In PCa, PI3K/AKT/mTOR signaling has been well studied and critical roles of PI3K/AKT signaling in proliferation [44], survival [45] and invasion [46] are known.

Our results demonstrate that HER2 cell surface expression becomes augmented by serum starvation (Fig. 2) or a CDK4/6 inhibitor (Fig. 4), when PCa cells are cultured with OBs (Fig. 5), and when DTCs are present in the marrow of experimental animals (Fig. 6). While this may seem paradoxical to upregulate HER2 on non-proliferating cells, one intriguing possibility is that HER2 may serve as an alert system for the reactivation of proliferation in dormant cells. A second hypothesis is that HER2 expression may serve as a distress signal for cells which are induced towards a dormant phenotype in a foreign environment. Investigating these possibilities

will be challenging since it will necessitate the isolation of human DTCs from marrow, followed by an evaluation of HER2 expression and the signaling pathways which are activated at the time of isolation.

One strategy to consider in the development of an adjuvant approach to treat DTCs to prevent disease progression is to enhance HER2 expression prior to targeted therapy. Toward this goal, it may be valuable that Abemaciclib, a FDA-approved medicine to treat advanced BCa [47], enhanced HER2 expression on both PCa cells and BCa cells in our studies. It is also reported that cholesterol-lowering drug lovastatin increases HER2 availability at the cell membrane to enhance the binding of trastuzumab to gastric cancer cells [48]. We envision that the combination of drugs that enhance HER2 expression on the cell membrane and HER2 targeted therapies may be a rationale strategy to treat cancer which shows low expression of HER2.

Late recurrences in PCa are relatively common, with 20% of recurrences occurring more than five years after curative intent radiation or prostatectomy [49]. These recurrences are thought to result from DTCs, which can exhibit dormant behavior for months or years, followed by re-activation and subsequent clinical recurrence [8]. Estimates of DTC frequency at the time of disease diagnosis are about 40 % of men undergoing radical prostatectomy prior to surgery [50]. Efforts to eradicate DTCs with systemic adjuvant therapy in PCa have far proven unsuccessful. However, our *in vivo* experiments modeling an early stage of metastasis suggest that T-DM1 effectively targets dormant DTCs and dramatically suppressed their growth or metastasis. We believe that this approach delivered chemotherapy to HER2 expressing cells but may have also worked by other mechanisms. A mechanism which may have produced the results we observed includes the induction of ADCC. Yet, some mice demonstrated a significant delay in the formation of metastasis, suggesting that some DTCs survived even after the T-DM1 treatments. This could have been due to a lack of HER2 expression or resistance to the therapy. Although trastuzumab-based chemotherapy is associated with excellent outcomes in BCa treatments, long-term follow-up data from adjuvant pivotal trials indicate that 15-24% of patients still develop recurrent disease [23] [24]. Several resistance mechanisms have been identified including impaired drug binding to HER2 due to molecular masking [51] and constitutive activation of signaling pathways parallel or downstream of HER2[52] [53]. Impaired drug binding is a consideration as there appears to be a positive correlation between HER2 protein levels and the efficacy of trastuzumab therapy [54]. From our FACS analyses, we observed that HER2 cell

surface expression on DTCs isolated from BM or liver is relatively high (Fig. 6), however this may not be the case with all DTCs as HER2 expression in DTCs in situ for all cells was not elucidated. Further, it has been reported that HER2 is masked by membrane-associated mucin 4 (MUC4) in the microenvironment, which interferes with trastuzumab's ability to bind HER2 [51]. Thus, further investigation is required to figure out how some DTCs survived through the treatments using T-DM1 in animal models of tumor metastasis.

In sum, our data suggest high expression of HER2 is one of the features for dormant PCa cells, which are the source of disease recurrence. In addition, our work demonstrated that cell surface HER2 levels can be enhanced when PCa cell proliferation is inhibited by a CDK inhibitor, Abemaciclib, which suggests that HER2 targeted therapies in combination with Abemaciclib may be a novel strategy to treat cancer which shows low expression of HER2. Finally, our data showing that T-DM1 significantly suppresses PCa metastasis in our animal model indicating that T-DM1 should be considered as a potential therapeutic focus to target dormant DTCs to prevent metastases.

Methods

Cell culture

The human prostate cancer cell lines, PC3 (Cat #: CRL-1435), DU145 (Cat #: HTB-81), LNCaP (Cat #: CRL-1740), and an osteoblast precursor cell line, MC3T3-E1 (Cat #: CRL-2593) were obtained from the American Type Culture Collection. The C4-2B is a derivative subline of human prostate cancer LNCaP, originally isolated from a lymph node of a prostate cancer patient [55]. Normal human prostate epithelial PNT2 cells (Cat #: 95012613) was purchased from Sigma (St. Louis, MO). The human breast cancer cell lines, SKBR3 and BT-474 were gifts from Dr. Max S. Wicha (Department of Internal Medicine, University of Michigan Comprehensive Cancer Center). Luciferase-expressing prostate cancer cells were established by lentiviral transduction. All prostate cancer cell lines, normal human prostate epithelial PNT2 cells and BT-474 were routinely grown in RPMI 1640 (Life Technologies, Cat #: 11875-093) supplemented with 10% (v/v) fetal bovine serum (FBS) (GEMINI Bio-Products, Cat #: 900-208), 1% (v/v) penicillin-streptomycin (Life Technologies, Cat #: 15140-122). SKBR3 cells were grown in DMEM (Gibco, Cat #: 11960) containing 10% (v/v) FBS, 1% (v/v) penicillin-streptomycin, 1% (v/v) Glutamax (Gibco, Cat #: 35050-061) and 1 mM sodium pyruvate (Gibco, Cat #: 11360).

MC3T3-E1 cells were grown in minimal essential medium (MEM) alpha (Life Technologies, Cat #: 12561-056) containing 10% (v/v) FBS, 1% (v/v) penicillin-streptomycin. All cells were maintained at 37 °C, 5% CO2, and 100% humidity.

PC3 integrated with cell cycle reporters

To develop a method to identify dormant cells, we transduced a human prostate cancer cell line, PC-3 with lentiviruses containing the fluorescent ubiquitination-based cell cycle reporters [29]. Both of the CDT1-mCherry reporter (pMXs-mCherry-hCdt1) and the p27 cyclin-dependent kinase inhibitor protein -Venus reporter (pMXs-IP-mVenus-p27) were packaged into lentivirus at the University of Michigan Vector Core Facility. PC-3 cells infected with both of the lentiviral reporters were selected for 7 days in RPMI media containing 10 μg/ml puromycin. To isolate the cells which are successfully integrated with both reporters, Venus and mCherry double positive cells were sorted by flow cytometry. Isolated PC-3 Venus mCherry (PC3VC) cells were cultured in the RPMI containing 10% FBS. p27-Venus is upregulated upon entry into quiescence and is tagged for degradation by the Kip1 ubiquitination-promoting complex (KPC) in late G1 and the Skp2 ubiquitin ligase in the G1-S transition. Therefore, this reporter is high during G0, but low upon G1 entry and the G1-S transition [29]. The Cdt1-mCherry reporter is high during G0 and G1, but degraded during S phase by Skp2-dependent degradation [29]. Together, these two reporters can be used to identify dormant cells. Using this system, we isolated cells in G0 or in G1 phase by FACS.

Extraction of membrane proteins

PC3VC cells were cultured in the presence of 5% fetal bovine serum (FBS) for 48 hours, and cells were treated with Accutase (Innovatove cell technologies, Cat #: AT104-500) for 10 minutes at room temperature to harvest from culture flasks. The cell cycle reporters expression was analyzed by FACS, and G0 (p27+ Cdt1+) or G1 cells (p27- Cdt1+) were sorted by FACS. Membrane proteins were extracted from isolated PC3 cells in G0 or G1 phase using MEM-PER Plus Membrane Protein Extraction kit (Thermo Fisher Scientific, Cat. # 89842) following the manufacturer's directions.

Flow cytometry

The flow cytometric analyses and fluorescence-activated cell sorting (FACS) were performed on a FACS Aria II three-laser flow cytometer (Becton Dickinson, Franklin Lakes, NJ) and data were analyzed with DIVA software (Becton Dickinson). BD cytometer setup & tracking beads (BD Biosciences, Cat #: 642412) were used for the daily instrument standardization and validation. Sorting calibration was performed before each sort by drop-delay using Accudrop beads (BD Biosciences, Cat #: 345249). Sorting of cells was performed using a 70µm nozzle at 70 psi in purity mode.

Proteomic mass spectrometry analysis

Extracted membrane proteins (400 µg) in each of G0 and G1 samples were analyzed by proteomic mass spectrometry (Proteomics & Peptide Synthesis Core, University of Michigan) in order to identify and quantify proteins expressed in the samples.

Serum starvation

Cells (1 x 10^5 cells) were seeded in 6-well plates in culture media containing 10 % (v/v) FBS. The following day, cells were rinsed with phosphate buffered saline (PBS) once and cells were continued to culture in culture media without FBS for 3 days.

Analysis of cell surface protein expression by FACS

Cell surface protein expression was analyzed by a FACS Aria three-laser flow cytometer (Becton Dickinson, Franklin Lakes, NJ). Cells were treated with Accutase (Innovatove cell technologies, Cat #: AT104-500) for 10 minutes at room temperature to harvest from plates. Cells were stained with fluorescence conjugated primary antibodies in PBS containing 1% FBS for 30 minutes at 4°C. The following antibodies were used: HER2 (130-106-697), CD9 (130-103-990), CLDN4 (130-114-911), CD239 (130-104-885), CD81 (130-107-981), CD228 (130-111-410), CD87 (130-114-891), CD171 (130-100-701), CD146 (130-097-934), CD318 (130-101-212), CD10 (130-093-448), CD46 (130-104-507), EPHB4 (130-115-595), CD166 (130-106-621), Mouse IgG1 isotype (130-113-761), REA control PE-Vio770 (130-113-452) (all these antibodies were obtained from Miltenyi Biotec), SLC16A1 (FAB8275G), THBS1 (FAB5178V), TMEM87A (FAB7966V), SDC4 (Syndecan-4, FAB29181A), SEMA4B (FAB5485G), SLC12A7 (FAB9030G) (all these were obtained from R&D systems), CDH11 (368707), CD18 (366305), CD71 (334103), PODXL (330613), mouse IgG2a isotype (400207) (all these were obtained from

BioLegend), HSPG2 (Heparan Sulfate Proteoglycan, NBP2-47695F) was obtained from Novus Biologicals.

p27 protein expression detected by FACS

Cells were fixed with cold 70% ethanol, and stained with anti-p27 antibody (R&D systems, Cat #: IC2256V) in PBS containing 1% FBS for 30 minutes at room temperature. Monoclonal mouse IgG2B (R&D systems, Cat #: IC0041V) was used as isotype control.

Immunocytochemistry

Cells were fixed with 100% methanol (ice-cold) for 15 min at -20 °C. After the removal of methanol, cells were rinsed three times in PBS for 5 min each. To detect HER2 and p27, anti-HER2 (1:200) (Cell signaling, Cat #: 2165), anti-p27 (1:1600) (Cell signaling, Cat #: 3698) were used as the primary antibodies, respectively. Anti-rabbit IgG conjugated with Alexa Fluor 594 (Cell Signaling Tech, Cat #: 8889) and anti-mouse IgG conjugated with Alexa Fluor 488 (Cell Signaling Tech, Cat #: 4408) were used as the secondary antibodies. The slides were mounted with ProLong Gold antifade reagent with DAPI (Invitrogen, Cat #: P36931). Images were taken with Nikon C1 confocal microscope.

Co-culture experiments using PCa cells and OBs *in vitro*

MC3T3-E1 cells (4 x10^5 cells) were seeded in 6-well plates in MEM-alpha containing 10 % (v/v) FBS, and 24 hours later, PCa cells (4 x 10^4 cells) were plated on the subconfluent MC3T3-E1 cells and cultured for 3 days.

HER2 expression on the surface of DTCs *in vivo*

PC3 cells (1 × 10^6 cells) were injected into male CB.17. SCID mice (8-10 weeks of age: Charles River, Wilmington, MA) by intracardiac (i.c.) injection. Pelvis, femora and tibiae were harvested 48 hours after the injection, and the bones were crushed with a mortar and pestle and strained to remove debris. All steps used PBS buffer with 1% FBS unless otherwise noted. Single cell preparations were incubated with a FITC- anti-HLAABC antibody (BioLegend, Cat #: 311404) (dilution; 1:11), PE-Cy7-anti-mouse MHC (H-2Db) antibody (BioLegend, Cat #: 111516) (1:40), and APC-anti human HER2 antibody (Miltenyi Biotech, Cat #: 130-106-696) (1:11) for 30 min at 4°C. After washing cells with PBS buffer with 1% FBS, dead cells were excluded by DAPI

staining using a FACS Aria laser flow cytometer. Thereafter, DTCs of PC3 were identified as HLA-ABC positive, and mouse-MHC negative cells and the cell surface expression of HER2 on the DTCs was elucidated.

A xenograft model of prostate cancer metastasis

GFP/luciferase-expressing PC3 cells (5 x 10^5 cells) were suspended in 100 μl of PBS and injected into male CB.17. SCID mice (10–12 weeks of age: Charles River Labs) by left ventricle i.c. injection. For analysis of metastasis free survival, bioluminescence images were acquired after injection of luciferin using a PerkinElmer IVIS 2000 system. Animals that had a large portion of the signal in the lungs (indicative of a right ventricle injection) were removed from the analysis a priori. Time to metastasis formation visible by bioluminescence was then determined from the images. The data was analyzed by Kaplan-Meier analysis and the log-rank test. All experimental procedures were approved by the University of Michigan Committee for the Use and Care of Animals.

Cell viability assays

PC3 cells (1,000 cells) were plated into 96-well plates in growth medium with 10 % or 0.5% FBS. The following day, cells were treated with purified human IgG (1 or 10 μg/ml) (MP Biomedicals, Cat #:855908), T-DM1 (1 or 10 μg/ml) or Docetaxel (1 μg/ml) and viable cell numbers were evaluated by Cell Counting Kit-8 (CCK-8) (Dojindo, Cat #:CK04-13). Optical intensities were read on a multiwell scanning spectrophotometer at OD 450 nm (Thermo Labsystems). T-DM1 and Docetaxel were purchased from University of Michigan Cancer Center Pharmacy.

Flowcytometric ADCC analysis

ADCC analysis was performed basically following a method using flow cytometry [56]. We used PC3 cells as the target cells and mouse splenocytes collected from SCID mice as the effector cells. DiD-labeled PC3 cells were cultured overnight in a 96-well culture plate at 37 °C. Splenocytes were cultured in DMEM containing 10% FBS and IL-2 (Miltenyi Biotech, Cat #: 130-097-742) (1 ng/ml) for 24 hours before ADCC assays. PC3 cells were treated with T-DM1 (10 μg/mL) for 30 minutes and splenocytes were added to the culture (5:1as the effector: target (E:T) ratio). The culture media was DMEM containing 1% FBS and IL-2 (1ng/ml). The plate

was further incubated for 18 hours at 37°C (5% CO2, humidified atmosphere). The cells were harvested, and stained with DAPI (0.5 μg/ml) which stains dead cells. After 20 minutes of incubation, cells were subjected to FACS analysis.

Cell labeling with DiD dye

PC3 cells were stained with DiD dye (Molecular Probes, Cat #: v22887), according to manufacturer directions. Briefly, cells (1×10^6 cells / ml) were incubated with DiD dye (0.5 μM) in serum-free conditions at 37°C for 20 min, and then were washed three times with serum-free medium.

Statistical Methods

All numerical data are expressed as mean ± standard deviation (S.D.) unless specified otherwise. Two-tailed, unpaired Student's *t*-test was used for data analysis, with $p < 0.05$ considered to be statistically significant. Metastasis free survival was analyzed by Kaplan Meier plots and the log-rank test performed with GraphPad Prism software.

Acknowledgments

This work is directly supported by the University of Michigan MCubed Project, the National Cancer Institute (CA093900, CA163124, U54CA143803, CA143055 to R.T.), the Department of Defense (PCRP Idea award W81XW-15-1-0413, to L.B., and W81XWH-11-1-0636 and W81XWH-15-1-0637 to R.T.), and the Prostate Cancer Foundation (Challenge Award 16CHAL05 to R. T.). R. T. received support as the Major McKinley Ash Colligate Professor. F. C. receives support from a Career Enhancement Award from the NIH / NCI Prostate Cancer Specialized Program in Research Excellence (SPORE) at the University of Michigan and Prostate Cancer Foundation Young Investigator Award 18YOUN04. The overlay histograms were made by the University of Michigan's BRCF Flow Cytometry Core, which is supported by the National Cancer Institute of the National Institutes of Health under award number P30CA046592. We thank Dr. Max S. Wicha for providing the breast cancer cell lines.

Author Contributions

K.Y. and R.T. wrote the main manuscript text and discussed the results with all other authors. R.T. and L.B. supervised the project. H.R. performed the proteomics analysis, K.Y., F.C., M.O., D.S. and Y.W. carried out the experiments. Y.J., A.D. and Y.M. reviewed the manuscript and gave technical support and conceptual advice.

Disclosure of Potential Conflicts of Interest

No potential conflicts of interest were disclosed.

Table 1.

Proteins identified from proteomics data to examine cell surface expression

Twenty-seven proteins are selected from the proteomics data showing protein expression levels in both G0 and G1 samples to examine cell surface expression on PC3 cells.

Figures:

Figure 1. **Preparation of G_0 or G_1 membrane protein samples for proteomics analysis**

Sub-populations of PC3 cells in different cell cycle phases were identified by fluorescence intensity associated with the reporters p27 and Cdt1 by FACS. G_0 dormant cells ($p27^+$ $Cdt1^+$) and G_1 cycling cells ($p27^-$ $Cdt1^+$) were isolated by FACS, separately. Membrane proteins were extracted using MEM-PER Plus Membrane Protein Extraction kit from the isolated cells, and analyzed by proteomic mass spectrometry.

Figure 2. **Cell surface HER2 expression is increased on dormant PCa cells induced by serum starvation**

(A) Percentages of PC3 cell number after 3 days of culture in the presence or absence of FBS. Data are shown as mean ± S.D. (N=3). (**B**) p27 positive populations after 3 days of culture in the presence/absence of FBS. (**C**) Relative cell surface expression levels by mean fluorescence intensity (MFI), which is derived from fluorescence-conjugated specific antibodies against each of selected proteins, on PC3 cells after serum starvation compared to cells cultured in 10% FBS. MFI is shown as mean ± S.D. (N=2-3). *$p<0.05$, **$p<0.01$ compared to the cells cultured in 10% FBS. **(D**) Histograms showing cell surface HER2 expression on PCa cell lines and normal prostate epithelial cells, PNT2 cultured in 10% FBS. (**E**) Histograms showing HER2 cell surface expression on cells cultured in the presence or absence of FBS. (**F**) Relative expression levels (MFI) of HER2 on the surface of cells after serum starvation compared to cells cultured in 10 % FBS.

Figure 3. Cell surface HER2 expression is associated with p27 expression

(**A**) Histograms demonstrating cell surface HER2 expression on PC3 and C4-2B cells. Cells were gated by HER2 levels (HER2 low and HER2 high) populations, and p27 levels (MFI) were measured in the gated cell populations. p27 levels are shown as mean ± S.D. (N=3). (**B**)

Immunocytochemistry showing p27 expression and HER2 expression. HER2 (red), p27 (green) and nuclei (DAPI, blue) in the image. Scale bar, 50 μm.

Figure 4. HER2 cell surface expression on dormant PCa cells induced by a CDK4/6 inhibitor

(**A**) Percent of PCa cell number after 3 days of culture in the presence or absence of a CDK4/6 inhibitor, abemaciclib. Data are shown as mean ± S.D. (N=3). (**B**) Percent of dead cells after 3 days of culture in the presence or absence of abemaciclib. Data are shown as mean ± S.D. (N=3). (**C**) Relative expression of cell surface HER2 after 3 days of culture in the presence or absence of abemaciclib. Data are expressed as mean ± S.D. (N=3).

Figure 5. HER2 cell surface expression on PCa cells 3 days after co-culture with MC3T3-E1 cells.

(**A**) Human PCa cells were cultured with murine OBs, MC3T3-E1 cells for 3 days in the presence of 10% FBS, and PCa cells were identified as murine MHC negative populations (PC3 is shown here). (**B**) Relative HER2 expression (MFI) on PCa cells co-cultured with OBs, compared to PCa cells cultured alone. Data are expressed as mean ± S.D. (N=3).

Figure 6. HER2 cell surface expression on DTCs 48 hours after i.c. injection of PC3 cells into mice

(**A**) DTCs are identified in BM and liver using FACS as HLA positive and mouse MHC negative populations. (**B**) Cell surface HER2 expression on DTCs isolated from BM and liver. Data are shown as mean ± S.D. (N=3).

Figure 7. Cytotoxic effects of T-DM1 on dormant PC3 cells

(**A**) Viabilities of PC3 cells after 3 days of culture in the presence or absence of T-DM1. Top shows cells cultured in 10 % FBS, and bottom shows cells cultured in 0.5 % FBS. Cells were also cultured in the presence of Docetaxel (1 μg/ml). Data are shown as mean ± S.D. (N=3). (**B**) ADCC assays using FACS. DiD labeled PC3 cells were cultured in 1% FBS for 24 hours and were treated with T-DM1 (10 μg/ml) for 30 minutes. Later, splenocytes collected from SCID mice were added to the culture. After 18 hours, PC3 cells were identified as DiD positive and

dead PC3 cells were detected by DAPI staining. (**C**) Dead PC3 cells (%) are shown as mean ± S.D. (N=3).

Figure 8. Impacts of T-DM1 treatments on metastasis free survival in a prostate cancer left ventricle injection xenograft model

(**A**) Experimental design. GFP/luciferase-expressing PC3 cells were injected into male SCID mice by left ventricle intracardiac (i.c.) injection. Human IgG (15 mg/kg) or T-DM1(15 mg/kg) were injected by intraperitoneal (i.p.) injection every 3 days until 12 days after tumor injection. (**B**) Kaplan-Meier analysis of time to formation of metastases visible by bioluminescence imaging or death in mice. (**C**) Representative bioluminescence images of control mice (human IgG injected) and T-DM1 treated mice 124 days after tumor injection.

Supplemental Figure 1. Dormant cells induced by serum starvation in PCa cells and BCa cells

(**A**) Dead cells detected by trypan blue exclusion after 3 days of culture in the presence or absence of FBS. Data are shown as mean ± S.D. (N=3). (**B**) Cell surface expression on PC3 regarding 27 proteins selected from proteomics analysis. + ; expressed on cell surface. -; not detected. (**C**) Histograms showing expression levels of CD146 and CD71 on the surface of PC3 cells cultured in the presence or absence of FBS. (**D**) Cell number (%) after 3 days of culture in the presence or absence of FBS in PCa cells and normal prostate epithelial cells, PNT2. Data are shown as mean ± S.D. (N=3). (**E**) Histograms showing p27 expression. (**F**) Cell number (%) of BCa cells after 3 days of culture in the presence or absence of FBS. Data are shown as mean ± S.D. (N=3). (**G**) HER2 cell surface expression (MFI) are shown as mean ± S.D. (N=3).

Supplemental Figure 2. HER2 cell surface expression on dormant BCa cells induced by a CDK4/6 inhibitor

(**A**) Percent of BCa cells after 3 days of culture in the presence or absence of a CDK4/6 inhibitor, abemaciclib. Data are shown as mean ± S.D. (N=3). (**B**) Percent of dead cells after 3 days of culture in the presence or absence of abemaciclib. Data are shown as mean ± S.D. (N=3). (**C**) Relative expression of cell surface HER2 after 3 days of culture in the presence or absence of abemaciclib. Data are expressed as mean ± S.D. (N=3).

References

[1] G.D. Roodman, Mechanisms of bone metastasis, N Engl J Med, 350 (2004) 1655-1664.
[2] J. Ferlay, I. Soerjomataram, R. Dikshit, S. Eser, C. Mathers, M. Rebelo, D.M. Parkin, D. Forman, F. Bray, Cancer incidence and mortality worldwide: sources, methods and major patterns in GLOBOCAN 2012, Int J Cancer, 136 (2015) E359-386.
[3] N. Sathiakumar, E. Delzell, M.A. Morrisey, C. Falkson, M. Yong, V. Chia, J. Blackburn, T. Arora, M.L. Kilgore, Mortality following bone metastasis and skeletal-related events among men with prostate cancer: a population-based analysis of US Medicare beneficiaries, 1999-2006, Prostate Cancer Prostatic Dis, 14 (2011) 177-183.
[4] K. Pantel, C. Alix-Panabieres, S. Riethdorf, Cancer micrometastases, Nat Rev Clin Oncol, 6 (2009) 339-351.
[5] Y. Shiozawa, E.A. Pedersen, A.M. Havens, Y. Jung, A. Mishra, J. Joseph, J.K. Kim, L.R. Patel, C. Ying, A.M. Ziegler, M.J. Pienta, J. Song, J. Wang, R.D. Loberg, P.H. Krebsbach, K.J. Pienta, R.S. Taichman, Human prostate cancer metastases target the hematopoietic stem cell niche to establish footholds in mouse bone marrow, J Clin Invest, 121 (2011) 1298-1312.
[6] P.I. Croucher, M.M. McDonald, T.J. Martin, Bone metastasis: the importance of the neighbourhood, Nat Rev Cancer, 16 (2016) 373-386.
[7] L. Chery, H.M. Lam, I. Coleman, B. Lakely, R. Coleman, S. Larson, J.A. Aguirre-Ghiso, J. Xia, R. Gulati, P.S. Nelson, B. Montgomery, P. Lange, L.A. Snyder, R.L. Vessella, C. Morrissey, Characterization of single disseminated prostate cancer cells reveals tumor cell heterogeneity and identifies dormancy associated pathways, Oncotarget, 5 (2014) 9939-9951.
[8] K. Yumoto, M.R. Eber, J.E. Berry, R.S. Taichman, Y. Shiozawa, Molecular pathways: niches in metastatic dormancy, Clin Cancer Res, 20 (2014) 3384-3389.
[9] M.S. Sosa, P. Bragado, J.A. Aguirre-Ghiso, Mechanisms of disseminated cancer cell dormancy: an awakening field, Nat Rev Cancer, 14 (2014) 611-622.
[10] Y. Shiozawa, E.A. Pedersen, L.R. Patel, A.M. Ziegler, A.M. Havens, Y. Jung, J. Wang, S. Zalucha, R.D. Loberg, K.J. Pienta, R.S. Taichman, GAS6/AXL axis regulates prostate cancer invasion, proliferation, and survival in the bone marrow niche, Neoplasia, 12 (2010) 116-127.
[11] K. Yumoto, M.R. Eber, J. Wang, F.C. Cackowski, A.M. Decker, E. Lee, A.R. Nobre, J.A. Aguirre-Ghiso, Y. Jung, R.S. Taichman, Axl is required for TGF-beta2-induced dormancy of prostate cancer cells in the bone marrow, Sci Rep, 6 (2016) 36520.
[12] P. Bragado, Y. Estrada, F. Parikh, S. Krause, C. Capobianco, H.G. Farina, D.M. Schewe, J.A. Aguirre-Ghiso, TGF-beta2 dictates disseminated tumour cell fate in target organs through TGF-beta-RIII and p38alpha/beta signalling, Nat Cell Biol, 15 (2013) 1351-1361.
[13] A. Kobayashi, H. Okuda, F. Xing, P.R. Pandey, M. Watabe, S. Hirota, S.K. Pai, W. Liu, K. Fukuda, C. Chambers, A. Wilber, K. Watabe, Bone morphogenetic protein 7 in dormancy and metastasis of prostate cancer stem-like cells in bone, J Exp Med, 208 (2011) 2641-2655.
[14] S. Sharma, F. Xing, Y. Liu, K. Wu, N. Said, R. Pochampally, Y. Shiozawa, H.K. Lin, K.C. Balaji, K. Watabe, Secreted Protein Acidic and Rich in Cysteine (SPARC) Mediates Metastatic Dormancy of Prostate Cancer in Bone, J Biol Chem, 291 (2016) 19351-19363.
[15] D. Ren, Y. Dai, Q. Yang, X. Zhang, W. Guo, L. Ye, S. Huang, X. Chen, Y. Lai, H. Du, C. Lin, X. Peng, L. Song, Wnt5a induces and maintains prostate cancer cells dormancy in bone, J Exp Med, 216 (2019) 428-449.
[16] H.J. Burstein, The distinctive nature of HER2-positive breast cancers, N Engl J Med, 353 (2005) 1652-1654.
[17] Y. Yarden, M.X. Sliwkowski, Untangling the ErbB signalling network, Nat Rev Mol Cell Biol, 2 (2001) 127-137.
[18] J.W. Park, R.M. Neve, J. Szollosi, C.C. Benz, Unraveling the biologic and clinical complexities of HER2, Clin Breast Cancer, 8 (2008) 392-401.

[19] D.J. Slamon, G.M. Clark, S.G. Wong, W.J. Levin, A. Ullrich, W.L. McGuire, Human breast cancer: correlation of relapse and survival with amplification of the HER-2/neu oncogene, Science, 235 (1987) 177-182.
[20] D.J. Slamon, B. Leyland-Jones, S. Shak, H. Fuchs, V. Paton, A. Bajamonde, T. Fleming, W. Eiermann, J. Wolter, M. Pegram, J. Baselga, L. Norton, Use of chemotherapy plus a monoclonal antibody against HER2 for metastatic breast cancer that overexpresses HER2, N Engl J Med, 344 (2001) 783-792.
[21] M.J. Piccart-Gebhart, M. Procter, B. Leyland-Jones, A. Goldhirsch, M. Untch, I. Smith, L. Gianni, J. Baselga, R. Bell, C. Jackisch, D. Cameron, M. Dowsett, C.H. Barrios, G. Steger, C.S. Huang, M. Andersson, M. Inbar, M. Lichinitser, I. Lang, U. Nitz, H. Iwata, C. Thomssen, C. Lohrisch, T.M. Suter, J. Ruschoff, T. Suto, V. Greatorex, C. Ward, C. Straehle, E. McFadden, M.S. Dolci, R.D. Gelber, T. Herceptin Adjuvant Trial Study, Trastuzumab after adjuvant chemotherapy in HER2-positive breast cancer, N Engl J Med, 353 (2005) 1659-1672.
[22] E.H. Romond, E.A. Perez, J. Bryant, V.J. Suman, C.E. Geyer, Jr., N.E. Davidson, E. Tan-Chiu, S. Martino, S. Paik, P.A. Kaufman, S.M. Swain, T.M. Pisansky, L. Fehrenbacher, L.A. Kutteh, V.G. Vogel, D.W. Visscher, G. Yothers, R.B. Jenkins, A.M. Brown, S.R. Dakhil, E.P. Mamounas, W.L. Lingle, P.M. Klein, J.N. Ingle, N. Wolmark, Trastuzumab plus adjuvant chemotherapy for operable HER2-positive breast cancer, N Engl J Med, 353 (2005) 1673-1684.
[23] E.A. Perez, E.H. Romond, V.J. Suman, J.H. Jeong, G. Sledge, C.E. Geyer, Jr., S. Martino, P. Rastogi, J. Gralow, S.M. Swain, E.P. Winer, G. Colon-Otero, N.E. Davidson, E. Mamounas, J.A. Zujewski, N. Wolmark, Trastuzumab plus adjuvant chemotherapy for human epidermal growth factor receptor 2-positive breast cancer: planned joint analysis of overall survival from NSABP B-31 and NCCTG N9831, J Clin Oncol, 32 (2014) 3744-3752.
[24] D. Cameron, M.J. Piccart-Gebhart, R.D. Gelber, M. Procter, A. Goldhirsch, E. de Azambuja, G. Castro, Jr., M. Untch, I. Smith, L. Gianni, J. Baselga, N. Al-Sakaff, S. Lauer, E. McFadden, B. Leyland-Jones, R. Bell, M. Dowsett, C. Jackisch, T. Herceptin Adjuvant Trial Study, 11 years' follow-up of trastuzumab after adjuvant chemotherapy in HER2-positive early breast cancer: final analysis of the HERceptin Adjuvant (HERA) trial, Lancet, 389 (2017) 1195-1205.
[25] N. Sharifi, A. Salmaninejad, S. Ferdosi, A.N. Bajestani, M. Khaleghiyan, M.A. Estiar, M. Jamali, M.R. Nowroozi, A. Shakoori, HER2 gene amplification in patients with prostate cancer: Evaluating a CISH-based method, Oncol Lett, 12 (2016) 4651-4658.
[26] G. Di Lorenzo, G. Tortora, F.P. D'Armiento, G. De Rosa, S. Staibano, R. Autorino, M. D'Armiento, M. De Laurentiis, S. De Placido, G. Catalano, A.R. Bianco, F. Ciardiello, Expression of epidermal growth factor receptor correlates with disease relapse and progression to androgen-independence in human prostate cancer, Clin Cancer Res, 8 (2002) 3438-3444.
[27] K.C. Day, G. Lorenzatti Hiles, M. Kozminsky, S.J. Dawsey, A. Paul, L.J. Broses, R. Shah, L.P. Kunja, C. Hall, N. Palanisamy, S. Daignault-Newton, L. El-Sawy, S.J. Wilson, A. Chou, K.W. Ignatoski, E. Keller, D. Thomas, S. Nagrath, T. Morgan, M.L. Day, HER2 and EGFR Overexpression Support Metastatic Progression of Prostate Cancer to Bone, Cancer Res, 77 (2017) 74-85.
[28] H. Takahashi, K. Yumoto, K. Yasuhara, E.T. Nadres, Y. Kikuchi, R.S. Taichman, K. Kuroda, Anticancer polymers designed for killing dormant prostate cancer cells, Sci Rep, 9 (2019) 1096.
[29] T. Oki, K. Nishimura, J. Kitaura, K. Togami, A. Maehara, K. Izawa, A. Sakaue-Sawano, A. Niida, S. Miyano, H. Aburatani, H. Kiyonari, A. Miyawaki, T. Kitamura, A novel cell-cycle-indicator, mVenus-p27K-, identifies quiescent cells and visualizes G0-G1 transition, Sci Rep, 4 (2014) 4012.
[30] C.G. Murphy, The Role of CDK4/6 Inhibitors in Breast Cancer, Curr Treat Options Oncol, 20 (2019) 52.
[31] Q. Pan, A. Sathe, P.C. Black, P.J. Goebell, A.M. Kamat, B. Schmitz-Draeger, R. Nawroth, CDK4/6 Inhibitors in Cancer Therapy: A Novel Treatement Strategy for Bladder Cancer, Bladder Cancer, 3 (2017) 79-88.

[32] E. Hamilton, J.R. Infante, Targeting CDK4/6 in patients with cancer, Cancer Treat Rev, 45 (2016) 129-138.
[33] T.K. Eggersmann, T. Degenhardt, O. Gluz, R. Wuerstlein, N. Harbeck, CDK4/6 Inhibitors Expand the Therapeutic Options in Breast Cancer: Palbociclib, Ribociclib and Abemaciclib, BioDrugs, 33 (2019) 125-135.
[34] A. Palumbo, G. Lau, M. Saraceni, Abemaciclib: The Newest CDK4/6 Inhibitor for the Treatment of Breast Cancer, Ann Pharmacother, 53 (2019) 178-185.
[35] E.A. Pedersen, Y. Shiozawa, A. Mishra, R.S. Taichman, Structure and function of the solid tumor niche, Front Biosci (Schol Ed), 4 (2012) 1-15.
[36] T.T. Junttila, G. Li, K. Parsons, G.L. Phillips, M.X. Sliwkowski, Trastuzumab-DM1 (T-DM1) retains all the mechanisms of action of trastuzumab and efficiently inhibits growth of lapatinib insensitive breast cancer, Breast Cancer Res Treat, 128 (2011) 347-356.
[37] M. Barok, M. Tanner, K. Koninki, J. Isola, Trastuzumab-DM1 causes tumour growth inhibition by mitotic catastrophe in trastuzumab-resistant breast cancer cells in vivo, Breast Cancer Res, 13 (2011) R46.
[38] Z. Mitri, T. Constantine, R. O'Regan, The HER2 Receptor in Breast Cancer: Pathophysiology, Clinical Use, and New Advances in Therapy, Chemother Res Pract, 2012 (2012) 743193.
[39] D.Y. Oh, Y.J. Bang, HER2-targeted therapies - a role beyond breast cancer, Nat Rev Clin Oncol, (2019).
[40] M. Javle, C. Churi, H.C. Kang, R. Shroff, F. Janku, R. Surapaneni, M. Zuo, C. Barrera, H. Alshamsi, S. Krishnan, L. Mishra, R.A. Wolff, A.O. Kaseb, M.B. Thomas, A.B. Siegel, HER2/neu-directed therapy for biliary tract cancer, J Hematol Oncol, 8 (2015) 58.
[41] A. Sartore-Bianchi, L. Trusolino, C. Martino, K. Bencardino, S. Lonardi, F. Bergamo, V. Zagonel, F. Leone, I. Depetris, E. Martinelli, T. Troiani, F. Ciardiello, P. Racca, A. Bertotti, G. Siravegna, V. Torri, A. Amatu, S. Ghezzi, G. Marrapese, L. Palmeri, E. Valtorta, A. Cassingena, C. Lauricella, A. Vanzulli, D. Regge, S. Veronese, P.M. Comoglio, A. Bardelli, S. Marsoni, S. Siena, Dual-targeted therapy with trastuzumab and lapatinib in treatment-refractory, KRAS codon 12/13 wild-type, HER2-positive metastatic colorectal cancer (HERACLES): a proof-of-concept, multicentre, open-label, phase 2 trial, Lancet Oncol, 17 (2016) 738-746.
[42] B.T. Li, R. Shen, D. Buonocore, Z.T. Olah, A. Ni, M.S. Ginsberg, G.A. Ulaner, M. Offin, D. Feldman, T. Hembrough, F. Cecchi, S. Schwartz, N. Pavlakis, S. Clarke, H.H. Won, E.B. Brzostowski, G.J. Riely, D.B. Solit, D.M. Hyman, A. Drilon, C.M. Rudin, M.F. Berger, J. Baselga, M. Scaltriti, M.E. Arcila, M.G. Kris, Ado-Trastuzumab Emtansine for Patients With HER2-Mutant Lung Cancers: Results From a Phase II Basket Trial, J Clin Oncol, 36 (2018) 2532-2537.
[43] V. Roy, E.A. Perez, Beyond trastuzumab: small molecule tyrosine kinase inhibitors in HER-2-positive breast cancer, Oncologist, 14 (2009) 1061-1069.
[44] N. Gao, Z. Zhang, B.H. Jiang, X. Shi, Role of PI3K/AKT/mTOR signaling in the cell cycle progression of human prostate cancer, Biochem Biophys Res Commun, 310 (2003) 1124-1132.
[45] S.M. Kim, J.H. Park, K.D. Kim, D. Nam, B.S. Shim, S.H. Kim, K.S. Ahn, S.H. Choi, K.S. Ahn, Brassinin induces apoptosis in PC-3 human prostate cancer cells through the suppression of PI3K/Akt/mTOR/S6K1 signaling cascades, Phytother Res, 28 (2014) 423-431.
[46] B.T. Vo, D. Morton, Jr., S. Komaragiri, A.C. Millena, C. Leath, S.A. Khan, TGF-beta effects on prostate cancer cell migration and invasion are mediated by PGE2 through activation of PI3K/AKT/mTOR pathway, Endocrinology, 154 (2013) 1768-1779.
[47] M.P. Goetz, M. Toi, M. Campone, J. Sohn, S. Paluch-Shimon, J. Huober, I.H. Park, O. Tredan, S.C. Chen, L. Manso, O.C. Freedman, G. Garnica Jaliffe, T. Forrester, M. Frenzel, S. Barriga, I.C. Smith, N. Bourayou, A. Di Leo, MONARCH 3: Abemaciclib As Initial Therapy for Advanced Breast Cancer, J Clin Oncol, 35 (2017) 3638-3646.

[48] P.M.R. Pereira, S.K. Sharma, L.M. Carter, K.J. Edwards, J. Pourat, A. Ragupathi, Y.Y. Janjigian, J.C. Durack, J.S. Lewis, Caveolin-1 mediates cellular distribution of HER2 and affects trastuzumab binding and therapeutic efficacy, Nat Commun, 9 (2018) 5137.
[49] C.R. Pound, A.W. Partin, M.A. Eisenberger, D.W. Chan, J.D. Pearson, P.C. Walsh, Natural history of progression after PSA elevation following radical prostatectomy, JAMA, 281 (1999) 1591-1597.
[50] F.C. Cackowski, Y. Wang, J.T. Decker, C. Sifuentes, S. Weindorf, Y. Jung, Y. Wang, A.M. Decker, K. Yumoto, N. Szerlip, L. Buttitta, K.J. Pienta, T.M. Morgan, R.S. Taichman, Detection and isolation of disseminated tumor cells in bone marrow of patients with clinically localized prostate cancer, Prostate, 79 (2019) 1715-1727.
[51] P. Nagy, E. Friedlander, M. Tanner, A.I. Kapanen, K.L. Carraway, J. Isola, T.M. Jovin, Decreased accessibility and lack of activation of ErbB2 in JIMT-1, a herceptin-resistant, MUC4-expressing breast cancer cell line, Cancer Res, 65 (2005) 473-482.
[52] Y. Kataoka, T. Mukohara, H. Shimada, N. Saijo, M. Hirai, H. Minami, Association between gain-of-function mutations in PIK3CA and resistance to HER2-targeted agents in HER2-amplified breast cancer cell lines, Ann Oncol, 21 (2010) 255-262.
[53] S. Chandarlapaty, R.A. Sakr, D. Giri, S. Patil, A. Heguy, M. Morrow, S. Modi, L. Norton, N. Rosen, C. Hudis, T.A. King, Frequent mutational activation of the PI3K-AKT pathway in trastuzumab-resistant breast cancer, Clin Cancer Res, 18 (2012) 6784-6791.
[54] C.L. Vogel, M.A. Cobleigh, D. Tripathy, J.C. Gutheil, L.N. Harris, L. Fehrenbacher, D.J. Slamon, M. Murphy, W.F. Novotny, M. Burchmore, S. Shak, S.J. Stewart, M. Press, Efficacy and safety of trastuzumab as a single agent in first-line treatment of HER2-overexpressing metastatic breast cancer, J Clin Oncol, 20 (2002) 719-726.
[55] T.T. Wu, R.A. Sikes, Q. Cui, G.N. Thalmann, C. Kao, C.F. Murphy, H. Yang, H.E. Zhau, G. Balian, L.W. Chung, Establishing human prostate cancer cell xenografts in bone: induction of osteoblastic reaction by prostate-specific antigen-producing tumors in athymic and SCID/bg mice using LNCaP and lineage-derived metastatic sublines, Int J Cancer, 77 (1998) 887-894.
[56] M. Yamashita, S. Kitano, H. Aikawa, A. Kuchiba, M. Hayashi, N. Yamamoto, K. Tamura, A. Hamada, A novel method for evaluating antibody-dependent cell-mediated cytotoxicity by flowcytometry using cryopreserved human peripheral blood mononuclear cells, Sci Rep, 6 (2016) 19772.

Figure 1

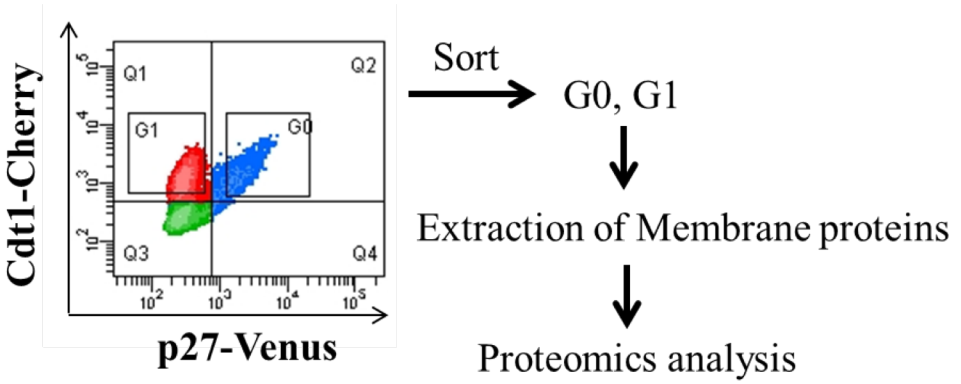

Table 1

G0 > G1		G0	G1
	SLC16A1	45	13
	CD9	30	27
	HSPG2	24	7
	THBS1	21	0
	CDH11	10	7
	CLDN4	8	4
	HER2	5	0
	CD239	4	2
	CD81	4	0
	TMEM87A	4	0
	CD228	4	0
	CD18	4	0
	CD87	3	0
	CD148	2	0
	CD171	2	0
	SDC4	2	0

G0 < G1		G0	G1
	CD71	154	206
	PODXL	55	82
	PLXNA1	22	34
	CD146	17	46
	SEMA4B	11	23
	CD318	5	18
	SLC12A7	0	6
	CD10	0	5
	CD46	0	4
	EPHB4	0	4

G0 = G1		G0	G1
	CD166	45	45

Figure 2

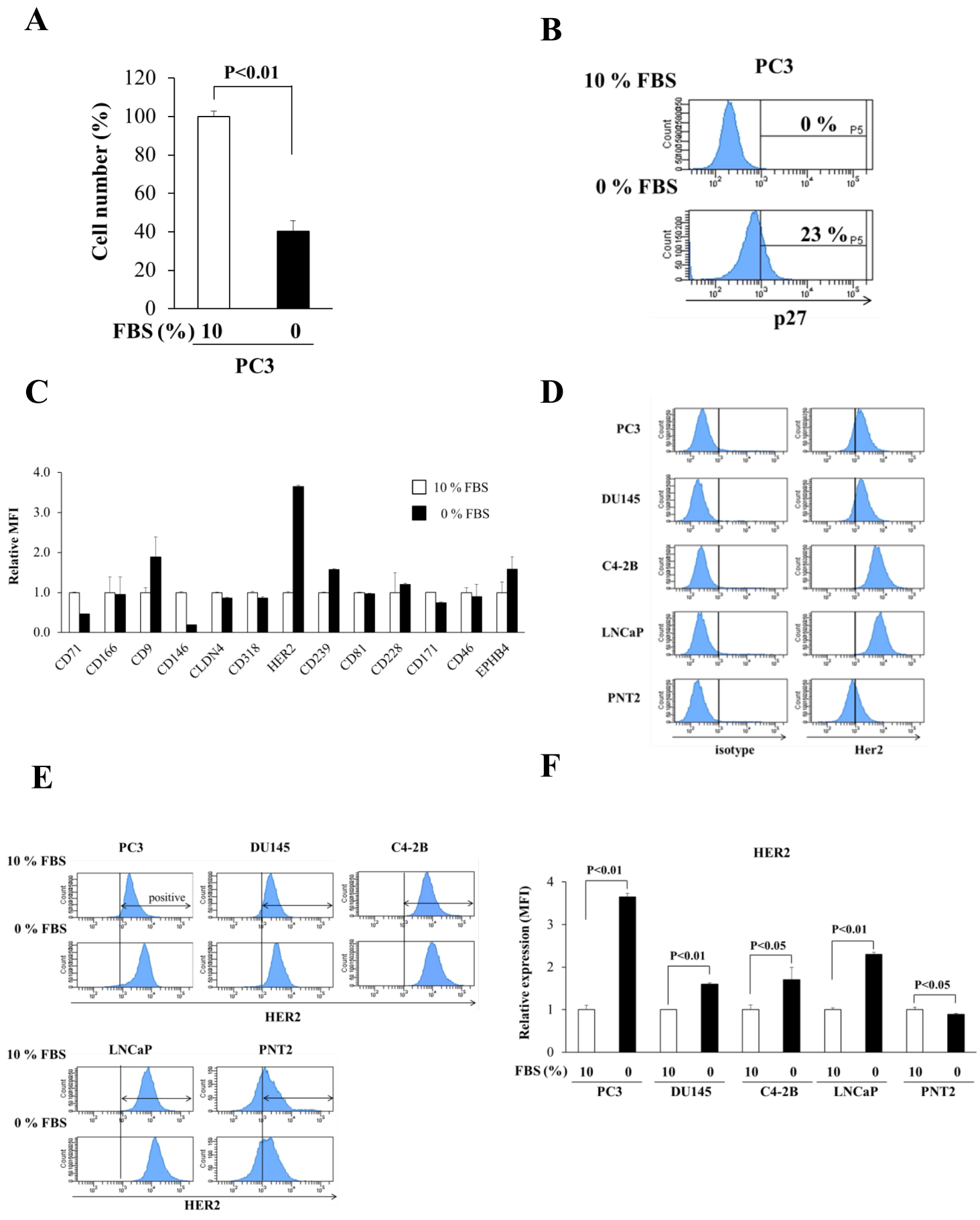
A
P<0.01
Cell number (%)
120
100
80
60
40
20
0
FBS (%) 10
0
PC3
B
PC3
10 % FBS
0 %
P5
Count
0 % FBS
23 %
P5
Count
p27
C
Relative MFI
4.0
3.0
2.0
1.0
0.0
10 % FBS
0 % FBS
CD71
CD166
CD9
CD146
CLDN4
CD318
HER2
CD239
CD81
CD228
CD171
CD46
EPHB4
D
PC3
DU145
C4-2B
LNCaP
PNT2
isotype
Her2
E
PC3
DU145
C4-2B
10 % FBS
0 % FBS
positive
HER2
LNCaP
PNT2
10 % FBS
0 % FBS
HER2
F
HER2
Relative expression (MFI)
P<0.01
P<0.01
P<0.05
P<0.01
P<0.05
4
3
2
1
0
FBS (%) 10 0 10 0 10 0 10 0 10 0
PC3
DU145
C4-2B
LNCaP
PNT2

Figure 3

A

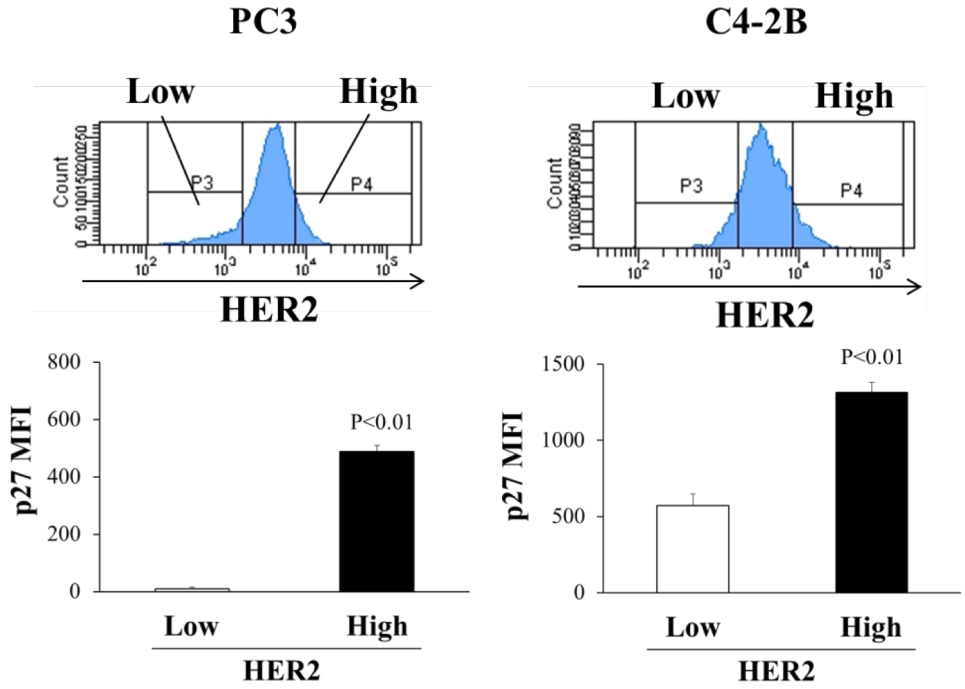
PC3
C4-2B
Low
High
P3
P4
Count
HER2
p27 MFI
P<0.01
800
600
400
200
0
1500
1000
500
Low
High
HER2

B

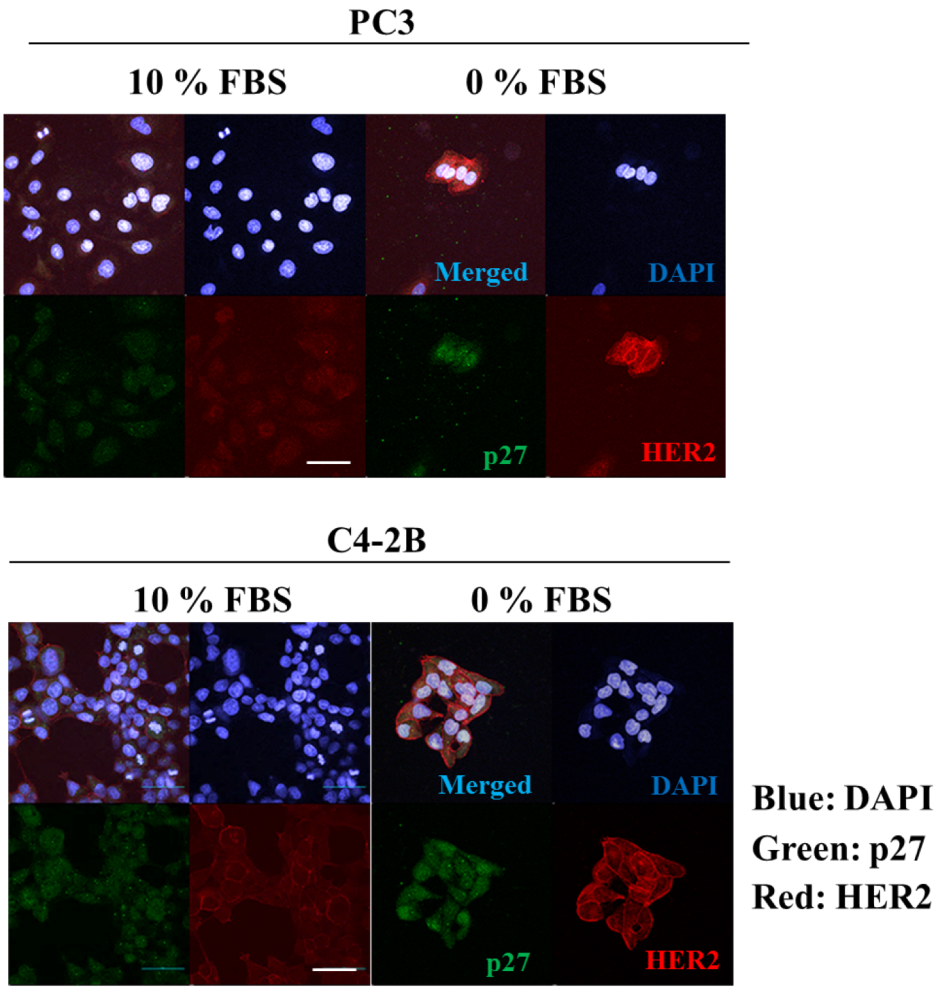
PC3
10 % FBS
0 % FBS
Merged
DAPI
p27
HER2
C4-2B
10 % FBS
0 % FBS
Merged
DAPI
p27
HER2
Blue: DAPI
Green: p27
Red: HER2

Figure 4

A

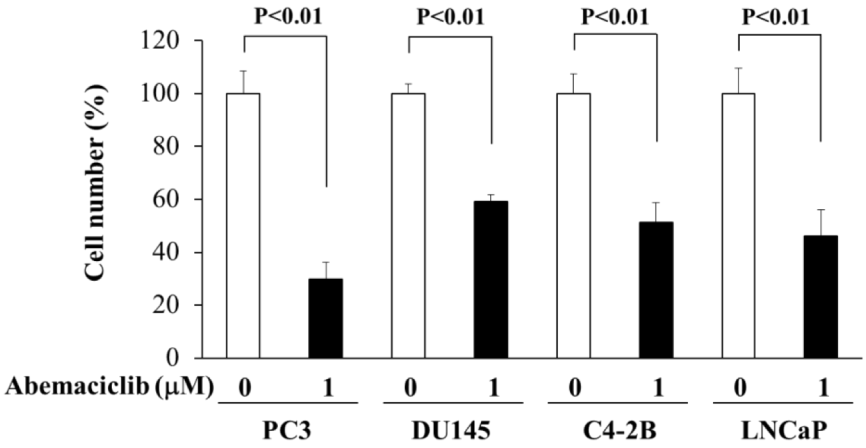
P<0.01
P<0.01
P<0.01
P<0.01
120
100
80
60
40
20
0
Cell number (%)
Abemaciclib (μM)
0
1
0
1
0
1
0
1
PC3
DU145
C4-2B
LNCaP

B

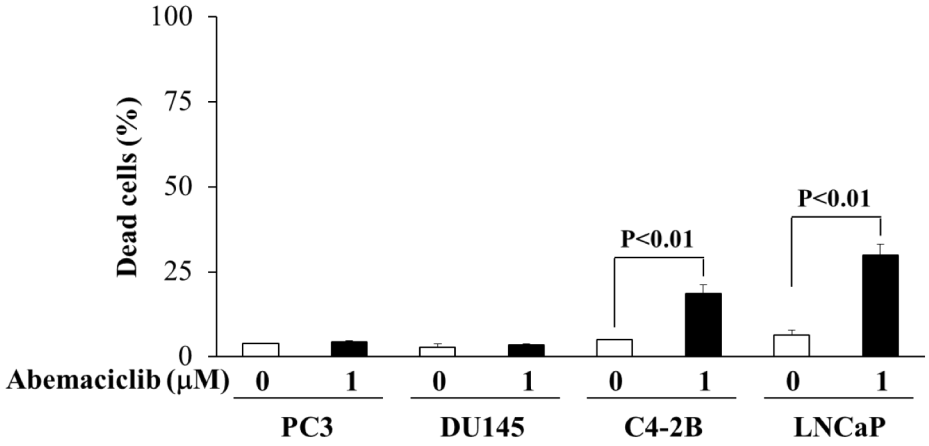
100
75
50
25
0
Dead cells (%)
P<0.01
P<0.01
Abemaciclib (μM)
0
1
0
1
0
1
0
1
PC3
DU145
C4-2B
LNCaP

C

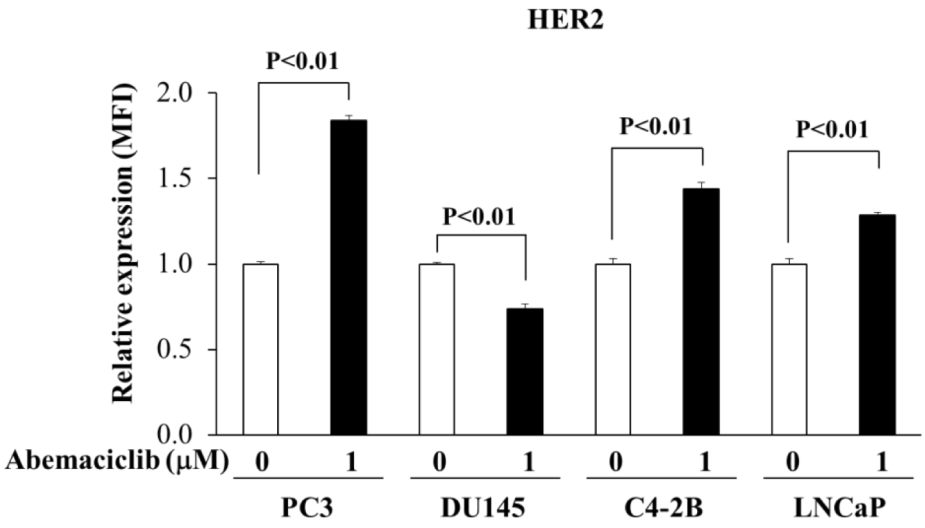
HER2
P<0.01
P<0.01
P<0.01
P<0.01
2.0
1.5
1.0
0.5
0.0
Relative expression (MFI)
Abemaciclib (μM)
0
1
0
1
0
1
0
1
PC3
DU145
C4-2B
LNCaP

Figure 5

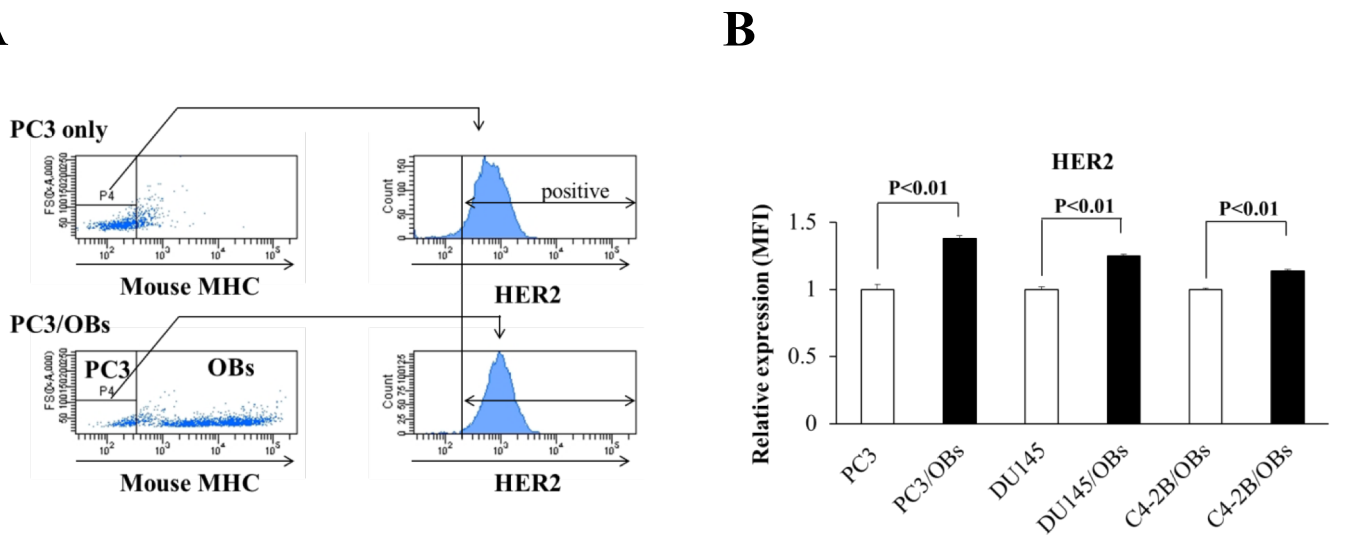

Figure 6

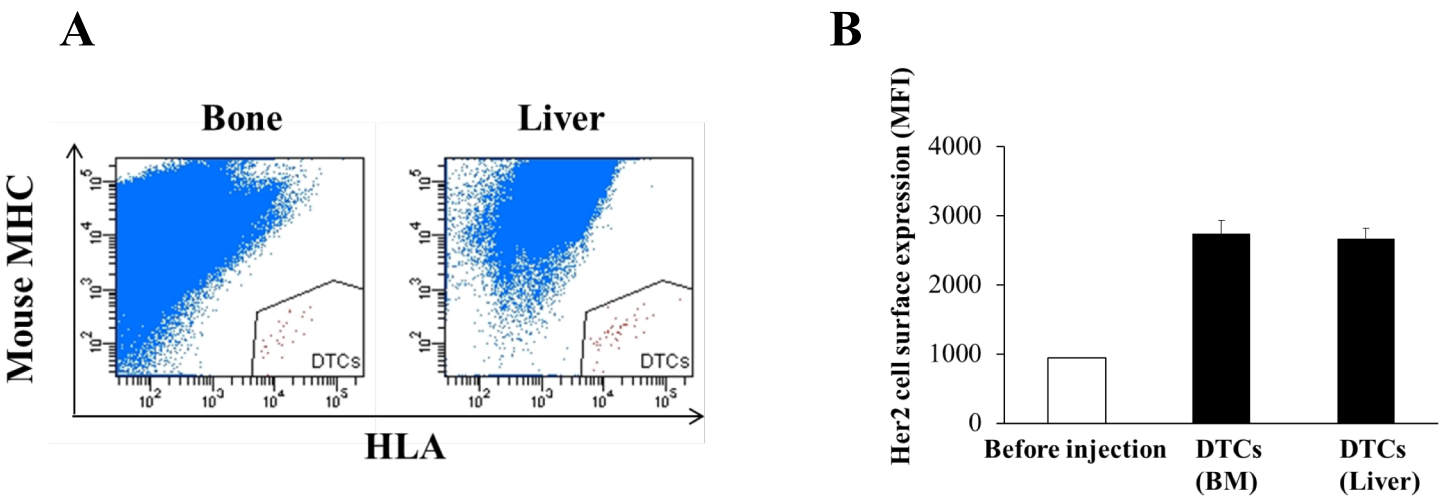

Figure 7

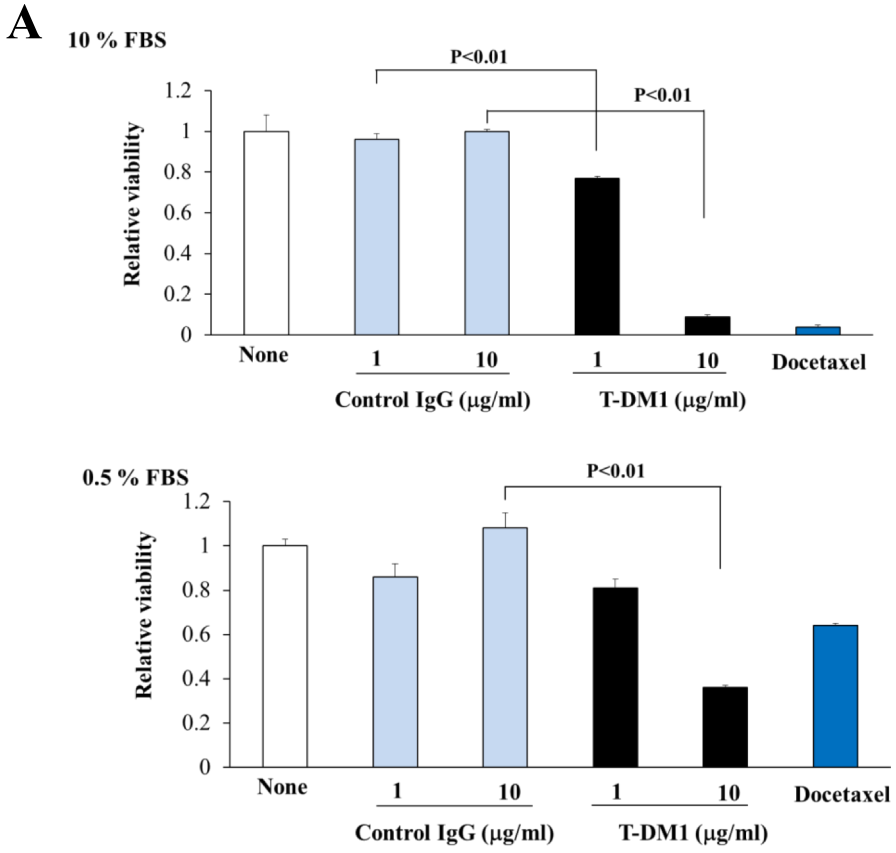
A
10 % FBS
P<0.01
P<0.01
Relative viability
1.2
1
0.8
0.6
0.4
0.2
0
None
1
10
1
10
Docetaxel
Control IgG (μg/ml)
T-DM1 (μg/ml)
0.5 % FBS
P<0.01
Relative viability
1.2
1
0.8
0.6
0.4
0.2
0
None
1
10
1
10
Docetaxel
Control IgG (μg/ml)
T-DM1 (μg/ml)

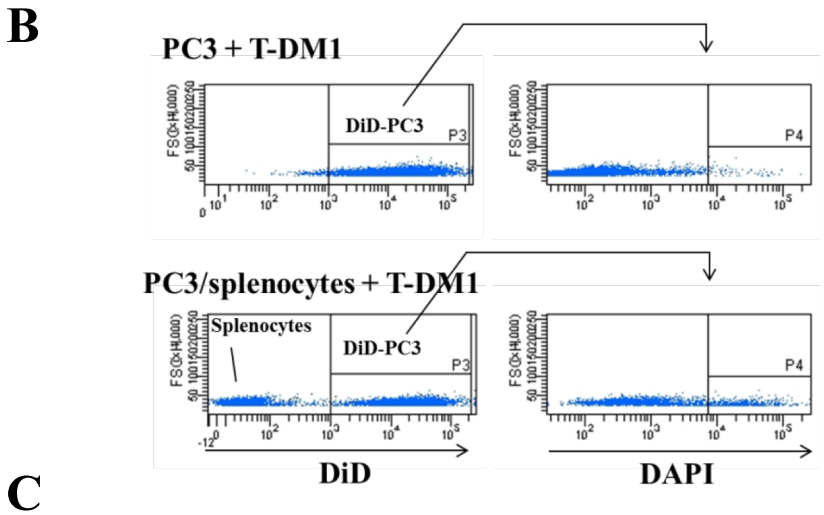
B
PC3 + T-DM1
DiD-PC3
P3
P4
PC3/splenocytes + T-DM1
Splenocytes
DiD-PC3
P3
P4
DiD
DAPI

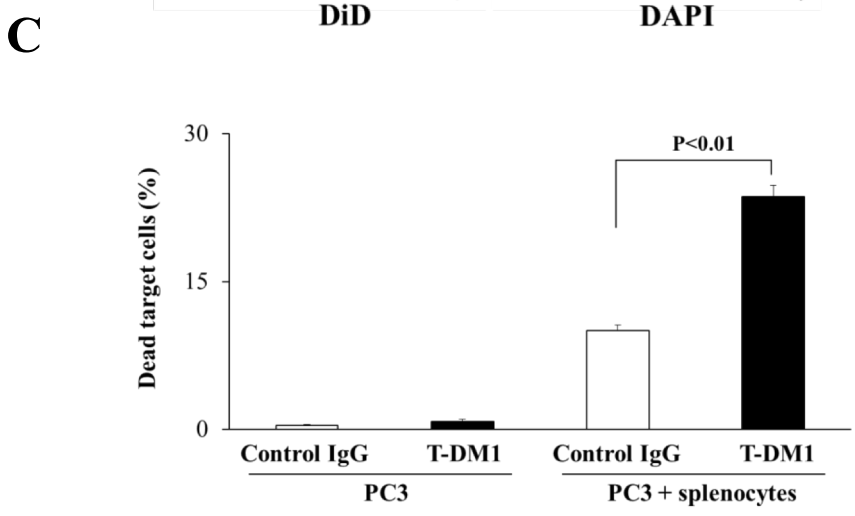
C
Dead target cells (%)
30
15
0
P<0.01
Control IgG
T-DM1
Control IgG
T-DM1
PC3
PC3 + splenocytes

Figure 8

A

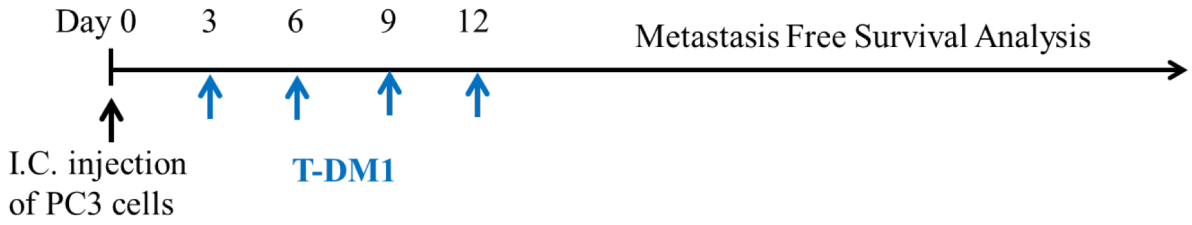
Day 0
3
6
9
12
Metastasis Free Survival Analysis
I.C. injection of PC3 cells
T-DM1

B

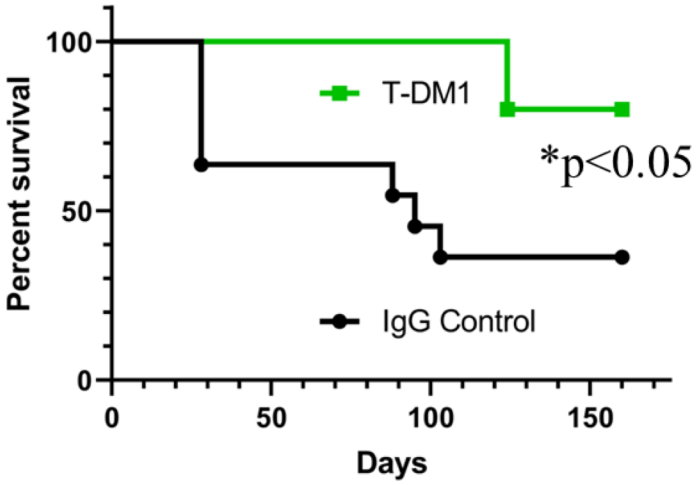
Percent survival
100
50
0
0
50
100
150
Days
T-DM1
IgG Control
*p<0.05

C

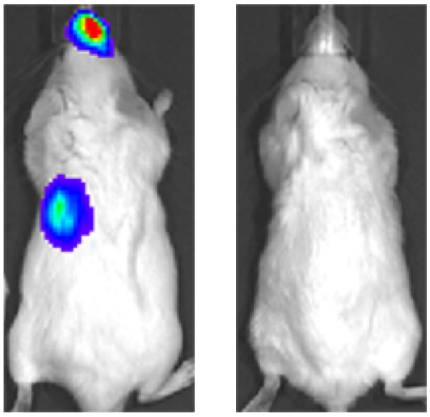
Day 124
Control IgG
T-DM1

Supplemental figure 1

A

	FBS (%)	Dead cells (%) ± S.D.
PC3	10	0
	0	0
C42B	10	0
	0	0
DU145	10	0
	0	0
LNCaP	10	0
	0	0
PNT2	10	0
	0	4.3 ±1.5

B

G0 > G1		G0	G1	Cell surface expression
	SLC16A1	45	13	–
	CD9	30	27	+
	HSPG2	24	7	–
	THBS1	21	0	–
	CDH11	10	7	–
	CLDN4	8	4	+
	HER2	5	0	+
	CD239	4	2	+
	CD81	4	0	+
	TMEM87A	4	0	–
	CD228	4	0	+
	CD18	4	0	–
	CD87	3	0	–
	CD148	2	0	–
	CD171	2	0	+
	SDC4	2	0	–

G0 < G1		G0	G1	Cell surface expression
	CD71	154	206	+
	PODXL	55	82	–
	PLXNA1	22	34	–
	CD146	17	46	+
	SEMA4B	11	23	–
	CD318	5	18	+
	SLC12A7	0	6	–
	CD10	0	5	–
	CD46	0	4	+
	EPHB4	0	4	+

G0 = G1		G0	G1	Cell surface expression
	CD166	45	45	+

C

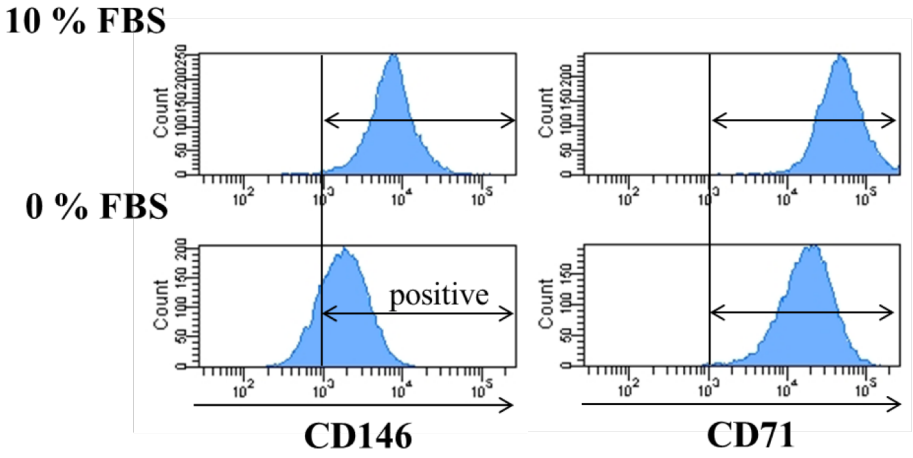

Supplemental figure 1

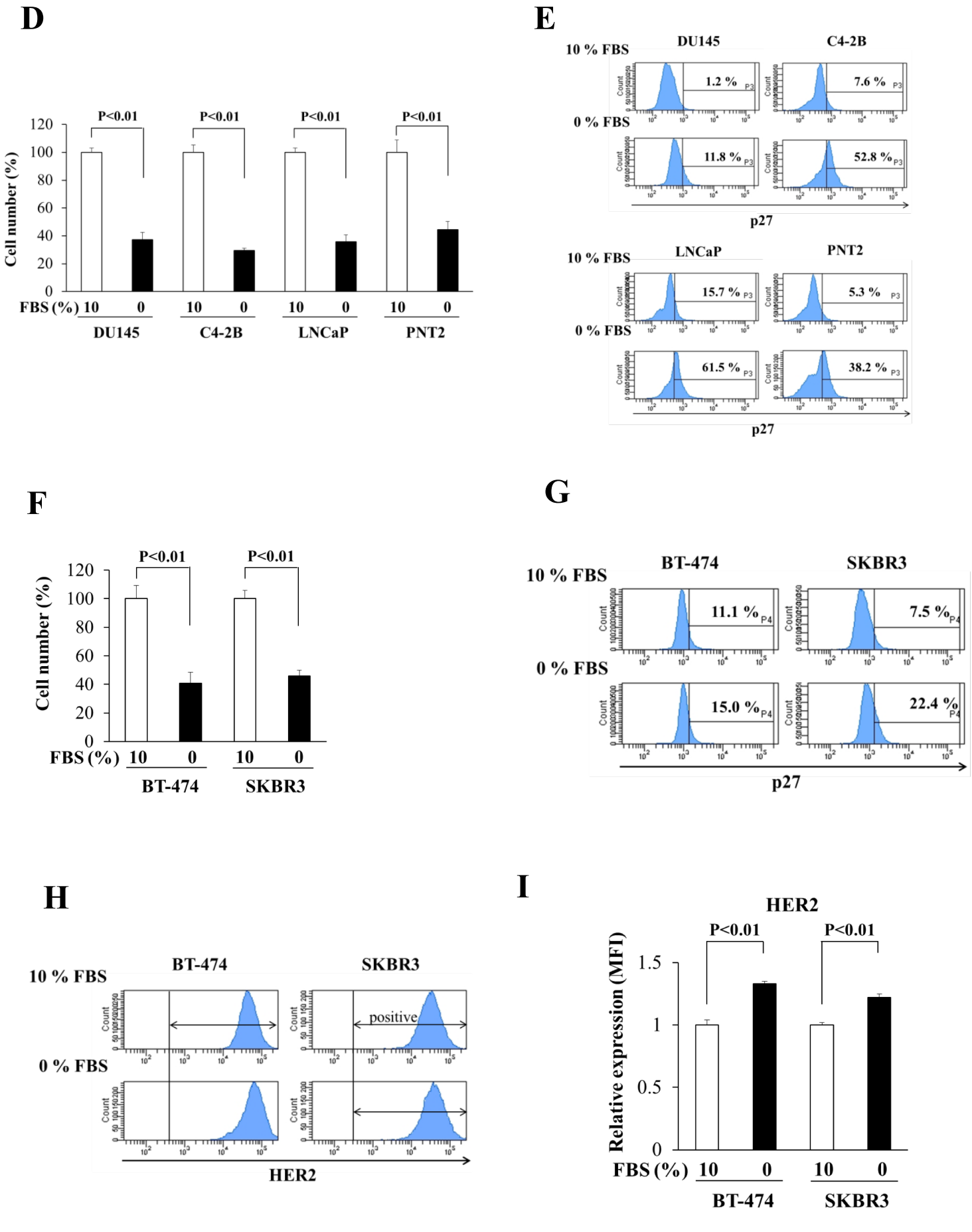

Supplemental figure 2

A

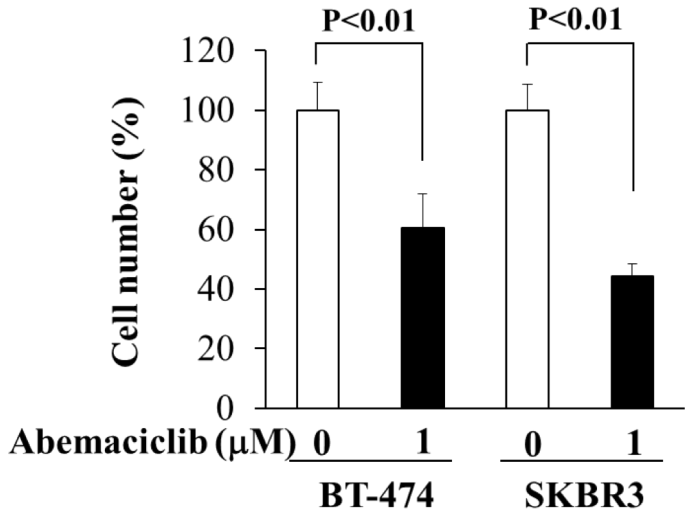

B

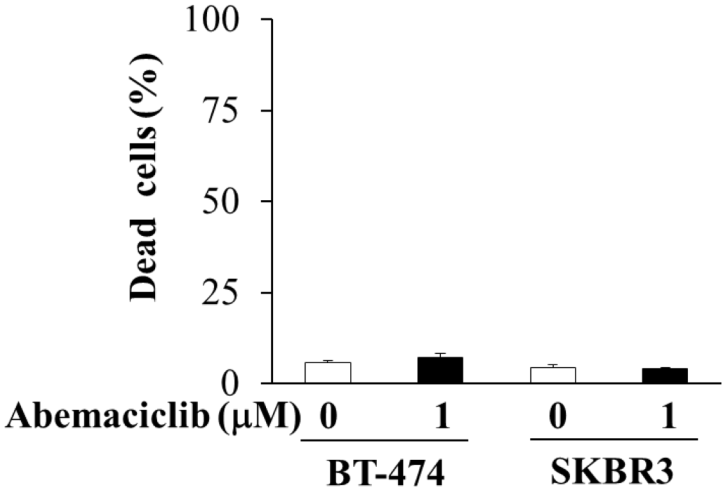

C

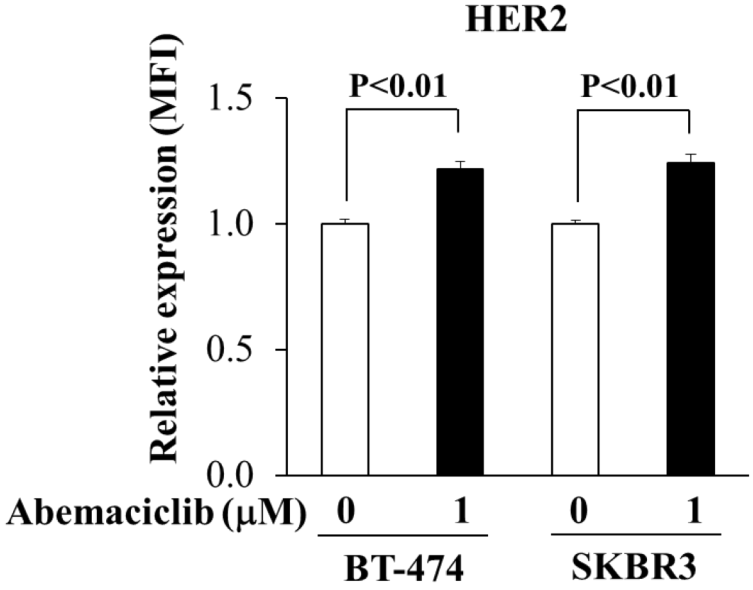

Prostate Cancer Cells Stimulate Macrophages to Express Transferrin in Bone Marrow

Kenji Yumoto[1], Maiko Omi[2], Frank C. Cackowski[1,3], Yu Wang[1], Ann Decker[1], Younghun Jung[1], Yuji Mishina[2], Laura Buttitta[4] and Russell S. Taichman[1]

[1]Department of Periodontics and Oral Medicine, University of Michigan School of Dentistry, Ann Arbor, MI 48109, USA
[2]Department of Biological and Materials Sciences, University of Michigan School of Dentistry, Ann Arbor, MI 48109, USA
[3]Department of Internal Medicine, Division of Hematology and Oncology, University of Michigan School of Medicine, Ann Arbor, MI 48109, USA
[4]Department of Molecular Cellular and Developmental Biology, University of Michigan College of Arts and Sciences

Corresponding Author:
Russell S. Taichman D.M.D., D.M.Sc.
Department of Periodontics
University of Alabama at Birmingham School of Dentistry
SDB #406
1720 2nd Avenue South
Birmingham, AL 35294-0007
Telephone: 205.934.4720
Email: taichman@uab.edu

Abstract

Transferin (TF) is an iron-transporting protein, which was found in high levels in the bone marrow (BM), promotes the proliferation of prostate cancer (PCa) cells. Yet how TF levels are altered in response to bone metastasis and PCa progression, and what cells are the sources of TF in the context of metastasis remains unclear. In this study, we injected PCa cells into the tibiae of mice to explore TF expression in BM. We found that TF protein levels are enhanced in marrow in the presence of PCa cells, and observed that osteoclasts express TF. Critically, we demonstrate that PCa cells stimulate macrophages to express TF during their differentiation into osteoclasts. Further, both RANKL and TNF-α induce the expression of TF by macrophages. These data suggest that a vicious cycle may be established between osteoclasts and PCa cells, to promote the growth of PCa in marrow through TF expression

Introduction

More than 70% of prostate cancer (PCa) patients develop bone metastases [1] [2], which ultimately are a major cause of death in the patients [3] [4]. Bone metastases cause severe pain, impaired mobility, pathologic fractures, and lead to increased risk of patient mortality [1].

Current treatments including radiotherapy and bisphosphonates can slow the growth of bone metastases, but rarely cure the disease [1]. Therefore, an urgent unmet medical need is to establish new therapies to treat bone metastases.

Metastasis is a multistep process comprised of the loss of intercellular adhesion, cell migration, angiogenesis, survival in the circulation, evasion of local and systemic immune surveillance, and ultimately growth at distant organs [5]. In PCa, approximately many men undergoing radical prostatectomy have disseminated tumor cells (**DTCs**) in their bone marrow (**BM**) prior to surgery [6], suggesting that DTCs exist in their BM even in the early progression when the patients are diagnosed.

In the context of patients whose disease is undetectable for years or even decades, bone metastasis is the result of the reactivation of dormant DTCs [7]. Accumulating evidence suggests that the tumor microenvironment plays a pivotal role in the regulation of tumor growth [8] [7] and may do so by activating dormancy pathways regulated by growth arrest specific 6 (GAS6) [9] [10], bone morphogenetic protein 7 (BMP-7) [11] and transforming growth factor β-2 (TGF-β2) [12]. Adding additional complexity is the process are findings that these pathways are interconnected; for example we previously reported that osteoblast expressed GAS6 binds to Axl expressed by DTCs, and its signaling induces the expression of both TGF-β ligands and their receptors (TGFBR2 and TGFBR3) [10]. Moreover, both TGF-β 2 and BMP-7 induce the expression of p27, a potent endogenous cell cycle inhibitor, by increasing phosphorylation of p38 [12] [11].

While dormancy is poorly understood, what regulates reactivation of DTC proliferation also remains largely unknown. One candidate for an activation molecule is transferrin (TF), an iron-transporting protein. Prior work demonstrated that conditioned medium (CM) derived from human BM strongly stimulated the proliferation of PCa cells in vitro, and it was revealed that this ability was due to the high expression of TF in the CM[13]. This suggests that TF can induce growth of PCa in BM. TF is abundantly produced in the liver, and the main function of TF is to bind and bring iron into cells [14]. Iron-bind TF is taken up by TF receptor (TfR) expressing cells through receptor mediated endocytosis [15]. There are two TfRs in humans; transferrin receptor 1 (TfR1) and transferrin receptor 2 (TfR2) [14]. TfR1 is expressed by all cell types, whereas TfR2 is selectively expressed by hepatocytes, erythroblasts and peripheral blood mononuclear cells [16] [17]. A reasonable explanation as to why many cancers express high levels of TfR1 is that they may require more iron as a nutrient and a co-factor of the ribonucleotide reductase enzyme involved in DNA synthesis, and energy production in mitochondria for the rapid cell proliferation [14].

Although it was reported years ago that TF derived from bones strongly promotes the proliferation of PCa cells [13], it has not been shown how TF expression is changed during the progression of bone metastasis, or which BM cells produce TF in tumor microenvironments. In this study, we showed that TF strongly promotes the proliferation of high bone metastatic PCa cell lines (PC3, DU145), but not a low bone metastatic LnCaP subline (C4-2B) nor normal prostatic epithelial cells (RWPE-1). We also found that TF activates p27-positive dormant PC3 cells into proliferation. In addition, we demonstrated that TF levels are increased in the BM when PCa cells grow in bones. Further, we identified that PCa cells stimulate macrophages to

express TF. These observations suggest that the increase in TF expression in the BM, stimulated by PCa cells may play a significant role in the growth of PCa.

Results

TF facilitates the proliferation of bone metastatic PCa cells

To examine the effects of TF on the proliferation of PCa cells (PC3, DU145, C4-2B) and normal prostate epithelial cells (RWPE-1), cells were cultured in the presence or absence of TF for 3 days, and MTS assays were performed to evaluate proliferation. As it was reported, TF significantly increased the proliferation of bone metastatic PCa cells (PC3 and DU145) (Fig. 1A). Yet RWPE-1 cells did not respond in a similar fashion to TF stimulation (Fig. 1A). C4-2B cells, which are rarely metastasize to bone following intracardiac injections, failed to proliferate in response to TF stimulation (Fig. 1A).

Next, we evaluated the PCa cells for their expression of TF receptors using specific antibodies against TfR1 and TfR2 (Fig. 1B). Although TF receptor 2 (TfR2) is not detected on the cell surface of these PCa cells (data not shown), TF receptor 1 (TfR1) is detected on all these cells. Both PC3 and DU145 cells have significantly higher TfR1 levels than do RWPE-1 cells (Fig. 1B). However, C4-2B cells had higher expression of TfR1than do PC3 or DU145 cells, yet C4-2B cells do not proliferate in response to TF (Fig. 1B).

To further explore the impact of TF on the cell proliferation, we examined whether TF stimulation alters the expression of p27 protein, an endogenous cell cycle inhibitor, which may induce or maintain the cellular dormancy of tumor cells in the bone [12] [11] (Fig. 1C). The percentages of p27 positive cells are significantly decreased both in PC3 and DU145, but not in C4-2B cells by TF stimulation, consistent with the findings of the impact of TF on cell proliferation (Fig. 1A). Next, we deployed cell cycle reporters (G0-Venus, p27 and G1-Cherry, Cdt1) in PC3 cells, which report the phase of cell cycle by fluorescence activities [18] [19]. WE used this approach to isolate PC3 in G0 ($p27^{+}$ $Cdt1^{+}$) and cultured in the presence or absence or of TF. We observed that TF exposure induces PC3 cells to leave the G0 stage of the cell cycle and enter the cell cycle into G1 and S-phases (Fig. 1D). The number of PC3 cells in the G0 phase was reduced, while increased numbers of cells in G1 and S/G2/M cell cycle phases were observed (Fig. 1E).

Statins inhibit both the cell surface expression of TfR1 and TF-induced proliferation of PCa cells

Accumulating epidemiologic data suggest that statins, medications which effectively lower serum cholesterol levels by inhibiting 3-hydroxy-3-methylglutaryl coenzyme A (**HMG-CoA**) reductase **(HMGCR**) [20], may be linked to a reduced risk of prostate cancer in patients [21] [22, 23] [24]. Further, statins may not influence the incidence of prostate cancer, but decrease the risk of prostate cancer recurrence [25], and reduce prostate cancer-specific mortality [26]. Here we tested whether stains inhibit the proliferation of PCa cells induced by TF (Fig. 2A). The data demonstrate that Fluvastatin prevents TF induced proliferation of PC3 and DU145 cells (Fig.

2A). In order to identify the mechanism as to how Fluvastatin alters TF induced proliferation, we evaluated the impact of Fluvastatin on the cell surface expression of TfR1. We found that Fluvastatin significantly suppressed the cell surface expression of TfR1 on PC3 (Fig. 2B), reducing TfR1 high populations from 95 % down to 44% and 32% at the concentration of 5 μM and 10 μM, respectively (Fig. 2B). Fluvastatin reduces the TfR1 levels both on PC3 and DU145 cells (Fig. 2C), suggesting that one of the mechanisms by which Fluvastatin suppresses TF-induced PCa proliferation is the reduction of TfR1 cell surface expression.

TF protein is increased in the BM after the inoculation of PCa cells into bones

A prior study found the high expression of TF in BM, however, it has not been shown how TF expression is changed during the progression of bone metastasis, or which BM cells produce TF in tumor microenvironments. In order to explore it, we inoculated luciferase-expressing PC3 cells into the tibiae of severe combined immunodeficiency (SCID) mice. The cancer growth in the tibiae was monitored by Bioluminescence (BLI) (Fig. 3A). Twenty-eight days later TF protein levels in the extracelluar supernatant in the marrow were measured by ELISA. We found that TF levels were significantly increased in BM when PCa cells grow in the marrow compared to control tissues (Fig. 3B), whereas neither TF protein levels in plasma (Fig. S1) nor TF mRNA levels in the liver were elevated (Fig. S1). TF mRNA expression is not detected by qPCR in vitro PC3 culture (data not shown), taken together, these observations suggest that TF is locally produced in the marrow in response to PCa in bones. We also stained bone sections with the anti-TF antibodies (Fig. 3C). PC3 inoculation dramatically augmented the presence of TF-expressing cells which were large and presented near the growth plates (Fig. 3C). Based on the location and size of the TF-positive cells, and increased numbers present in the marrow in conjunction with tumor cells we suspected that the cells were osteoclasts (OCs). To test this hypothesis, we performed immunocytochemistry (IHC) using specific antibodies against tartrate-resistant acid phosphatase (TRAP), a well-known marker of osteoclasts and antibodies against TF (Fig. 3D). Many but not all of TF-positive cells were stained by TRAP antibodies (Fig. 3D, enlarged image). These observations suggest that OC is one of the cells which produce TF in response to PCa metastasis. To further examine whether OCs express TF, we stained human bone sections isolated from individuals with PCa bone metastases (Fig. 3E). As in the animal experiments, many mononuclear and multinuclear cells which stained for TRAP expressed TF (Fig. 3E).

PCa cells stimulate macrophages to express TF

We found that OCs express TF in bones containing PCa (Fig. 3D, E), while previous studies demonstrated that PCa cells stimulate macrophages to differentiate into OCs [27] [28]. Based on these observations, we hypothesized that PCa cells stimulate macrophages to express TF in the process of osteoclastogenesis. To test this hypothesis, PC3 cells were co-cultured with macrophage cell line, RAW264.7 cells. We observed that TF mRNA levels are significantly elevated in macrophages cultured with PC3 cells (Fig. 4A) and are the levels of TRAP mRNA (Fig. 4A). Next, we tested whether conditioned medium (CM) derived from PCa cells stimulate macrophages to express TF (Fig. 4B). Interestingly, CM either derived from PC3 or DU145 significantly elevates TF mRNA expression in macrophages, but CM from C4-2B reduces TF mRNA expression (Fig. 4B), although C4-2B CM increases TRAP mRNA more effectively than does PC3 or DU145 CM. These data suggest that factors secreted from PC3 or DU145 cells

induce both TF and TRAP expression by macrophages, however, TF expression is not always associated with TRAP expression.

To further explore the factors which induce TF expression by macrophages, macrophages were cultured in the presence of cytokines or lipopolysaccharides (LPS) which activate macrophages. We found that both receptor activator of nuclear factor kappa-B ligand (RANKL) and tumor necrosis factor alpha (TNF-α) increase TF mRNA expression by macrophages (Fig. 4C), while IL-6, IL-17 and LPS failed to induce TF mRNA expression. In addition, LPS increases TRAP mRNA, but not TF mRNA, further suggesting that TRAP expression is not always associated with TF expression as we observed in BM (Fig 3D). Further, immunocytochemistry showed that both TRAP and TF proteins are induced by RANKL in consistent with mRNA expression (Fig. 4C, D), suggesting that osteoclast progenitors or osteoclasts produce TF.

Discussion

Accumulating evidence suggests that TF is a pivotal factor for the growth of a variety of cancers including PCa [13], breast cancer [29], and lung cancer [30] [31]. Although the mechanisms underlying the growth of PCa in bones are poorly understood, TF extracted from bones were demonstrated to have strong abilities to promote the proliferation of PCa cells [13]. Yet what is the source of TF and how TF levels change in response to tumor in marrow has not been explored.

In this study, we demonstrate that TF levels increase in the BM in response to the presence of PCa cells (Fig. 3B). The source of TF in marrow appears to be predicated on local production as the TF-positive cells are dramatically expanded in the presence of tumor (Fig. 3D). We also observed that many although not all OCs express TF (Fig. 3D, E), and cells which are not identified by TRAP staining also express TF in the BM (Fig. 3D). The identity of these cells remains unclear however in a recent study examining lung cancer, neutrophils were shown to produce TF [31], suggesting that it is possible that bone marrow neutrophils also may be involved in TF elevation in bone metastases.

We found that both RANKL and TNF-α significantly increase TF expression by macrophages (Fig. 4C). Both cytokines have been reported to be expressed by PCa cells [27] [32], further osteoblasts produce significant quantities of RANKL when stimulated by PCa [33], and TNF-α production is induced by activated macrophages [34]. Therefore, it is likely that these cytokines may be involved in the induction of TF by macrophages in the marrow of individuals with metastatic PCa.

Our data show that TF increases the proliferation of PCa cells, PC3 and DU145, but not C4-2B (Fig. 1 A). Yet, the levels of TfR1 expression are comparable across these cell lines (Fig. 1B). In an attempt to explore the mechanisms regulating proliferation, mRNA expression in PCa cells after TF stimulation was examined (Fig. S2). We found that both tumor necrosis factor alpha-induced protein 2 (TNFAIP2) and hypoxia inducible factor 1 subunit alpha (Hif1α) are significantly increased by TF in both PC3 and DU145, but not in C4-2B cells (Fig. S2), which is associated with the TF-induced proliferation in these tested PCa cells (Fig. 1A). TNFAIP2 is a

recently identified gene which promotes the proliferation of esophageal squamous cell carcinoma [35] and breast cancer [36]. HIF-1α is a subunit of HIF-1, which is a transcription factor, primarily mediates the reaction of cells to low oxygen and affects the cell survival, proliferation and cell death [37]. HIF-1 overexpression is involved in promoting tumor growth and metastasis through its role in initiating angiogenesis and regulating cellular metabolism to overcome hypoxia [38]. Although further studies are required, our data implies that TNFAIP2 and HIF-1α may be involved in the molecular mechanisms by which TF-induced proliferation in PCa cells.

In this study, we also found that TF activates dormant PCa cells in G0 to enter the cell cycle (G1 and S-phases) (Fig.1D, E). Taken together, our data suggest that TF may play a pivotal role in PCa growth in bones by stimulating dormant PCa cells, and may warrant the development of methods to target TF in individuals with metastatic cancer. In this regard, we demonstrate that statins suppress TF-induced proliferation of PCa cells. In addition, statins significantly reduces TfR1 cell surface expression. Another group also reported that stains inhibited the expression of TfR1 in breast cancer [39]. In a xenograft prostate cancer model, it has been demonstrated that statins inhibit the proliferation of PCa in soft tissues [40] [41] [42], but the influence of statins on the proliferation of PCa cells in bones remains unexplored. Our results support the notion that statins should be evaluated of their therapeutic potential in the context of PCa bone metastases.

In conclusion, TF has a strong ability to promote the proliferation of bone metastatic PCa cells, and TF levels increase in response to the presence of tumor in marrow. Further, we showed that PCa cells stimulate macrophages to express TF. Finally, we show that statins inhibit the proliferation of PCa cells promoted by TF in part by down regulating expression of TF receptors. Together, targeting TF may be an efficacious strategy to suppress PCa growth in bone, and statins may serve as a useful tool in this regard.

Methods

Cell culture

The human prostate cancer cell lines, PC3 (Cat #: CRL-1435), DU145 (Cat #: HTB-81), normal human prostate epithelial RWPE-1 cells (Cat #: CRL-11609), murine macrophages, RAW264.7 (Cat #: TIB-71) and murine pre-osteoblastic cell line, MC3T3-E1 (Cat #: CRL-2593) were obtained from the American Type Culture Collection. The C4-2B is a derivative subline of human prostate cancer LNCaP, originally isolated from a lymph node of a prostate cancer patient [43]. All prostate cancer cell lines were routinely grown in RPMI 1640 (Life Technologies, Cat #: 11875-093), MC3T3-E1 cells and RAW264.7 cells were each grown in α-MEM (Life Technologies, Cat #: 12561-056) and DMEM (Life Technologies, Cat #: 11995-065), respectively. Cultures were supplemented with 10% (v/v) fetal bovine serum (GEMINI Bio-Products, Cat #: 900-208), 1% (v/v) penicillin-streptomycin (Life Technologies, Cat #: 15140-122) and maintained at 37°C, 5% CO2, and 100% humidity. RWPE-1 cells were cultured in Keratinocyte-SFM (Life Technologies) with supplements (17005-042, Life Technologies) and maintained at 37°C, 5% CO2, and 100% humidity.

Proliferation assays

PCa cells (1,000 cells) were plated into 96-well plates in growth medium with 0.5% FBS. The following day, cells were stimulated with TF (Millipore Sigma, Cat #: 616424) and viable cell numbers were evaluated by One Solution Cell Proliferation Assay kit (Promega, Cat #: G3580), which contains a tetrazolium compound [3-(4,5-dimethylthiazol-2-yl)-5-(3-carboxymethoxyphenyl)-2-(4-sulfophenyl)-2Htetrazolium, inner salt; MTS]. Optical intensities were read on a multiwell scanning spectrophotometer at OD 492 nm (Thermo Labsystems). An automatic blanking measurement was performed immediately before a measurement.

Flow cytometry

The flow cytometric analyses and fluorescence-activated cell sorting (FACS) were performed on a FACS Aria dual-laser flow cytometer (Becton Dickinson, Franklin Lakes, NJ) and data were analyzed with DIVA software (Becton Dickinson). Cells were stained with an APC/Cy7-anti-human TfR1 antibody (Cat #:334110, BioLegend) to evaluate the cell surface expression of TfR1. BD cytometer setup & tracking beads (BD Biosciences, Cat #: 642412) were used for the daily instrument standardization and validation. Sorting calibration was performed before each sort by drop-delay using Accudrop beads (BD Biosciences, Cat #: 345249). Sorting of cells was performed using a 70µm nozzle at 70 psi in purity mode.

PC3 integrated with cell cycle reporters

To develop a method to identify dormant, we transduced the human prostate cancer cell line, PC3 with lentiviruses containing the fluorescent ubiquitination-based cell cycle reporters [18]. Both of the CDT1-mCherry reporter (pMXs-mCherry-hCdt1(30/120) and the p27 cyclin-dependent kinase inhibitor protein –Venus reporter (pMXs-IP-mVenus-p27) were packaged into lentivirus at the University of Michigan Vector Core Facility. PC3 cells infected with both of the lentiviral reporters were selected for 7 days in RPMI media containing 10µg/ml puromycin. To isolate the cells which are successfully integrated with both reporters, Venus and mCherry double positive cells were sorted by flow cytometry. Isolated PC3 Venus mCherry cells were cultured in the RPMI containing 10% FBS. P27-Venus is upregulated upon entry into quiescence and is tagged for degradation by the Kip1 ubiquitination-promoting complex (KPC) in late G1 and the Skp2 ubiquitin ligase in the G1-S transition. Therefore, this reporter is high during G0, but low upon G1 entry and the G1-S transition [18]. The Cdt1-mCherry reporter is high during G0 and G1, but degraded during S phase by Skp2-dependent degradation [18]. Together, these two reporters can be used to identify dormant cells.

Immunostaining

Bone sections were fixed with 10% formalin overnight at 4°C. After antigen unmasking using Citrate Unmasking Solution (Cell Signaling Tech, Cat #: 14746) according to manufacturer directions, to detect mouse TF and mouse TRAP in bone marrow sections, anti-transferrin antibodies (rabbit IgG), (Boster, Cat. #:PB9827) and anti-TRAP antibodies (mouse IgG), (NSJ Bioreagents, Cat. #:V2794) were used as the primary antibodies, respectively. Anti-rabbit IgG conjugated with Alexa Fluor 594 (Cell Signaling Tech, Cat #: 8889) and anti-mouse IgG conjugated with Alexa Fluor 488 (Cell Signaling Tech, Cat #: 4408) were used as the secondary antibodies. After washing with PBS, the slides were mounted with ProLong Gold antifade reagent with DAPI (Invitrogen). Images were taken with Nikon A-1-B confocal microscope.

RNA Extraction and Real-Time RT-PCR
Total RNA was isolated using RNeasy Mini Kit (QIAGEN, Cat #: 74104). First-strand cDNA was synthesized in a 20μL reaction volume using 1 μg of total RNA. RT products were analyzed by real-time RT-PCR in TaqMan® Gene Expression Assays (Applied Biosystems, Foster City, CA), using human-specific or mouse-specific TaqMan MGB probes (Applied Biosystems). PCR products were detected as an increase in fluorescence using an ABI PRISM 7700 instrument (Applied Biosystems). TaqMan MGB probes (Applied Biosystems) were as follows: Mouse-specific probes; Transferrin (Mm00446715_m1) and TRAP (ACP5) (Mm00475698_m1) and Gapdh (Mm99999915_g1). Human-specific probes; Hif1α (Hs00936368_m), TNFAIP2 (Hs00196800_m1) and GAPDH (Hs99999905_m1). Gapdh (Mm99999915_g1) and Gapdh (Hs99999905_m1) were used as internal controls for the normalization of target gene expression in murine RAW264.7 cells and human PCa cells, respectively.

Animal experiments
All experimental animal procedures were performed in compliance with the institutional ethical requirements and approved by the University of Michigan Institutional Animal Care and Use Committee (IACUC). GFP/luciferase-expressing PC3 cells (2 x 10^5 cells) were suspended in 20 μl of PBS and injected into male CB.17. SCID mice (6-8 weeks of age, Charles River,Wilmington, MA) by intratibial (i.t.) injection. Tumor growth was monitored by bioluminescence images (BLI). At the experimental endpoint, mice were sacrificed, and the tibiae were collected for further histological analysis. The extracelluar supernatant in the BM was prepared by flushing out BM cells with 500 μl of PBS, and then the BM cells were centrifuged to acquire the extracelluar supernatant. The extracelluar supernatant was used to quantify TF protein levels by enzyme-linked immunosorbent assay (ELISA) (Aviva Systems Biology, Cat. #: OKIA00115) according to manufacturer directions.

Statistical Methods
All numerical data are expressed as mean ± standard deviation unless specified otherwise. Two-tailed, unpaired Student's *t*-test was used for data analysis, with $p < 0.05$ considered to be statistically significant.

Acknowledgments
This work is directly supported by the University of Michigan MCubed Project, the National Cancer Institute (CA093900, CA163124, U54CA143803, CA143055 to R.T.), the Department of Defense (PCRP Idea award W81XW-15-1-0413, to L.B., and W81XWH-11-1-0636 and W81XWH-15-1-0637 to R.T.), and the Prostate Cancer Foundation (Challenge Award 16CHAL05 to R. T.). R. T. received support as the Major McKinley Ash Colligate Professor. F. C. receives support from a Career Enhancement Award from the NIH / NCI Prostate Cancer Specialized Program in Research Excellence (SPORE) at the University of Michigan and Prostate Cancer Foundation Young Investigator Award 18YOUN04. The overlay histograms were made by the University of Michigan's BRCF Flow Cytometry Core, which is supported by the National Cancer Institute of the National Institutes of Health under award number P30CA046592. We thank Dr. Max S. Wicha for providing the breast cancer cell lines.

Author Contributions

K.Y. and R.T. wrote the main manuscript text and discussed the results with all other authors. R.T. and L.B. supervised the project. K.Y., M.O. and Y.W. carried out the experiments. F.C., Y.J. and A.D. reviewed the manuscript and gave technical support and conceptual advice.

Disclosure of Potential Conflicts of Interest
No potential conflicts of interest were disclosed.

Figure 1. **The influence of TF stimulation on the proliferation of PCa cells**
(**A**) MTS assays after 3 days of culture in the presence or absence of TF stimulation. The culture media was RPMI1640 containing 0.5% FBS. Relative cell proliferation levels are shown as mean ± S.D. (N=3). **p <0.01 compared to PC3, none. ##p < 0.01 compared to DU145, none. (**B**) Cell surface TfR1 levels detected using anti-TfR1 abs in FACS. (C) The sub-populations of PC3 cells in different cell cycles were identified by fluorescence signals associated with the reporters p27 and Cdt1 in FACS, and G0 dormant cells ($p27^+$ $Cdt1^+$) were isolated by FACS sorting. The isolated dormant cells were cultured in the presence or absence of TF (5 μg/ml). The culture media was RPMI1640 containing 0.5% FBS. After 3 days of the culture, cell cycle phases were identified by FACS. (D) The impact of TF on the each G0, G1 and S/G2/M cell cycle phase was shown as cells (%), mean ± S.D. (N=3). **p <0.01 compared to PC3, none. (E) p27 positive PCa cells (%) are shown after 3 days of culture in the presence or absence of TF (1 μg/ml). The culture media was RPMI1640 containing 0.5% FBS. p27 positive cells (%) are shown as mean ± S.D. (N=3). *p <0.05 compared to the PC3 cultured without TF. ##p < 0.01 compared to DU145 cultured without TF.

Figure 2. **Fluvastatin inhibits the cell surface expression of TfR1 and TF-induced proliferation of PCa cells**
(A) Number of PC3cells and DU145 cells after 3 days of culture in the presence or absence of TF or fluvastain (Sigma-Ald, Cat #:344096). Cells were pretreated with fluvastatin for 2 days, and then cultured in the presence or absence of TF for another 3 days in the presence of fluvastatin. Cell number is shown as mean ± S.D. (N=3). **p <0.01 compared to PC3, none. ##p <0.01 compared to DU145, none. (**B**) Cell surface expression of TfR1 by PC3 cells after 2 days of culture in the presence or absence of fluvastatin. TfR1 high cells (%) are shown as mean ± S.D. (N=3). **p <0.01 compared to PC3, vehicle (PBS). (C) TfR1 cell surface expression levels by PC3 and DU145 cells are quantified by the fluorescence from anti-TfR1 abs (APC-Cy7) in FACS after 2 days of culture in the presence or absence of TF. TfR1 cell surface expression levels are shown as mean ± S.D. (N=3). **p <0.01 compared to PC3, none. ##p <0.01 compared to DU145, none.

Figure 3. TF protein levels are increased in the BM after PC3 i.t. injection
(**A**) Cancer growth in tibiae monitored by BLI after the inoculation of PC3 into the tibiae of SCID mice. Data are shown as mean ± S.D. (N=5). (**B**) TF protein levels in the extracelluar

supernatant in the marrow 28 days after the inoculation. Data are shown as mean ± S.D. (N=5). *p <0.05 compared to Control (PBS) i.t. injection. (C) IHC showing TF expression in the bone sections 28 days after i.t. injection of PBS (Control) and PC3 cells. TF (red) and nuclei (DAPI, blue) in the image. Scale bar, 20 μm. (D) IHC showing both TF (red) and TRAP (green) expression in the bone sections 28 days after i.t. injection of PBS (Control) and PC3 cells. Scale bar, 20 μm. (E) IHC showing TF expression by TRAP-positive osteoclasts in human bone metastases. Scale bar, 20 μm.

Figure 4. PCa cells stimulate macrophages to produce TF

(**A**) Relative TF and TRAP mRNA expression by macrophages (RAW264.7 cells) in the presence or absence of PC3 cells. Data are shown as mean ± S.D. (N=3). mRNA was extracted after 3 days of the co-cultutre. **p <0.01 compared to RAW264.7 cells alone. (**B**) Relative mRNA expression of TF and TRAP by RAW cells were detected after RAW cells were cultured for 4 days in the CM prepared from PCa cells. The CM was prepared by 3 days of PCa cell culture in RPMI1640 medium with 1% FBS. Data are shown as mean ± S.D. (N=3). **p <0.01 compared to RAW264.7 cells without PCa CM. (C) Relative mRNA expression of TF and TRAP by RAW cells. mRNA was extracted after 3 days of stimulation with recombinant human RANKL, TNF-α, IL-6, IL-17 (each 50 ng/ml), or LPS (1μg/ml) while RAW cells were cultured in DMEM medium with 10% FBS. Data are shown as mean ± S.D. (N=3). **p < 0.01 compared to Control (PBS). (D) Immunocytochemistry for TF expression by RAW264.7 cells after 3 days of RANKL (50 ng/ml) stimulation. Scale bar, 20 μm.

Supplemental Figure 1. TF protein levels in plasma and TF mRNA levels in liver after PC3 i.t. injection

(A) TF protein levels in plasma 28 days after i.t. injection of PBS (Control) and PC3 cells. Data are shown as mean ± S.D. (N=5). (B) Relative TF mRNA expression levels in liver 28 days after i.t. injection of PBS (Control) and PC3 cells. Data are shown as mean ± S.D. (N=5).

Supplemental Figure 2. TF stimulation increases both HIF-1A and TNFAIP2 mRNA expression

Relative mRNA expression by PCa cells. mRNA was extracted 24 hours after TF stimulation (1μg/ml). Data are shown as mean ± S.D. (N=3). **p <0.01 compared to PC3, none. #p < 0.05, ##p < 0.01 compared to DU145, none.

[1] F. Macedo, K. Ladeira, F. Pinho, N. Saraiva, N. Bonito, L. Pinto, F. Goncalves, Bone Metastases: An Overview, Oncol Rev, 11 (2017) 321.
[2] R.B. Shah, R. Mehra, A.M. Chinnaiyan, R. Shen, D. Ghosh, M. Zhou, G.R. Macvicar, S. Varambally, J. Harwood, T.A. Bismar, R. Kim, M.A. Rubin, K.J. Pienta, Androgen-independent prostate cancer is a heterogeneous group of diseases: lessons from a rapid autopsy program, Cancer Res, 64 (2004) 9209-9216.
[3] J. Ferlay, I. Soerjomataram, R. Dikshit, S. Eser, C. Mathers, M. Rebelo, D.M. Parkin, D. Forman, F. Bray, Cancer incidence and mortality worldwide: sources, methods and major patterns in GLOBOCAN 2012, Int J Cancer, 136 (2015) E359-386.
[4] N. Sathiakumar, E. Delzell, M.A. Morrisey, C. Falkson, M. Yong, V. Chia, J. Blackburn, T. Arora, M.L. Kilgore, Mortality following bone metastasis and skeletal-related events among men with prostate cancer: a population-based analysis of US Medicare beneficiaries, 1999-2006, Prostate Cancer Prostatic Dis, 14 (2011) 177-183.
[5] K.J. Luzzi, I.C. MacDonald, E.E. Schmidt, N. Kerkvliet, V.L. Morris, A.F. Chambers, A.C. Groom, Multistep nature of metastatic inefficiency: dormancy of solitary cells after successful extravasation and limited survival of early micrometastases, Am J Pathol, 153 (1998) 865-873.
[6] T.M. Morgan, P.H. Lange, M.P. Porter, D.W. Lin, W.J. Ellis, I.S. Gallaher, R.L. Vessella, Disseminated tumor cells in prostate cancer patients after radical prostatectomy and without evidence of disease predicts biochemical recurrence, Clin Cancer Res, 15 (2009) 677-683.
[7] C. Morrissey, R.L. Vessella, The role of tumor microenvironment in prostate cancer bone metastasis, J Cell Biochem, 101 (2007) 873-886.
[8] K. Yumoto, M.R. Eber, J.E. Berry, R.S. Taichman, Y. Shiozawa, Molecular pathways: niches in metastatic dormancy, Clin Cancer Res, 20 (2014) 3384-3389.
[9] Y. Shiozawa, E.A. Pedersen, L.R. Patel, A.M. Ziegler, A.M. Havens, Y. Jung, J. Wang, S. Zalucha, R.D. Loberg, K.J. Pienta, R.S. Taichman, GAS6/AXL axis regulates prostate cancer invasion, proliferation, and survival in the bone marrow niche, Neoplasia, 12 (2010) 116-127.
[10] K. Yumoto, M.R. Eber, J. Wang, F.C. Cackowski, A.M. Decker, E. Lee, A.R. Nobre, J.A. Aguirre-Ghiso, Y. Jung, R.S. Taichman, Axl is required for TGF-beta2-induced dormancy of prostate cancer cells in the bone marrow, Sci Rep, 6 (2016) 36520.
[11] A. Kobayashi, H. Okuda, F. Xing, P.R. Pandey, M. Watabe, S. Hirota, S.K. Pai, W. Liu, K. Fukuda, C. Chambers, A. Wilber, K. Watabe, Bone morphogenetic protein 7 in dormancy and metastasis of prostate cancer stem-like cells in bone, J Exp Med, 208 (2011) 2641-2655.

[12] P. Bragado, Y. Estrada, F. Parikh, S. Krause, C. Capobianco, H.G. Farina, D.M. Schewe, J.A. Aguirre-Ghiso, TGF-beta2 dictates disseminated tumour cell fate in target organs through TGF-beta-RIII and p38alpha/beta signalling, Nat Cell Biol, 15 (2013) 1351-1361.
[13] M.C. Rossi, B.R. Zetter, Selective stimulation of prostatic carcinoma cell proliferation by transferrin, Proc Natl Acad Sci U S A, 89 (1992) 6197-6201.
[14] T.R. Daniels, T. Delgado, J.A. Rodriguez, G. Helguera, M.L. Penichet, The transferrin receptor part I: Biology and targeting with cytotoxic antibodies for the treatment of cancer, Clin Immunol, 121 (2006) 144-158.
[15] C.E. Herbison, K. Thorstensen, A.C. Chua, R.M. Graham, P. Leedman, J.K. Olynyk, D. Trinder, The role of transferrin receptor 1 and 2 in transferrin-bound iron uptake in human hepatoma cells, Am J Physiol Cell Physiol, 297 (2009) C1567-1575.
[16] H. Kawabata, R.S. Germain, T. Ikezoe, X. Tong, E.M. Green, A.F. Gombart, H.P. Koeffler, Regulation of expression of murine transferrin receptor 2, Blood, 98 (2001) 1949-1954.
[17] A. Nai, M.R. Lidonnici, M. Rausa, G. Mandelli, A. Pagani, L. Silvestri, G. Ferrari, C. Camaschella, The second transferrin receptor regulates red blood cell production in mice, Blood, 125 (2015) 1170-1179.
[18] T. Oki, K. Nishimura, J. Kitaura, K. Togami, A. Maehara, K. Izawa, A. Sakaue-Sawano, A. Niida, S. Miyano, H. Aburatani, H. Kiyonari, A. Miyawaki, T. Kitamura, A novel cell-cycle-indicator, mVenus-p27K-, identifies quiescent cells and visualizes G0-G1 transition, Sci Rep, 4 (2014) 4012.
[19] H. Takahashi, K. Yumoto, K. Yasuhara, E.T. Nadres, Y. Kikuchi, R.S. Taichman, K. Kuroda, Anticancer polymers designed for killing dormant prostate cancer cells, Sci Rep, 9 (2019) 1096.
[20] A. Endo, Chemistry, biochemistry, and pharmacology of HMG-CoA reductase inhibitors, Klin Wochenschr, 66 (1988) 421-427.
[21] M.A. Alfaqih, E.H. Allott, R.J. Hamilton, M.R. Freeman, S.J. Freedland, The current evidence on statin use and prostate cancer prevention: are we there yet?, Nat Rev Urol, 14 (2017) 107-119.
[22] J. Shannon, S. Tewoderos, M. Garzotto, T.M. Beer, R. Derenick, A. Palma, P.E. Farris, Statins and prostate cancer risk: a case-control study, Am J Epidemiol, 162 (2005) 318-325.
[23] E.J. Jacobs, C. Rodriguez, E.B. Bain, Y. Wang, M.J. Thun, E.E. Calle, Cholesterol-lowering drugs and advanced prostate cancer incidence in a large U.S. cohort, Cancer Epidemiol Biomarkers Prev, 16 (2007) 2213-2217.
[24] T.J. Murtola, T.L. Tammela, J. Lahtela, A. Auvinen, Cholesterol-lowering drugs and prostate cancer risk: a population-based case-control study, Cancer Epidemiol Biomarkers Prev, 16 (2007) 2226-2232.
[25] E.H. Allott, L.E. Howard, M.R. Cooperberg, C.J. Kane, W.J. Aronson, M.K. Terris, C.L. Amling, S.J. Freedland, Postoperative statin use and risk of biochemical recurrence following radical prostatectomy: results from the Shared Equal Access Regional Cancer Hospital (SEARCH) database, BJU Int, 114 (2014) 661-666.
[26] O. Yu, M. Eberg, S. Benayoun, A. Aprikian, G. Batist, S. Suissa, L. Azoulay, Use of statins and the risk of death in patients with prostate cancer, J Clin Oncol, 32 (2014) 5-11.
[27] Y. Lu, Z. Cai, G. Xiao, E.T. Keller, A. Mizokami, Z. Yao, G.D. Roodman, J. Zhang, Monocyte chemotactic protein-1 mediates prostate cancer-induced bone resorption, Cancer Res, 67 (2007) 3646-3653.
[28] K. Mizutani, S. Sud, K.J. Pienta, Prostate cancer promotes CD11b positive cells to differentiate into osteoclasts, J Cell Biochem, 106 (2009) 563-569.
[29] T. Inoue, P.G. Cavanaugh, P.A. Steck, N. Brunner, G.L. Nicolson, Differences in transferrin response and numbers of transferrin receptors in rat and human mammary carcinoma lines of different metastatic potentials, J Cell Physiol, 156 (1993) 212-217.
[30] P.G. Cavanaugh, G.L. Nicolson, Lung-derived growth factor that stimulates the growth of lung-metastasizing tumor cells: identification as transferrin, J Cell Biochem, 47 (1991) 261-271.

[31] W. Liang, Q. Li, N. Ferrara, Metastatic growth instructed by neutrophil-derived transferrin, Proc Natl Acad Sci U S A, 115 (2018) 11060-11065.
[32] H. Penno, O. Nilsson, H. Brandstrom, O. Winqvist, O. Ljunggren, Expression of RANK-ligand in prostate cancer cell lines, Scand J Clin Lab Invest, 69 (2009) 151-155.
[33] H. Inoue, K. Nishimura, D. Oka, Y. Nakai, M. Shiba, T. Tokizane, Y. Arai, M. Nakayama, K. Shimizu, N. Takaha, N. Nonomura, A. Okuyama, Prostate cancer mediates osteoclastogenesis through two different pathways, Cancer Lett, 223 (2005) 121-128.
[34] T. Hagemann, S.C. Robinson, M. Schulz, L. Trumper, F.R. Balkwill, C. Binder, Enhanced invasiveness of breast cancer cell lines upon co-cultivation with macrophages is due to TNF-alpha dependent up-regulation of matrix metalloproteases, Carcinogenesis, 25 (2004) 1543-1549.
[35] Y. Xie, B. Wang, Downregulation of TNFAIP2 suppresses proliferation and metastasis in esophageal squamous cell carcinoma through activation of the Wnt/beta-catenin signaling pathway, Oncol Rep, 37 (2017) 2920-2928.
[36] L. Jia, Z. Zhou, H. Liang, J. Wu, P. Shi, F. Li, Z. Wang, C. Wang, W. Chen, H. Zhang, Y. Wang, R. Liu, J. Feng, C. Chen, KLF5 promotes breast cancer proliferation, migration and invasion in part by upregulating the transcription of TNFAIP2, Oncogene, 35 (2016) 2040-2051.
[37] G.L. Semenza, HIF-1: mediator of physiological and pathophysiological responses to hypoxia, J Appl Physiol (1985), 88 (2000) 1474-1480.
[38] P. Vaupel, A. Mayer, Hypoxia in cancer: significance and impact on clinical outcome, Cancer Metastasis Rev, 26 (2007) 225-239.
[39] A.K. Kanugula, P.N. Gollavilli, S.B. Vasamsetti, S. Karnewar, R. Gopoju, R. Ummanni, S. Kotamraju, Statin-induced inhibition of breast cancer proliferation and invasion involves attenuation of iron transport: intermediacy of nitric oxide and antioxidant defence mechanisms, FEBS J, 281 (2014) 3719-3738.
[40] Y. Miyazawa, Y. Sekine, H. Kato, Y. Furuya, H. Koike, K. Suzuki, Simvastatin Up-Regulates Annexin A10 That Can Inhibit the Proliferation, Migration, and Invasion in Androgen-Independent Human Prostate Cancer Cells, Prostate, 77 (2017) 337-349.
[41] S.T. Kochuparambil, B. Al-Husein, A. Goc, S. Soliman, P.R. Somanath, Anticancer efficacy of simvastatin on prostate cancer cells and tumor xenografts is associated with inhibition of Akt and reduced prostate-specific antigen expression, J Pharmacol Exp Ther, 336 (2011) 496-505.
[42] X. Zheng, X.X. Cui, G.E. Avila, M.T. Huang, Y. Liu, J. Patel, A.N. Kong, R. Paulino, W.J. Shih, Y. Lin, A.B. Rabson, B.S. Reddy, A.H. Conney, Atorvastatin and celecoxib inhibit prostate PC3 tumors in immunodeficient mice, Clin Cancer Res, 13 (2007) 5480-5487.
[43] T.T. Wu, R.A. Sikes, Q. Cui, G.N. Thalmann, C. Kao, C.F. Murphy, H. Yang, H.E. Zhau, G. Balian, L.W. Chung, Establishing human prostate cancer cell xenografts in bone: induction of osteoblastic reaction by prostate-specific antigen-producing tumors in athymic and SCID/bg mice using LNCaP and lineage-derived metastatic sublines, Int J Cancer, 77 (1998) 887-894.

Figure 1

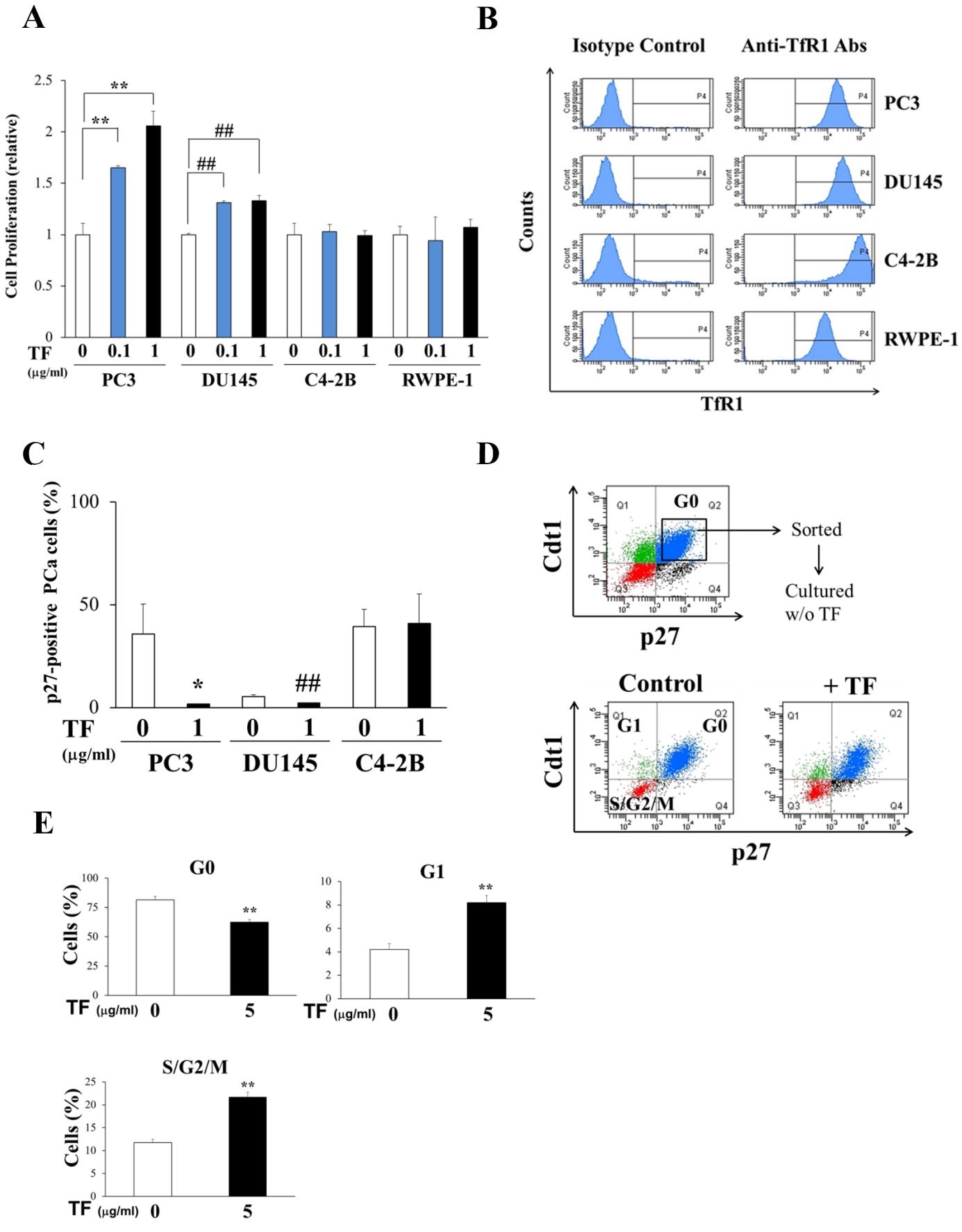
A
Cell Proliferation (relative)
2.5
2
1.5
1
0.5
0
**
**
##
##
TF (μg/ml)
0 0.1 1 0 0.1 1 0 0.1 1 0 0.1 1
PC3
DU145
C4-2B
RWPE-1
B
Isotype Control
Anti-TfR1 Abs
PC3
DU145
C4-2B
RWPE-1
Counts
TfR1
C
p27-positive PCa cells (%)
100
50
0
*
##
TF (μg/ml)
0 1 0 1 0 1
PC3
DU145
C4-2B
D
Cdt1
p27
G0
Q1
Q2
Q3
Q4
Sorted
Cultured w/o TF
Control
+ TF
G1
G0
S/G2/M
E
G0
Cells (%)
100
75
50
25
0
**
TF (μg/ml) 0 5
G1
10
8
6
4
2
0
**
TF (μg/ml) 0 5
S/G2/M
Cells (%)
25
20
15
10
5
0
**
TF (μg/ml) 0 5

Figure 2

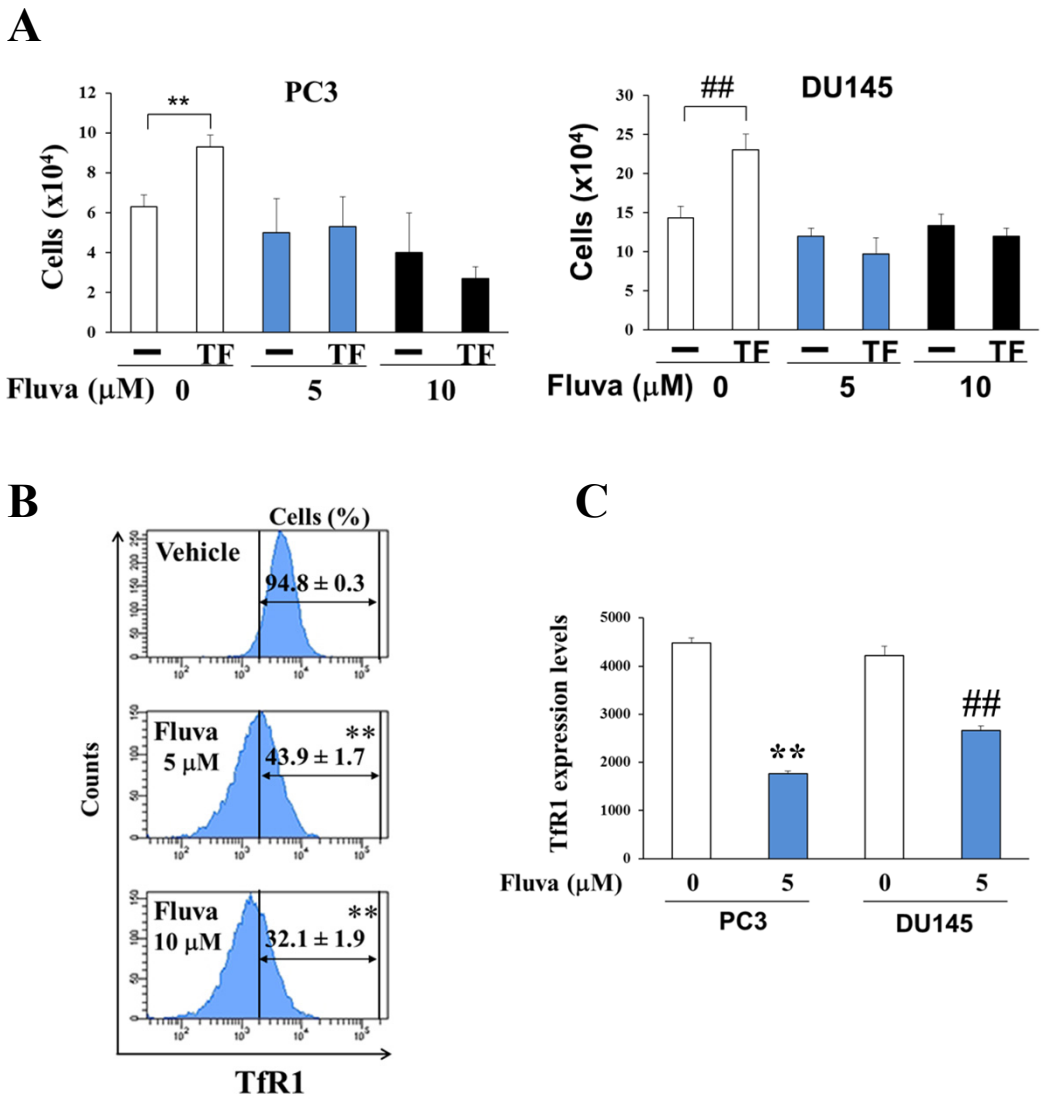
A
PC3
**
Cells (x10⁴)
12
10
8
6
4
2
0
— TF — TF — TF
Fluva (μM) 0 5 10
DU145
##
Cells (x10⁴)
30
25
20
15
10
5
0
— TF — TF — TF
Fluva (μM) 0 5 10
B
Cells (%)
Vehicle
94.8 ± 0.3
Fluva 5 μM
**
43.9 ± 1.7
Fluva 10 μM
**
32.1 ± 1.9
Counts
TfR1
C
TfR1 expression levels
5000
4000
3000
2000
1000
0
**
##
Fluva (μM) 0 5 0 5
PC3
DU145

Figure 3

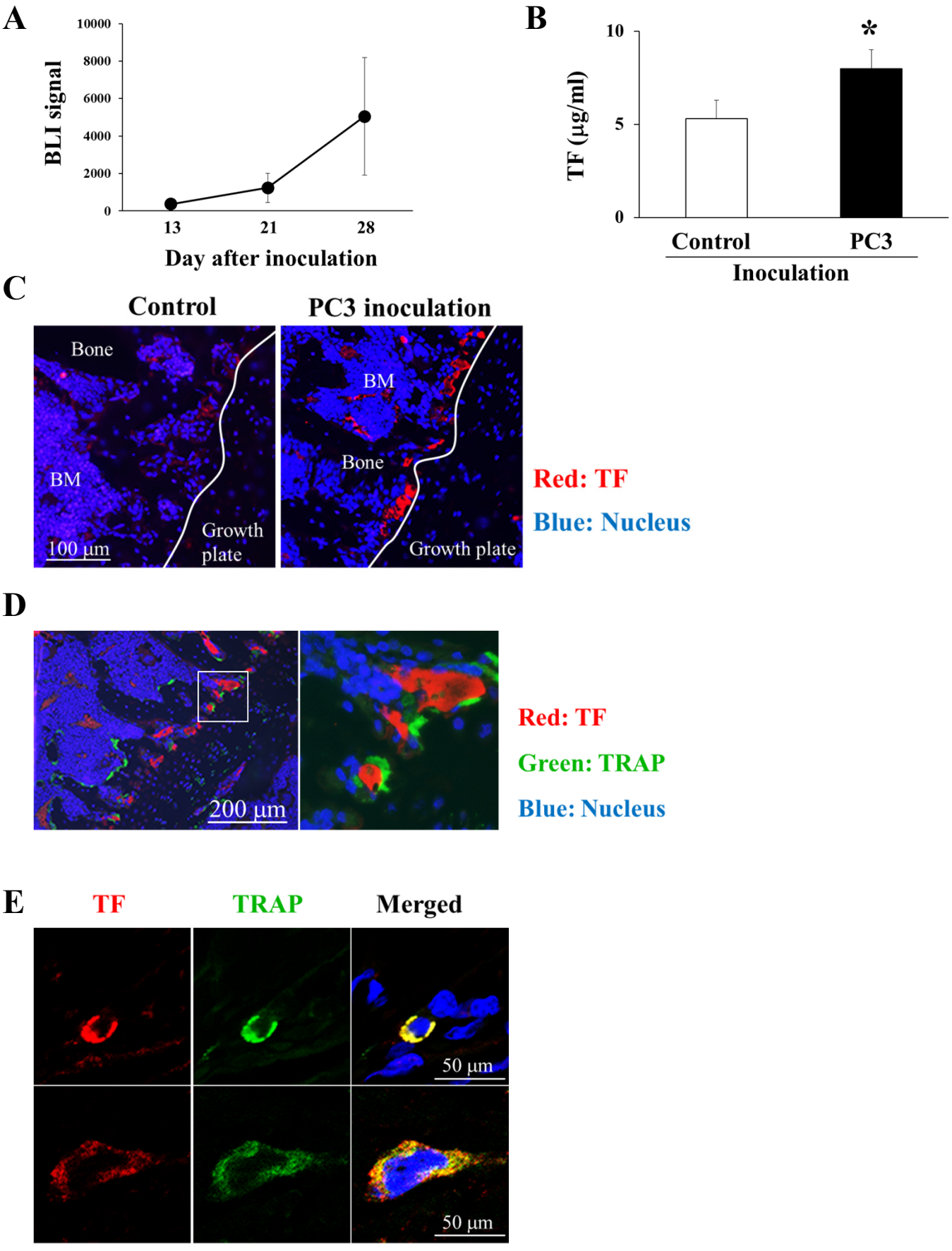
A
BLI signal
10000
8000
6000
4000
2000
0
13
21
28
Day after inoculation
B
TF (μg/ml)
10
5
0
*
Control
PC3
Inoculation
C
Control
PC3 inoculation
Bone
BM
Growth plate
100 μm
BM
Bone
Growth plate
Red: TF
Blue: Nucleus
D
200 μm
Red: TF
Green: TRAP
Blue: Nucleus
E
TF
TRAP
Merged
50 μm
50 μm

Figure 4

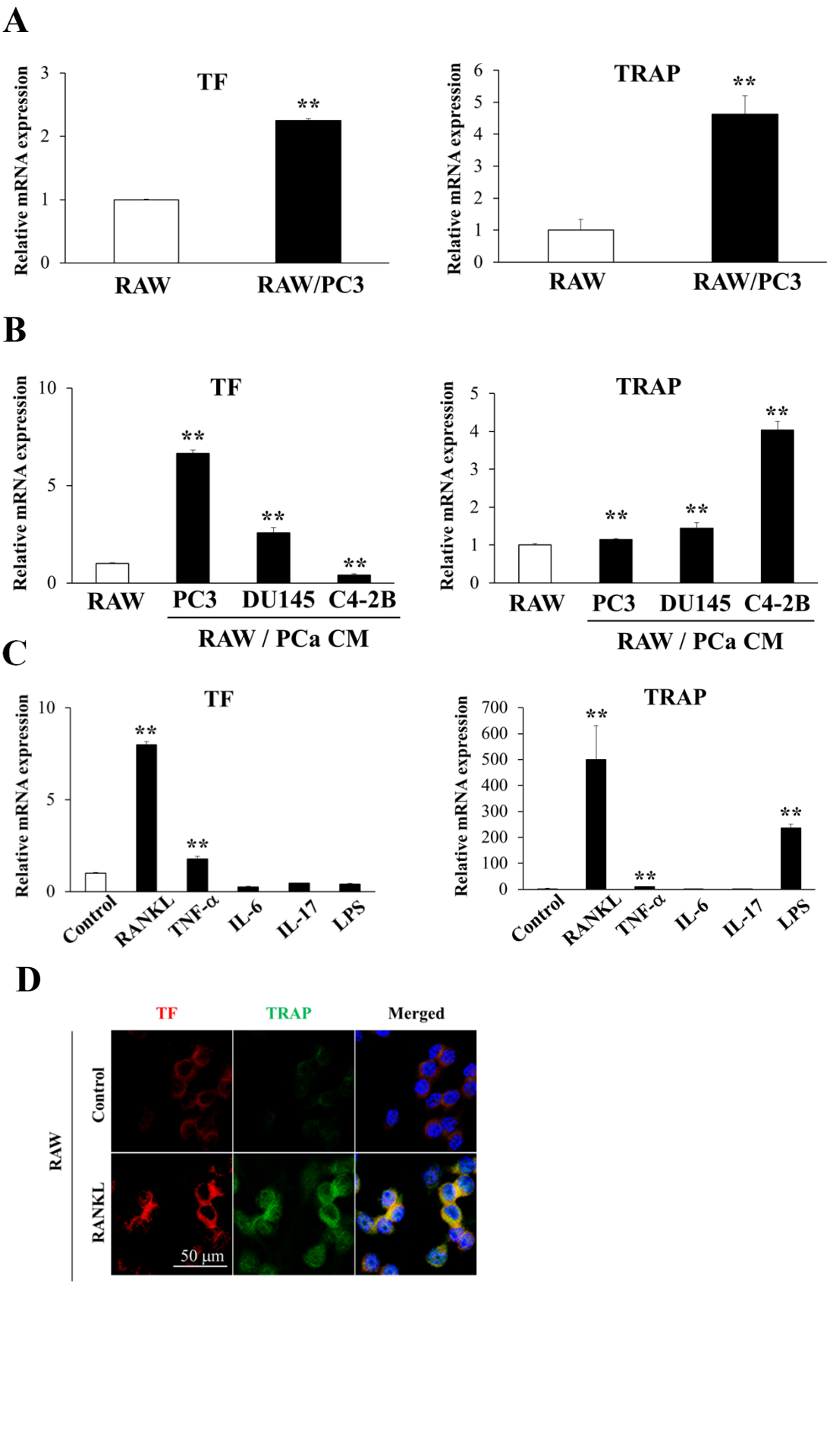
A
TF
Relative mRNA expression
RAW
RAW/PC3
TRAP
B
PC3
DU145
C4-2B
RAW / PCa CM
C
Control
RANKL
TNF-α
IL-6
IL-17
LPS
D
TF
TRAP
Merged
RAW
Control
RANKL
50 μm

Supplemental figure 1

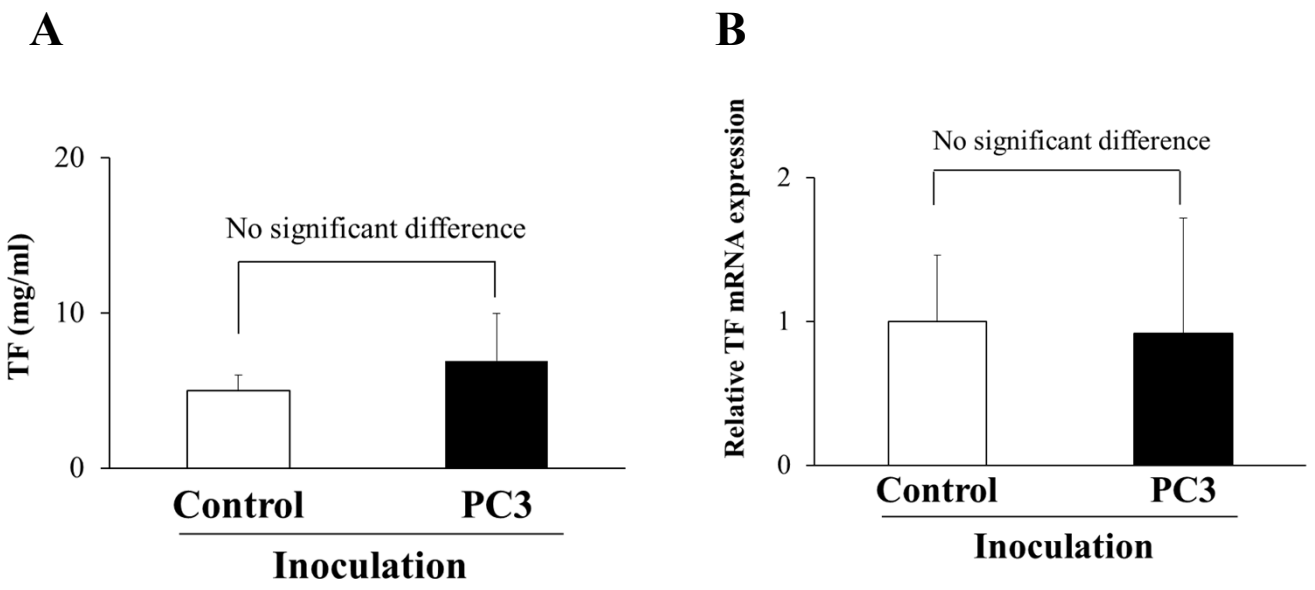

Supplemental figure 2